# STRUCTURAL AND DYNAMIC DESIGN OF VARIABLE GEOMETRY VERTICAL AXIS WIND TURBINE BLADE USING FEM

A Thesis Submitted

In Partial Fulfillment of the Requirements

for the Degree of

**MASTER OF TECHNOLOGY**

by

**SHEVADE ANIRUDDHA VASUDEV**

To the

**DEPARTMENT OF MECHANICAL ENGINEERING**

**INDIAN INSTITUTE OF TECHNOLOGY**

**KANPUR**

APRIL 1994

To

MY PARENTS AND SHRI DADAJI

## CERTIFICATE

21.4.94

It is certified that the work contained in the thesis entitled " **STRUCTURAL AND DYNAMIC DESIGN OF VARIABLE GEOMETRY VERTICAL AXIS WIND TURBINE BLADE USING FEM** ", by Shevade Aniruddha Vasudev, has been carried out under my supervision and that this work has not been submitted elsewhere for a degree.

Dr. P.M Dixit

Associate professor

Department of Mechanical Engineering

I.I.T Kanpur

April 1994

## ACKNOWLEDGEMENTS

I express my sincere thanks to Dr. P.M.Dixit for his able and precious guidance and for devoting his precious time to solve my difficulties. I consider it a privilege to have had an oppurtunity to get inspiration from his meticulous method of working and research apttitude.

I am grateful to Dr. Kunal Ghosh for his help in making me understand the basic principles of operations of a wind turbine.

I thank each and every person of Ghat Mandal for having created a homely atmosphere, conducive to work.My special thanks are due to Gharpure, Kopinesh, Rakesh, Bhat, Kamat, Pai and Dipayan for allowing me to use their computing facility at a very critical time. I also thank S.P.Chandrashekhar for having allowed me to use his graphics package. I consider myself to be very lucky to be associated with friends like Shrikant Sharma, Kelkar and Dindore whose enthusiasm and confidence have always encouraged me.

Words fail to describe my feelings towards my parents and Shri Dadaji, whose blessings have been a great source of power for me.

April 1994 Aniruddha V.shevade

I.I.T Kanpur

CONTENTS

# LIST OF TABLES

# LIST OF FIGURES

# LIST OF SYMBOLS

A) List of symbols common to all chapters

| Symbol | Description |
|---|---|
| $a_n$, $b_n$ | Fourier coefficients |
| A | Area of cross-section |
| C | Chord length |
| [ D ] | Matrix containing stiffness coefficients of the box beam |
| $C_n$, $C_t$ | Normal force coefficient and tangential force coefficient respectively |
| $E_1$, $E_2$ | Young's modulus i he direction of the fibre and perpendicular to the fibre respectively |
| FI | Failure index |
| { $F_g$ } | Global force vector |
| $F_n$, $F_t$ | Normal and tangential aerodynamic forces respectively |
| G | Mass centre |
| $I_p$ | Polar moment of inertia referred to the shear centre |
| $I_y$, $I_z$ | Moment of inertia about y and z axis respectively |
| $I_{y_1y_1}$, $I_{z_1z_1}$ | Moment of inertia about $y_1$ and $z_1$ axis respectively |
| J | Torsion constant of the section |
| K | Kinetic energy |
| [ $K^e$ ] | Elemental stiffness matrix |
| [ $K_g$ ] | Global stiffness matrix |
| l | Length of the beam |

| | |
|---|---|
| $M_t$ | Torque about the mass centre |
| $M_{tE}$ | Torque about the shear centre. |
| $M_y$, $M_z$ | Moments about y and z axis respectively |
| $M_1$, $M_2$ | Shape functions |
| $[ M^e ]$ | Elemental mass matrix |
| $[ M_g ]$ | Global mass matrix |
| $n_j$ | Co-ordinate along the normal to a point |
| $N_1$, $N_2$, $N_3$, $N_4$ | Shape functions |
| P(t), q(t), r(t) | Functions of time satisfying the homogeneous Part of equation of the beam. |
| P(x), Q(x), R(x) | Functions of x satisfying the homogeneous part of equation of vibration. |
| $p_g$ | Perpendicular distance of the element from the mass centre. |
| $q^j$ | Shear flow in cell j |
| $\{ Q \}$ | Matrix containing stiffness coefficient for a ply whose fibres are parallel to x axis. |
| $\overline{Q_{11}}'$, $\overline{Q_{16}}'$ etc. | Reduced stiffness coefficients |
| $r_s$, $r_n$ | The perpendicular distance of a cell element and the normal to the cell element from the shear centre. |
| $s_j$ | Co-ordinate measured along the contour of cell j |
| $\overrightarrow{r}$ | Position vector. |

| | |
|---|---|
| $u_1$, $v_1$ | Bending deflections/ Translations of the cross-section about the $y_1$-$z_1$ axis |
| $\overline{u}$, $\overline{v}$, $\overline{w}$ | Total displacements of a particle in the $x_1$, $y_1$ and $z_1$ directions respectively. |
| $v_o(x)$, $w_o(x)$, $\theta_o(x)$ | Functions of x satisfying the inhomogeneous part of equation of vibration of the blade. |
| $V_\alpha$ | Free stream wind velocity |
| $V_{sj}$, $V_{nj}$ | Tangential displacement and normal displacement at a point in cell j. |
| $\overrightarrow{Vel}$ | Velocity vector at a point |
| $y_P$ | Co-ordinate of the centre of pressure. |
| $V_y$, $V_z$ | Shear forces along the y and z directions respectively |
| $x_c$ | Global co-ordinate of the midpoint of the element |
| x,y,z | Inertial co-ordinate system |
| $x_e$, $x_{e+1}$ | Co-ordinates of the end nodes of a element |
| $X_t$, $X_c$ | Ultimate tensile strength and ultimate compressive strength in the fibre direction respectively |
| $\{ X^{ne} \}$ | Vector containing elemental degrees of freedom |
| $\{ X_g \}$ | Vector containing global degrees of freedom |
| $Y_t$, $Y_c$ | Ultimate tensile strength and ultimate compressive strength in the direction perpendicular to the fibre respectively. |
| $y_P$ | Co-ordinate of the centre of pressure. |

Greek symbols

| | |
|---|---|
| $\beta_y$, $\beta_z$ | Rotations of the cross-section about the y and z axis respectively |
| $\{ \varepsilon^e \}$ | Residue |
| $\gamma^o_{x\xi}$, $\gamma^o_{x\eta}$ | Transverse shear |
| $\lambda$ | Eigen value |
| $\nu_{12}$, $\nu_{21}$ | Poisson's ratio in the direction of the fibre and perpendicular to it respectively. |
| $\rho_\alpha$ | Density of air |
| $\sigma_{xx}$ | Normal stress |
| $\sigma_{xsj}$, $\sigma_{xnj}$ | Shear stress for the cell j |
| $\sigma_1$, $\sigma_2$ | Normal stress in the direction of the fibre and perpendicular to it respectively |
| $\{ \sigma_v \}$, $\{ \sigma_h \}$ | Vectors containing stress components of the vertical and horizontal wall respectively |
| $\omega$ | Frequency of vibration |

Mathematical symbols

| | |
|---|---|
| $\oint$ | Integration over the entire cell |
| $\int_{j-1,j}$ | Integration for the region common to j th cell and j-1 th cell |
| $\iint_V$ , $\iint_H$ | Integration over the horizontal and vertical walls of the composite box-beam |
| $\delta$ | Variational operator |

B) Symbols used in particular chapters

1) Chapter 2

| | |
|---|---|
| P | Axial force |
| t | Thickness of spar |

| | |
|---|---|
| $U$ | Potential energy |
| $( y_E, Z_E)$ | Co-ordinates of shear centre w.r.t (x,y,z) axes. |
| $\alpha_j$ | Constant for cell j which depends on its shape |
| $\phi$ | angle of twist |
| $\mu$ | Shear modulus |
| $\Omega_j$ | Area enclosed by the j th cell |

2) Chapter 3

| | |
|---|---|
| $t$ | time |
| $U$ | Potential energy |
| $x_1, y_1, z_1$ | Body fixed co-ordinate system |
| $y_E, z_E$ | Co-ordinates of the shear centre w.r.t $x_1, y_1, z_i$ co-ordinate system |
| $\mu$ | In - plane shear modulus |
| $\theta$ | Angle of twist |
| $\Omega$ | Angular velocity of the turbine |
| $\xi$ | Local co-ordinate of the element |

3) Chapter 4

| | |
|---|---|
| $F_x$ | Axial force |
| $G_{12}$ | In plane shear modulus |
| $U^e$ | Strain energy of a element |
| $\alpha$ | Local co-ordinate of the element. |
| $\phi$ | Angle of twist of the section |
| $\eta - \xi$ | Body fixed co-ordinate system |
| $\theta$ | Ply orientation angle |

# ABSTRACT

The structural and dynamic design has been done for a 10 KW VGAVWT to be set up by the Ministry of Non-conventional Energy Resources, Govt. of India and BHEL. The section consists of a standard 2 cell structure consisting of a D-shaped thick walled spar and thin skin. The blade is provided with stepped internal taper to reduce the weight and to bring down the position of the mass centre to facilitate centrifugal reef control. The stresses are determined using an iterative technique which uses the Engineer's theory of bending and the Bredt-Batho theory for torsion of multi-cell sections. The Tsai-Wu failure criterion for composite materials is used.

The Gallerkin finite element method is used to find the natural frequencies and the modes of vibration of the blade. The periodic aerodynamic forces are decomposed into harmonics to determine the dominant excitation frequencies. The campbell diagram is constructed to check for resonance. The effect of change in hinge location, shear centre position, thickness and taper on the frequencies of vibration is studied. This is done to check for resonance due to slight change in the construction of the VGVAWT blade.

A method of modelling high capacity VGVAWT blades as composite box-beam spar has been discussed. the variational FEM is used to study the response of the structure subjected to various loading conditions. It has been shown that by a proper selection of ply orientation angle and stacking sequence , the deflections in the structure can be reduced.

# CHAPTER 1

## INTRODUCTION

Winds result from the fact that the earth's equatorial regions receive more energy than the polar regions.This sets up large scale convection currents in the atmosphere. Meteorologists estimate that about 1% of the incoming solar radiation is converted into wind energy. Since the solar energy received by the earth in just ten days has an energy content equal to the entire fossil fuel reserves of the world , this means that the wind resource is extremely large. One percent of the daily wind energy input (i.e 0.01% of the incoming solar energy) is equivalent to the present daily energy consumption of the world. As the fossil fuels are exhaustible , sufficient power will not be produced using these conventional sources of energy in the near future. Naturally one has to go in for alternative sources of energy such as solar energy, wind energy , tidal energy and biomass energy etc. It has long been realized that wind is a clean and renewable source of energy from which electrical and mechanical power may be generated.

In India The Ministry Of Non -Conventional Energy Resources has identified the wind rich areas which have the potential of producing 2000 MW of electric power. The ministry has started wind energy programmes by setting up wind turbines at various places like Tuticorin (Tamilnadu), Mandvi, Okha (Gujrat), Puri( Orissa ) etc.

## 1.1 Wind Turbines

On the basis of the axis of rotation wind turbines can be classified into two types namely

1) Horizontal Axis Wind Turbine ( HAWT )

2) Vertical Axis Wind Turbine ( VAWT )

A HAWT requires a yawing system to align it with the direction of the wind. On the other hand,a VAWT is able to extract energy from the wind independent of the wind direction and thus one can avoid the cost and complexity of a yaw orientation sub system. Further advantage of the Vertical axis configuration is that it eliminates the cyclically varying stresses which the Horizontal Axis Wind Turbine experience due to their own weight . These cyclically varying gravity stress become progressively more predominant as the overall size of the turbine increases and imposes a theoretical limit on the size of the blade that can be constructed. Although VAWT blades experience cyclically varying aerodynamic loads,the resulting stresses remain substantially constant as the turbine size is increased. A major drawback of the vertical axis wind turbines is that they do not have a good self - starting characteristic and the usual low-solidity ( less number of blades ) machines will not reliably self start. A reliable self -starting capability can be provided by increasing the rotor solidity, but the increased rotor weight and cost make this approach unattractive, except

perhaps for smaller machines. Experience over the last decade has shown that VAWTs are best suited to applications at the tens of Kilowatts level and higher,where self - start is not important. These include the commercially dominant applications, where wind turbines are used in parallel with either a grid system or some auxiliary power source, such as a diesel engine.

However, HAWT have a long history and a mature technology. Most of the wind turbines in India and other countries are of the horizontal axis type.The VAWT is a relatively new concept. Hence, data and literature available for VAWT are very small in number.

### 1.1.1 Vertical Axis Wind Turbine

There are two types of VAWT

1) Darrieus rotor

2) Straight blade type

A typical VAWT ~~consists of~~ the straight blade type consists of a cross arm, blades, tower, electric generator, control and foundation. Figure 1.1 shows the general arrangement of a straight blade type VAWT. It is seen that each blade is divided into two halves and has a airfoil cross section. When wind flows over the blade it causes aerodynamic forces ( i.e lift and drag ) to act on the blade. It is seen from fig 1.2 that the lift force does not act radially . Hence it produces a torque about the axis of rotation and causes the blade to rotate. Also it is seen that

each blade of the VAWT interacts effectively with the on coming wind over two arcs, one upstream and one downstream of the tower, when it is crossing the wind. For the remaining of each revolution, when the blade is moving approximately parallel to the wind, there is little aerodynamic interaction. The optimum solidity is therefore somewhat higher than that for a comparable HAWT.

### 1.1.2 : Centrifugal Reef Control Mechanism.

The power produced by a turbine depends on the wind speed . Most of the wind turbines are located in coastal areas, since they have a high wind power potential throughout the year. The coast lines are often prone to cyclones and hence wind turbines may experience severe loading. In addition to this, the speed of rotation of the turbine also increases. It is necessary to maintain a constant speed of rotation to produce electric power with constant frequency. To maintain the speed of rotation, the blades are made to incline inward with respect to the vertical. This process is called reefing. The wind turbines which incorporate this feature are called Variable Geometry Vertical Axis Wind Turbines (VGVAWT).

Presently, reefing is achieved by a hydraulic system which senses the over speed of the wind turbine and allows the blade to reef through a telescopic cross-arm arrangement. However the hydraulic system can fail under extreme wind conditions. Dr.K.Ghosh (1990) suggested a novel method of reef control namely

centrifugal reef control technique.

Figure 1.3 shows the general arrangement for achieving centrifugal reef control. It consists of a telescopic cross - arm which supports two half blades at its either ends. The half blades are connected to the end of the cross arm through a base plate and a hinge. The end of the the cross - arm is connected through a spring to a point on the rotor axis.Each half blade is connected through a control strut to the sleeve which houses the cross - arm.

When the wind speed increases , it causes a increase in the lift force acting on the airfoil. This results in the increase of the torque and hence in the speed of rotation .When this happens, the cross - arm moves radially outward in the sleeve and causes the blade to reef. In the reefed position, there is a change in the distribution of the lift along the length of the blade because of which the effective torque decreases. This brings back the speed of rotation to its original value.

## 1.2: Structural and Vibration Design of VGVAWT

The design of a wind turbine consists of two stages namely aerodynamic design and the structural design. The aerodynamic design deals with the selection of approximate blade profile and other aerodynamic parameters to generate the required power. These include determination of the radius of rotation of the blade ,the length of the turbine blade , the chord length of

the airfoil, twist of the section if required etc. From this, aerodynamic forces viz. lift and drag can be estimated.

The structural design commences with the determination of various aspects of the blade structure. Normally it is a two or three cell structure consisting of a thick spar( D - shaped or rectangular shaped ) and a thin outer skin. The spar is the major load carrying member. The skin is essentially used to give the blade the desired aerodynamic shape although it can carry some shear stress. The hollow space adjacent to the spar is filled with foam to maintain the shape.

At present three main materials have emerged as practical alternatives for blade construction. These are Wood / Epoxy laminates, Glass Reinforced Polyester (GRP), and steel. The use of composite materials has the advantage that for the same strength the mass of the blade is very less compared to those fabricated from conventional materials. Also composite materials make it possible to form complex shapes.

The forces acting on the blade are

1) The drag and the lift forces (Aerodynamic forces)

2) The centrifugal force

3) The gravitational force (weight)

Since the resultant aerodynamic force does not pass through the shear centre , it causes both bending and twisting of the section. For a VAWT the centrifugal force is a transverse force and therefore it also causes bending and twisting. The gravitational force acts in the axial direction for a VAWT .

The thicknesses of the spar and the skin are chosen so that the stresses are less than the critical value at failure for the chosen material. Since the aerodynamic forces are periodic in nature, it is necessary to check that resonance does not occur at the operational speed. Both, the natural frequencies and the excitation frequencies vary with the rotational speed. Hence an interference diagram needs to be constructed to check for the resonance . Due to the asymmetry of the cross-section, the coupling between the bending and torsion needs to be taken into account while finding the natural frequencies. If the spar consists of composite material , there can be additional coupling effects.

Apart from fatigue failure and resonance, the third design criterion is aeroelastic instability. Some of the important types of instabilities are flap-lag instability, pitch -lag instability, classical flutter etc. For blades made up of composite materials, instability may not be a critical design criterion as the viscoelastic nature of the matrix is expected to damp out any external excitation.

### 1.3 Literature Survey :

Stress analysis of blades made up of isotropic materials or unidirectional fabric is done using the classical theories of bending of unsymmetric cross-sections and torsion of multi cell sections. These are described in standard texts on Aircraft structures like Megson [1(b)].

Ramesh Chandra .et.al. [2] have studied the behaviour of thin walled composite beam of rectangular cross section. The response of the structure at various points was measured using an optical system, and the results were correlated with the predicted values from a simple beam analysis as well as refined Finite element analysis. They found that symmetric ply lay up results in bending - twist coupling whereas antisymmetric lay up causes extension - twist coupling.

Alan D. Stemple and S.W.Lee [3] developed a finite element formulation to take into account the warping effect of composite beams of any arbitrary cross sections. For the fibre-reinforced composite beams, results were compared to those from a shell element formulation and a good agreement was found between these two formulations.

Inderjit Chopra and E.C.Smith [4] formulated a direct analytical model for predicting the effective elastic stiffness and corresponding load deformation of composite box - beams. They investigated the the importance of three non-classical structural phenomena. It was found that torsion related warping, shear deformation and two dimensional elasticity play an important role in the structural response of composite beams.

Ramesh Chadra .et.al. [5] presented an analytical cum experimental study for the static response of composite rotor blades with elastic couplings. They expanded Vlasov theory to analyze composite two cell rotor blades. The essence of this theory is the reduction of two - dimensional stress and

displacement fields ( associates with plate / shell segments of the blade ) to one - dimensional stress and displacements identified with the beam. The effect of shear deformation and constrained warping were not taken into account. The blades were tested under unit tip bending and torsional loads and the structural response was measured by using a laser-optical system. Good correlation between the theory and experiments was observed.

Most of the literature on vibration of rotary blades pertain to horizontal axis wind turbines. William Carnegie [6] applied the variational method to derive the equations of motion of rotating cantilever blading.

Ramesh Chandra et.al. [7] conducted a theoretical and experimental study of the free vibration characteristics of a rotating thin walled composite box. The governing equations in generalized displacement were derived using the Newtonian approach. It was shown that the bending - twist coupling influences the vibration of antisymmetric box beams. Extension - twist coupling on the other hand, does not influence the flexural - torsion vibration of symmetric box beams significantly.

C.P.Filipich and M.B.Rosales [8] studied the vibration of a uniform beam, ~~free vibration coupling of bending and torsion of a uniform beam~~ rotating about an axis parallel to the beam. They presented an analytical solution for isotropic material. A numerical example was solved to bring out the influence of the coupling. They compared their results with those obtained without considering bending - torsion coupling. They concluded that

flexural - torsional coupling is unavoidable. By neglecting it some fundamental frequencies are lost and others are in error.

### 1.4 Objective of the present work :

The present work deals with the structural and dynamic design of a variable geometry vertical axis wind turbine (VGVAWT). This has been done for an actual turbine to be set up by the Ministry Of Non Conventional Energy Resources and BHEL Hyderabad, for producing 10 KW power.

Prior to this work, the entire aerodynamic design of the turbine blade has been completed. It is decided to use straight ( untwisted ) and uniform ( externally un-tapered ) blade of symmetric airfoil section - NACA 0015. The half - blade length is chosen as 3.25m and the chord - length as 0.45m. The radius of rotation of the blade is decided to be 4.5m. ~~The position of the connecting strut is decided to be 4.5m.~~ The position of the connecting strut is fixed at the mass centre of the half - blade.

The cross section consists of a D - shaped spar and thin skin to give the blade the desired aerodynamic shape. The empty space within the spar and between the spar and the skin is filled with foam to maintain the shape. The blade is given internal stepped taper along its length by varying the spar thickness. This helps to reduce the mass of the blade and hence the centrifugal force acting on the blade. Moreover, it brings down the location

of the mass - centre which is desirable for centrifugal reef control mechanism. The blade material is E- glass/epoxy as it is easily available in India. It was decided to make both the spar and the skin from unidirectional fabric (UDF) as it simplifies the stress and vibration analysis. Initially a suitable thickness is assumed for the spar and the skin. Then Engineer's theory of bending and Bredt - Batho theory of torsion for multi - cell structure is used to calculate the normal and shear stresses. The failure index is evaluated at each critical point of the most stressed sections using the Tsai - Wu theory of failure for composite materials. If the failure index does not turn out to be sufficiently small, the procedure is repeated with higher values of thickness till it is achieved. After finding the spar and the skin thickness, the shear centre and the torsion constant are obtained.

The blade is analyzed as a rotating beam fixed at one end and hinged at the point where it is connected to the strut. The coupled equations of motions are first derived from Hamiltonian principle. The Galerkin finite element method is then used for conversion of these equations into an eigen value problem. The eigen value problem is solved numerically to obtain the natural frequencies and the mode shapes. The periodic aerodynamic force is decomposed into Fourier components to find out which harmonics are dominant in the excitation. These harmonics are plotted along with the variation of the first few natural frequencies (interference diagram) to check for resonance at the operating conditions.

.In the end, behavior of composite box shaped spar under static loading is studied. It was found that without neglecting the effects of warping, the displacement and rotations could be in error by as much as 200%. Due to lack of time, stress and vibration analysis of composite box shaped beams (with warping included) could not be undertaken.

Several assumptions have been made here for the sake of simplicity. The effects of shear deformation and constrained warping ~~warping~~ have been neglected in both the structural and vibration analysis. The effect of rotary inertia and the stiffness of other structures such as cross - arm, tower etc. have not been taken into account in vibration studies. Stability studies for the blade have not been carried out.

## 1.5 Plan of the thesis

Chapter 2 deals with structural design of the blade considering it to be made of an uni - directional fabric. The engineer's theory of bending and Bredt - Batho theory of torsion of multi - cell sections is are used to determine the spar and skin thickness.The Tsai - Wu theory of failure for composite material is used to determine the failure index. The shear centre and the torsion constant of the blade section are also evaluated.

Chapter 3 deals with dynamic aspects of blade design. The Galerkin finite element method is used to obtain the natural

frequencies and the mode shapes. The aerodynamic force is decomposed into a Fourier components to determine the dominant excitation frequencies. The first few natural frequencies and the dominant excitation frequencies are plotted against the speed of rotation to get an interference diagram to check for resonance at operational speed. Parametric studies of the natural frequencies is also carried out with shear centre location, spar thickness, hinge location and taper as parameters.

In chapter 4 the spar is modelled as a ~~as a~~ composite box beam. Here the shear deformation is included but not the constrained warping. The variational finite element method is used to study the effects of anisotropic nature of composite materials on static response of the spar. This is done for various cases of ply layups and loadings. Chapter 5 gives the summary of results and conclusions and suggests scope for future work.

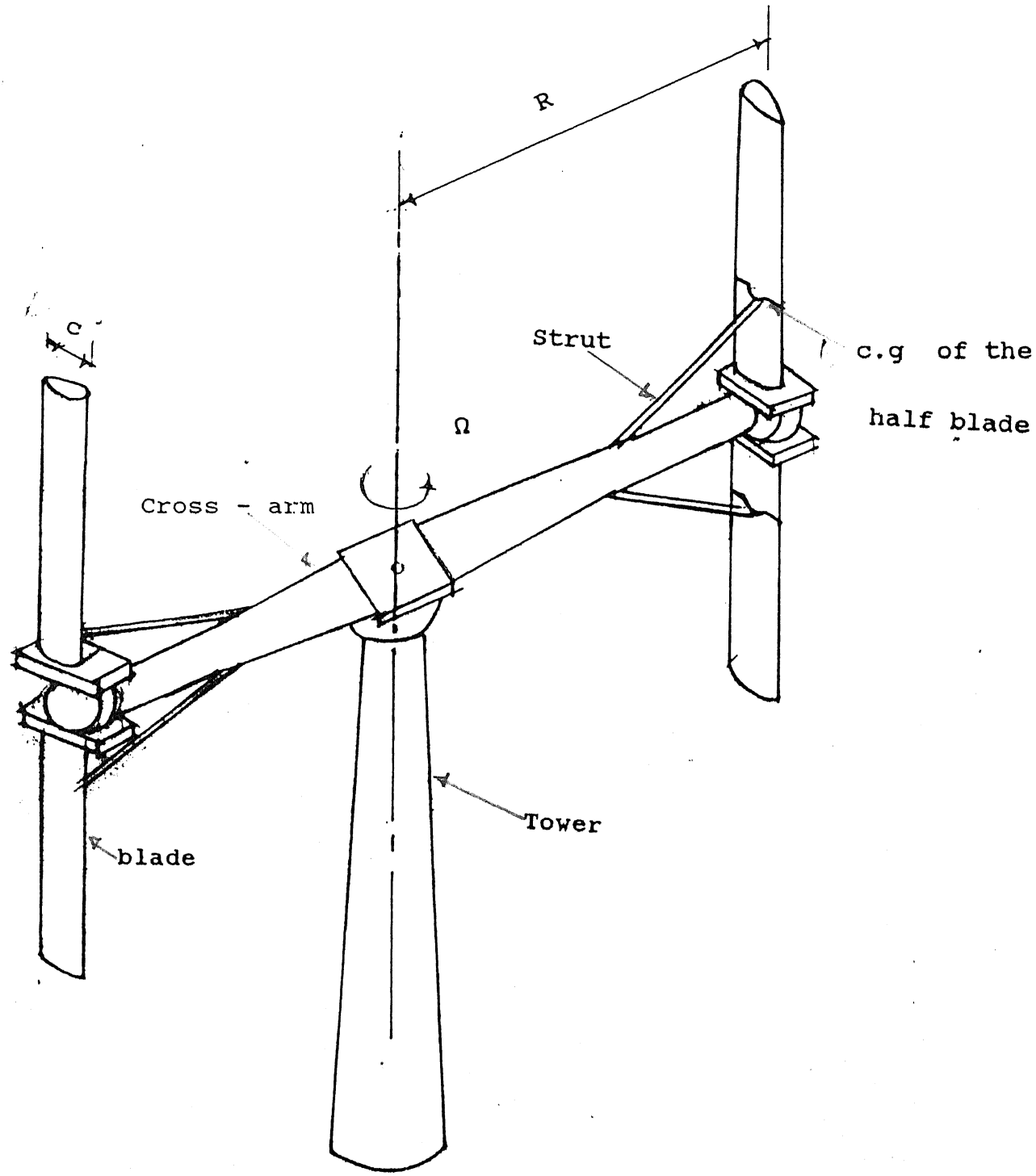


Fig 1.1 : A General Arrangement of a Typical VGAVWT

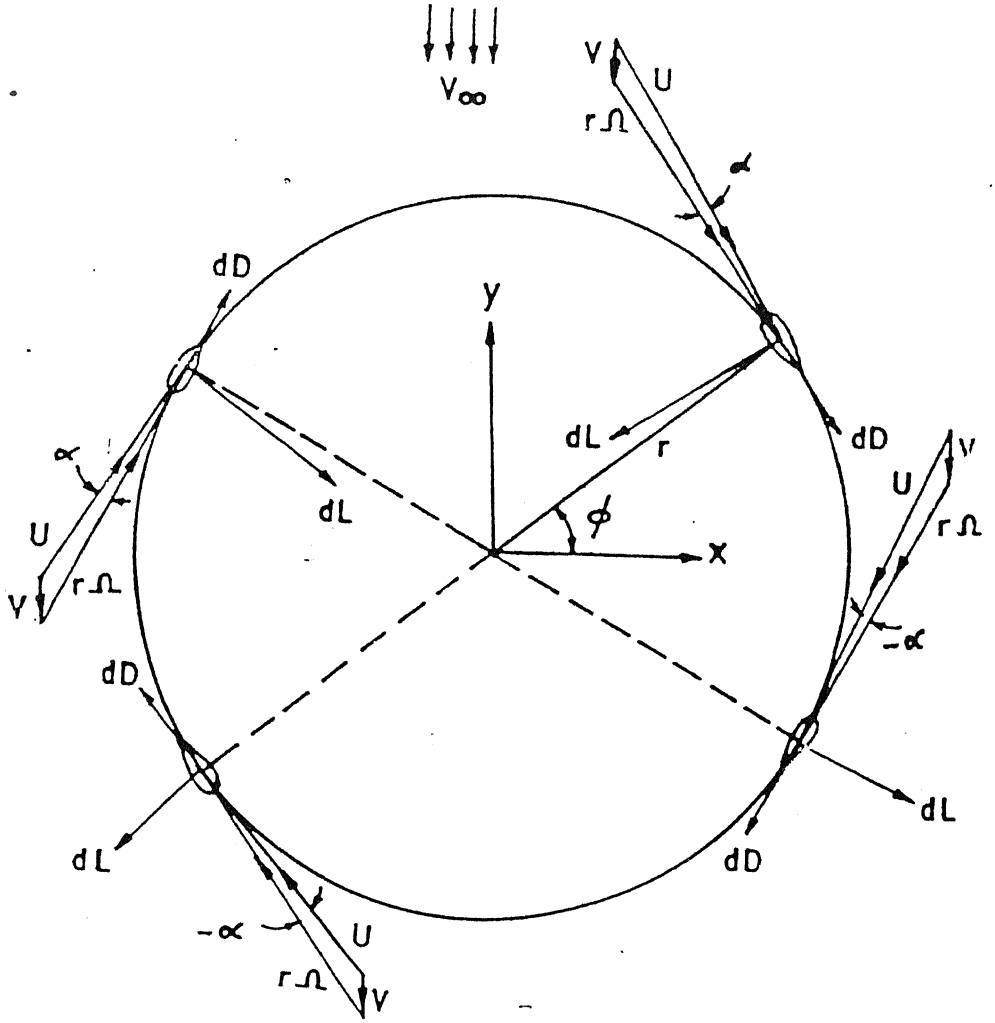


Fig 1.2 : Variation of Lift and Drag forces with azimuthal angle $\phi$

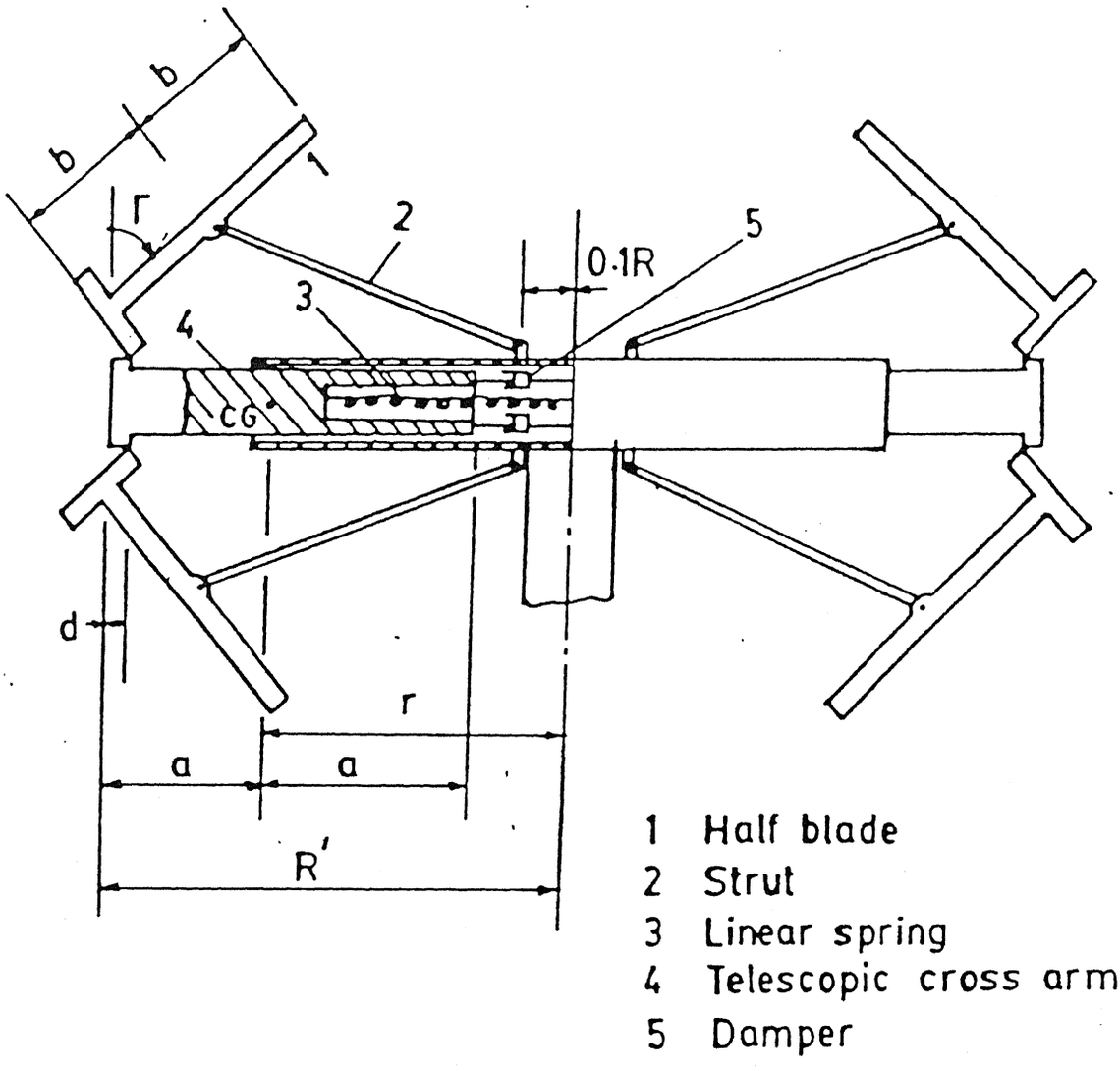


Fig 1.3 : Details of Centrifugal Reef Control Mechanism

# CHAPTER 2

# STRUCTURAL DESIGN OF VGVAWT BLADE

This chapter deals with the determination of wall thickness and other cross-sectional properties of the blade treating it as a beam. The beam is assumed fixed at one end (near the base plate) and hinged at the point where it is connected to the strut. The stresses in the blade are determined using the engineer's theory of bending ( for unsymmetric sections.) and Bredt - Batho theory of torsion for multi- cell sections. Since composite material ( unidirectional fabric ) is used in constructing the blade, Tsai - Wu failure theory is used to determine the failure index.

## 2.1 Blade structure

Based on the aerodynamic considerations, symmetric NACA - 0015 airfoil is selected for the blade cross - section. It is decided that the blade should be straight ( untwisted ) and uniform ( externally untapered ). The chord - length of the airfoil and the length of the blade are also selected on the basis of power considerations.

Generally the blade cross - section is a multi - cell structure. It consists of basically two parts the spar and the skin. The spar is the main load carrying member. The skin is the portion which forms the outer covering and gives the necessary aerodynamic shape to the structure. The skin, although normally not designed to carry any significant load, can carry some shear stresses. The hollow region adjacent to the spar can be filled with foam. This helps to to maintain the aerodynamic shape.

At present three main materials have emerged as practical alternatives for blade construction. These are Wood/Epoxy laminate, glass-reinforced polyester ( GRP ), and steel. The use of GRP has the advantage of an established technology and it is possible to form complex shapes. The blades made of GRP have high strength, low mass and low stiffness. However the tooling costs are high. Wood is used as a material for blade construction for low capacity turbines. However there is a lack of information on the long term material properties of wood and it can be affected by moisture. Steel is used for high capacity wind turbines and has advantage of low tooling costs, established technology and established long term material properties. The disadvantages of using steel include the difficulty in forming complex shapes and the high mass of the structure.

The most common forms of blade construction are shown in fig 2.1 . Figure 2.1.a shows a typical section from a wood blade. The nose is generally formed as a laminated D-spar. The trailing edge is a much lighter glass / epoxy and foam sandwich structure. Figure 2.1.b shows a structure made of GRP for low capacity turbines in which there is no seperate spar, but ribs are provided to provide stiffness. Larger GRP blades are manufactured with a filament wound spar as shown in fig 2.1.c. The trailing edge can be seperate GRP skin or can be wound as an integral part of the blade. Figure 2.1.d shows the use of a box - shaped steel spar with GRP skin for high capacity turbines.

The structure chosen for the the wind turbine blade under consideration is shown in Fig 2.2. The spar and the skin are to be

made from uni-directional fabric of E-glass / Epoxy with a fibre volume of 0.6 and density of 2000 Kg/$m^3$. The foam is polyurethene and has a density of 230 kg/$m^3$. It is assumed that the foam does not carry any loads.

The blade is provided with a taper. The purpose of the taper is to reduce the mass of the structure and to bring the position of the mass centre of the section nearer to the base of the blade. This is desirable in the centrifugal reef control mechanism which requires the strut be connected to the C.G of the blade. Uniform taper is not possible because maximum bending moment occurs at the intermediate support ( i.e at the hinge connected to the strut ). External taper is not desirable because it would change the aerodynamic loads along the length of the blade and reduce the power output. The blade structure has been provided stepped internal taper. It is seen from Fig 2.2 that the thickness of the spar varies in stages along the length of the blade while that of the skin remains constant.

We choose the origin of the co-ordinate axis at the mass centre of the combined section. The y axis is chosen along the chord of the airfoil and the z axis is perpendicular to it in the plane of the cross-section. The x axis is along the length of the blade ( Fig 2.2).

## 2.2 Loading on the blade:

The loading on the blade basically falls into three categories

1) Aerodynamic force

2) Inertial force

3) Centrifugal force

The aerodynamic force acts due to the interaction of the ambient with the airfoil. It is normally resolved along two directions: along the direction of the relative motion( drag ) and perpendicular to it ( lift ). For the purpose of stress analysis it is convenient to resolve the aerodynamic force into components along the chord( $F_t$ ) and perpendicular to it ( $F_n$ ). These are given by the expressions

$$F_n(\phi) = \frac{1}{2} \rho_\infty \left[ \frac{U}{V_\infty} \right]^2 V_\infty^2 C_n C \ ,$$

$$F_t(\phi) = \frac{1}{2} \rho_\infty \left[ \frac{U}{V_\infty} \right]^2 V_\infty^2 C_t C \ . \qquad \ldots 2.1$$

where,

$F_n$ = Normal force ,

$F_t$ = Tangential force,

$\phi$ = Azimuthal angle,

$\rho_\infty$ = Free stream air density = 1.224 $Kg/m^3$,

U = Relative velocity of the blade in the plane of the blade section,

$V_\infty$ = Free stream wind speed = 10 m/s ,

$C_n$ = Normal force coefficient,

$C_t$ = Tangential force coefficient,

C = Chord length = 0.45m .

The variation of $\left[ \frac{U}{V_\infty} \right]^2$, $C_n$ and $C_t$ as functions of azimuthal angle $\phi$ have been determined from the aerodynamic analysis [ 9 ]. From this the normal and the tangential forces can be determined. Figure 2.3 shows the variation of these forces over

one period.

The inertial and gravitational forces depend on the mass distribution of the structure. Since the structure has stepped taper, these forces vary from vary from section to section, however on each section they are uniform. These forces are not known a-priori as they depend on the thickness. For a typical value of t = 6mm the magnitude of these forces are shown in Table 2.1.

Table 2.1: Values of centrifugal and gravitational forces for a typical spar thickness.

| Section | Centrifugal force (N/m) $R\Omega^2 [(\rho A_c) + (\rho A_f)]$ | Gravitational force (N/m) $[(\rho A_c) + (\rho A_f)]g$ |
|---|---|---|
| AB | 4235.82 | 103.34 |
| BC | 3583.68 | 86.95 |
| CD | 2835.57 | 67.25 |

In the above table,

R = Radius of rotation of the blade = 4.5m,

$\Omega$ = Speed of rotation = 85 RPM ,

$A_c$ = Area of cross - section,

$A_f$ = Area of the region filled with foam .

Thus the loads on the blade are

1) Loads in the x - z plane :

Normal aerodynamic force ( $F_n$ )

Centrifugal force

2) Loads in the x - y plane

Tangential aerodynamic load ( $F_t$ )

3) Gravitational load can be assumed to act in x-y or x-z plane.

Figure 2.4.a shows the loading in the the the x - z plane while fig 2.4.b shows the loading diagram in the x - y plane. The aerodynamic loads pass through the centre of pressure of the airfoil while the centrifugal force acts at the C.G of the section. These forces cause bending and torsion. The gravitational forces cause axial stresses.

From the table 2.1 and Fig 2.3 we see that the value of the centrifugal force ( which is constant for a particular rotational speed ) far exceeds that of the cyclic aerodynamic forces. So we feel that static failure criterion with sufficiently large factor of safety can be used instead of fatigue failure criterion.

## 2.3 Engineer's theory of bending.

The basic assumption of the Engineer's theory of bending is that plane sections of the beam remain plane after deformation produced by the loading. It also assumes that the stress component $\sigma_{yy}$ and $\sigma_{zz}$ are zero. Although a composite material is used, the fibres are along the blade length. Therefore the anisotropy of the blade material does not affect the derivation.

The expression for the axial stress $\sigma_{xx}$ at a point A(y,z) of the cross -section is given by

$$\sigma_{xx} = \frac{P}{A_c} + \frac{\overline{M_z}}{I_{zz}} y + \frac{\overline{M_y}}{I_{yy}} z \qquad \ldots 2.2$$

where,

$P$ = axial force

$A_c$ = area of cross section

$$\overline{M_z} = \frac{1}{1 - \frac{I_{yz}^2}{I_{yy} I_{zz}}} \left( M_z - \frac{M_y I_{yz}}{I_{yy}} \right)$$

$$\overline{M_y} = \frac{1}{1 - \frac{I_{yz}^2}{I_{yy} I_{zz}}} \left( M_y - \frac{M_z I_{yz}}{I_{zz}} \right)$$

where,

$M_y$ = Moment about the y axis

$M_z$ = Moment about the z axis

$I_y$ and $I_z$ = Moment of inertia of the cross-section about the y and z axis respectively.

$I_{yz}$ = Product of inertia of the cross - section about the y and z axis.

In the present case, since the y axis is an axis of symmetry, $I_{yz} = 0$. So the expression for the normal stress reduces to

$$\sigma_{xx} = \frac{P}{A_c} + \frac{M_z}{I_{zz}} y + \frac{M_y}{I_{yy}} z \qquad \ldots 2.3$$

The above theory is applicable to beams possessing any form of cross-sections. However, in the analysis of thin walled sections some simplifying assumptions can be made as follows. The thickness t of a thin walled section is normally small compared to other cross- sectional dimensions so that stresses can be

assumed to be constant over the thickness. In fact stress can be calculated at the mid line of the the section wall and this represents the average value over the thickness. Furthermore, in the calculation of section properties, we neglect squares and higher powers of the thickness and assume the section profile to be represented by the mid line of its wall. Thus the expression for the moment of inertia $I_{yy}$ and $I_{zz}$ can be written as follows

$$I_{yy} = \oint_{1,2} z^2 t \, ds$$

$$I_{zz} = \oint_{1,2} y^2 t \, ds \qquad \ldots 2.4$$

where $\oint_{1,2}$ represents the integration along the mid line contour of both cell 1 and cell 2.

## 2.4 Bredt - Batho theory of torsion for multi - cell sections:

Figure 2.5 shows the blade cross section with the shear forces acting on it. It is seen that a part of the shear force passes through the centre of pressure and a part passes through the mass centre of the section. Since they do not pass through the shear centre there is a torque. The shear stresses in the section are due to both, the shear forces and the torque.

The equations for shear stress for a general case containing m sections ~~is~~ are developed. A typical multi - cell section is shown in Fig 2.6. We choose a different co-ordinate system for each cell. A point on the mid line of the top skin of cell j is chosen as the origin for the co-ordinate $s_j$, which is measured along mid line

of the cell j in the clockwise direction. The co-ordinate $n_j$ is measured in the outward direction along the normal of the mid line.

The shear stress components associated with the cell j are denoted by $\sigma_{xnj}$ and $\sigma_{xsj}$. These are considered positive when they act in the positive $n_j$ and $s_j$ directions respectively. Besides the usual assumptions of the Engineers theory of bending, we further assume that

1) The shear stress component $\sigma_{nj}$ is negligible.

2) The shear stress component $\sigma_{xsj}$ is almost uniform over the thickness of the wall.

3) The contribution of P to the stress $\sigma_{xx}$ is negligible. Since the shear stress $\sigma_{xsj}$ is assumed to be almost uniform over the thickness, it is convenient to introduce the shear flow. For a cell j, it is defined by

$$q^j = \sigma_{xsj}\, t \,. \qquad \ldots 2.5$$

To find the shear flow $q^j$, an element on the top / bottom wall is considered. It implies

$$\frac{\partial q^j}{\partial s_j} + t\,\frac{\partial \sigma_{xx}}{\partial s_j} = 0. \qquad \ldots 2.6$$

Integrating we get

$$q^j = q_o^j - \int_0^{s_j} t\,\frac{\partial \sigma_{xx}}{\partial x}\,ds \qquad \ldots 2.7$$

where $q_o^j$ is the shear flow at the origin of co-ordinate $s_j$.

Differentiating 2.3 and under the assumption 3 above we have

$$\frac{\partial \sigma_{xx}}{\partial x} = \frac{V_y\, y}{I_{zz}} + \frac{V_z\, z}{I_{yy}} . \qquad \ldots 2.8$$

Substituting 2.3.d in 2.3.c gives

$$q^j = q_o^j - \left[ \frac{V_y\, Q_y^j}{I_{zz}} + \frac{V_z\, Q_z^j}{I_{yy}} \right] \qquad \ldots 2.9$$

where

$$Q_y^j = \int_0^{s_j} y\, t\, ds$$

$$Q_z^j = \int_0^{s_j} z\, t\, ds \qquad \ldots 2.10$$

As seen from Fig 2.7, at the junction of the vertical wall with the top or bottom wall, conservation of shear flow implies the following expression for the shear flow in the vertical wall common to the cells j and j + 1

$$q^j - q^{j+1} \quad \text{in the } s_j \text{ direction.} \qquad \ldots 2.11$$

The expression 2.9 and 2.10 for the shear flow involve m unknowns $q_o^j$ (j = 1, 2, ...m ). To find these, we need m equations. We get one equation by equating the moment of the shear flows $q^j$ about the mass centre G with the torque $M_t$. The equation has the form

$$M_t = \sum_{j=1}^{m} \oint q^j p_g \, ds_j \qquad \ldots 2.12$$

where $P_g$ is the perpendicular distance of the cell element $\Delta s_j$ from G. $P_g$ is considered positive if it is in the positive $n_j$ direction.

To get m - 1 more equations, the deformation of the cross - section is considered. It is assumed that the cross - section is free to deform in the axial direction ( i.e it is free to warp ), but within their own plane they can only undergo rigid displacement. The most general rigid displacement consists of translation along y and z directions and rotation about the x axis. However there exists a point in the plane of the cross - section which remains stationary. This is called the centre of twist and it coincides with the shear centre ~~for an asymmetric cross - section~~. The displacement components can be expressed in terms of the twist $\phi$ about this point. Let $V_{sj}$ and $V_{nj}$ be the tangential and normal displacements of point a point p. We can express these as( see Fig 2.7):

1) In thetop and bottom walls

$$V_{s,j} = r_s \phi$$
$$V_{n,j} = r_n \phi \qquad \ldots 2.13.a$$

2) In thevertical wall common to the cells j-1 and j

$$V_{s,j} - V_{s,j-1} = r_s \phi$$
$$V_{n,j} - V_{n,j-1} = - r_n \phi \qquad \ldots 2.13.b$$

3) In thevertical wall common to cells j and j + 1

$$V_{s,j} - V_{s,j+1} = r_s \phi$$
$$V_{n,j} - V_{n,j+1} = - r_n \phi \qquad \ldots 2.13.c$$

The shear strain component $\varepsilon_{xnj}$ is assumed negligible. The other shear strain component $\varepsilon_{xsj}$ is given by

$$\varepsilon_{xsj} = \frac{1}{2} \left( \frac{\partial u_j}{\partial s_j} + \frac{\partial V_{s,j}}{\partial s_j} \right) \qquad \ldots 2.14$$

The strain $\varepsilon_{xsj}$ and the shear flow $q^j$ are related by

$$\varepsilon_{xsj} = \frac{q^j}{2\mu t} \qquad \ldots 2.15$$

Using the fact that $\oint du = 0$ for j th cell, we get

$$\oint \frac{q^j}{\mu t} ds_j - \int_{j-1,j} \frac{q^{j-1}}{\mu t} ds_j - \int_{j,j+1} \frac{q^{j+1}}{\mu t} = 2 \Omega_j \frac{d\phi}{dx}$$

$\ldots 2.16$

where $\oint$ represents integration over the entire cell j, $\int_{j-1,j}$ and $\int_{j,j+1}$ denote the integration over the region common to j-1 and j th cell and the region common to the j and j+1 cell respectively and

$$\Omega_j \cong \frac{1}{2} \oint r_s \, ds_j$$
$$\cong \frac{1}{2} \oint p_g \, ds_j \qquad \ldots 2.17$$

is the area enclosed by the cell j.

We get similar equations for the other cells. We note that for the first cell, the second integral does not exist, while for the last cell, the third integral does not exist.

Now we have (m + 1) equations

1) m equations of the type 2.16

2) equation 2.12

These are solved to get (m + 1) unknowns i.e $q_o^j$ ( j = 1,...m) and $\frac{d\phi}{dx}$. Once $q_o^j$ is known we use equation 2.9 to find the shear flow.For our case m = 2. Therefore there are three unknowns namely $q_o^1$, $q_o^2$ and $\frac{d\phi}{dx}$.

## 2.5 Determination of torsional constant of the cross - section:

The torsional constant is a property which is essential for the vibration analysis of the turbine blade. To determine it, consider pure torsion of a multi - cell section as shown in Fig 2.8. Here since the normal stress $\sigma_{xx}$ is zero everywhere, equation 2.6 implies that

$$\frac{\partial q^j}{\partial s_j} = 0 \qquad \ldots 2.18$$

This indicates that the shear flow associated with each cell is constant. Then equations 2.12 and 2.20 reduce to

$$M_t = 2 \sum_{j=1}^{m} q^j \Omega_j \qquad \ldots 2.19$$

$$q^{j} \oint \frac{ds_j}{t} - q^{j-1} \int_{j-1,j} \frac{ds_j}{t} - q^{j+1} \int_{j,j+1} \frac{ds_j}{t} = 2\mu\Omega_j \frac{d\phi}{dx} \quad \ldots 2.20$$

The equations 2.19 and 2.20 comprise (m+1) equations in (m+1) unknowns namely $\frac{d\phi}{dx}$ and $q^j$( j = 1, 2, ... m ). First we find $q^j$ in terms of $\frac{d\phi}{dx}$ by solving equation 2.20 . The solution can be expressed in the form

$$q^{j} = \alpha_j \mu \frac{d\phi}{dx} \quad \ldots 2.21$$

where $\alpha_j$ are the constants which depend on the shapes and thickness of the cells. Substituting 2.21 in 2.19, we get

$$M_t = \mu J \frac{d\phi}{dx} \quad \ldots 2.22$$

where

$$J = 2 \sum_{j=1}^{m} \alpha_j \Omega_j \quad \ldots 2.23$$

This is the expression for torsion constant of the thin walled closed multi - cell section.

## 2.6 Determination of shear centre:

Determination of shear centre is essential for vibration analysis of the turbine blade. It also provides an alternate method to determine the shear stress in the structure.

Earlier, in the first approach given in section 2.4, the

moment equation was used as one of the equation to determine the constants $q_o^j$. Here we use the fact that when the shear forces $V_y$ and $V_z$ act at the shear centre, there is no twisting of the cross - section ( see Fig 2.9 ). With this condition, equation 2.16 reduces to

$$\oint \frac{q^j \, ds_j}{\mu t} - \int_{j-1,j} \frac{q^{j-1} \, ds_j}{\mu t} - \int_{j+1,j} \frac{q^{j+1} ds_j}{\mu t} = 0$$

for $j = 1,2,\ldots m.$ ... 2.24

For convenience, the expression 2.7 for the shear flow $q^j$ can be decomposed as

$$q^j = q^j(V_y) + q^j(V_z) \quad \ldots 2.25$$

where,

$$q^j(V_y) = q_{oy}^j - \frac{V_y Q_y^j}{I_{zz}} \quad \ldots 2.26.a$$

$$q^j(V_z) = q_{oz}^j - \frac{V_z Q_z^j}{I_{yy}} \quad \ldots 2.26.b$$

Here $q^j(V_y)$ is the shear flow due to shear force $V_y$ and $q^j(V_z)$ is due to $V_z$. Substituting expression 2.26.a and 2.26.b seperately into 2.24, we get 2m equations in 2m unknowns in 2m unknowns $q_{oy}^j$ and $q_{oz}^j$ for ($j = 1,2, .. m$ ). By solving these equations, we find the shear flows due to $V_y$ and $V_z$ from the expression 2.26.a and 2.26.b.

To find the position of the shear centre, we equate the the moments of the shear flows $q^j(V_y)$ and $q^j(V_z)$ about the mass centre those of $V_y$ and $V_z$. This gives the following expressions for the co-ordinates of the shear centre

$$y_E = \sum_{j=1}^{m} \oint \frac{q^j (V_z) P_G \, ds_j}{V_z}$$

$$z_E = \sum_{j=1}^{m} \oint \frac{q^j (V_y) P_G \, ds_j}{V_y} \qquad \ldots 2.27$$

Note that for the section under consideration, $z_E$ should come out to be zero as y - axis is the axis of symmetry.

Once the shear centre position is determined, the shear flow due to torsion can be determined as follows. Note that the torque about the shear centre is given by

$$M_{tE} = V_{z1} ( y_p - y_E ) - V_{z2} y_E \qquad \ldots 2.28$$

where $y_p$ is the co-ordinate of the centre of pressure (Fig 2.5). Then using the theory of pure torsion of multi - cell sections described in the previous section, we get the shear flow due to $M_{tE}$ by solving equations 2.19 and 2.20 . The shear flow due to $V_y$ and $V_z$ are given by equations 2.26.a and 2.26.b. By adding these shear flows, we get the net shear flow due to $V_y$, $V_z$ and $M_{tE}$.

In this work , the shear stresses were found by two methods: by applying the method described in section 2.4 and the method mentioned in this section. The values obtained by these methods match very well. This shows that the position of the shear centre has been determined accurately.

## 2.7 Tsai - Wu failure theory

The aerodynamic forces acting on the blade are periodic in nature. Hence fatigue failure criterion should be used for determination of the wall thickness. However, reliable values for the fatigue strength of the blade material are not available. Moreover, the periodic forces are small compared to the centrifugal force which is a static force. Hence the static failure criterion has been used.

We use the Tsai-Wu failure theory [10]. In this theory, for plane stress problems, the failure index at a point is given by

$$FI = F_1 \sigma_1 + F_2 \sigma_2 + F_{11} \sigma_1^2 + F_{22} \sigma_2^2 + F_{33} \sigma_{12}^2 + 2 F_{12} \sigma_1 \sigma_2 \quad \ldots 2.29$$

where,

$$F_1 = \frac{1}{X_t} - \frac{1}{X_c}$$

$$F_2 = \frac{1}{Y_t} - \frac{1}{Y_c}$$

$$F_{11} = \frac{1}{X_t X_c}$$

$$F_{22} = \frac{1}{Y_t Y_c}$$

$$F_{33} = \frac{1}{S^2}$$

$$F_{12} = (F_{12}^*) \sqrt{F_{11} F_{12}} \quad \ldots 2.30$$

Here, $X_t$ = Ultimate tensile strength in the longitudinal (fibre) direction or direction 1.

$X_c$ = Ultimate compressive strength in the fibre direction.

$Y_t$ = Ultimate tensile strength in the transverse

direction or direction 2.

S = In plane ultimate shear strength.

$\sigma_1$, $\sigma_2$, $\sigma_{12}$ = state of stress with respect to directions 1 and 2.

The value of the coefficient $F_{12}^*$ is determined from a biaxial test. Performing such a test on a ply is not straightforward. Tsai and Hahn [10] have shown that the value of the coefficient $F_{12}^*$ lies between the limits of -1 and 1. In the absence of a measured value, $F_{12}^*$ is generally set to -0.5 without loss of accuracy.

According to this theory, failure occurs when the failure index exceeds 1. To account for uncertainties in the determination of the loads, stresses and strengths, a factor of safety n is used. Then failure is said to occur when

$$FI = \frac{1}{n} \qquad \ldots 2.31$$

For static case, n can be chosen as 3. However the aerodynamic forces are periodic in nature.. Therefore to avoid fatigue failure due to these forces, the factor of safety should be increased. Normally it is taken as three times the static value. Thus, the value of n = 10 is reasonable. then for failure , FI should be less than 0.1.

Since the blade is made of unidirectional fabric with fibres referred to along the length direction of the blade, the axes 1 and 2 of equation 2.29 coincide with the x and s axes.

## 2.8 Determination of spar/skin thickness

The spar thickness in section AB i.e $t_1$ ( Fig 2.2 ) is determined iteratively as follows. In the first iteration, some value of $t_1$ is chosen. This enables us to calculate the centrifugal and gravitational forces. The reactions at the fixed and hinged support are then determined using the procedure for statically indeterminate problem.Next, the axial force, shear forces and bending moments ( P, $V_y$, $V_z$, $M_y$, $M_z$ ) are obtained at the three critical sections E, B and C (Fig 2.4). Then the normal stress $\sigma_{xx}$ at the critical points of the three critical sections is found by applying the theory of section 2.3. Then the shear flows $q^1$ and $q^2$ and $\sigma_{xs1}$ and $\sigma_{xs2}$ are determined at the critical points of the critical sections using the theory described in section 2.4. Finally the failure index is calculated by using the Tsai - Wu theory of section 2.7. If the failure index exceeds 0.1, the next iteration is carried out by increasing the thickness. Iterations are continued till the failure index becomes less than or equal to 0.1. Once the spar/skin thicknesses are determined, the torsion constant J and the co-ordinate of the shear centre $y_E$ are calculated using the procedures of sections 2.5 and 2.6 .

A software was developed to perform the structural design. The step wise procedure used for this purpose is as follows

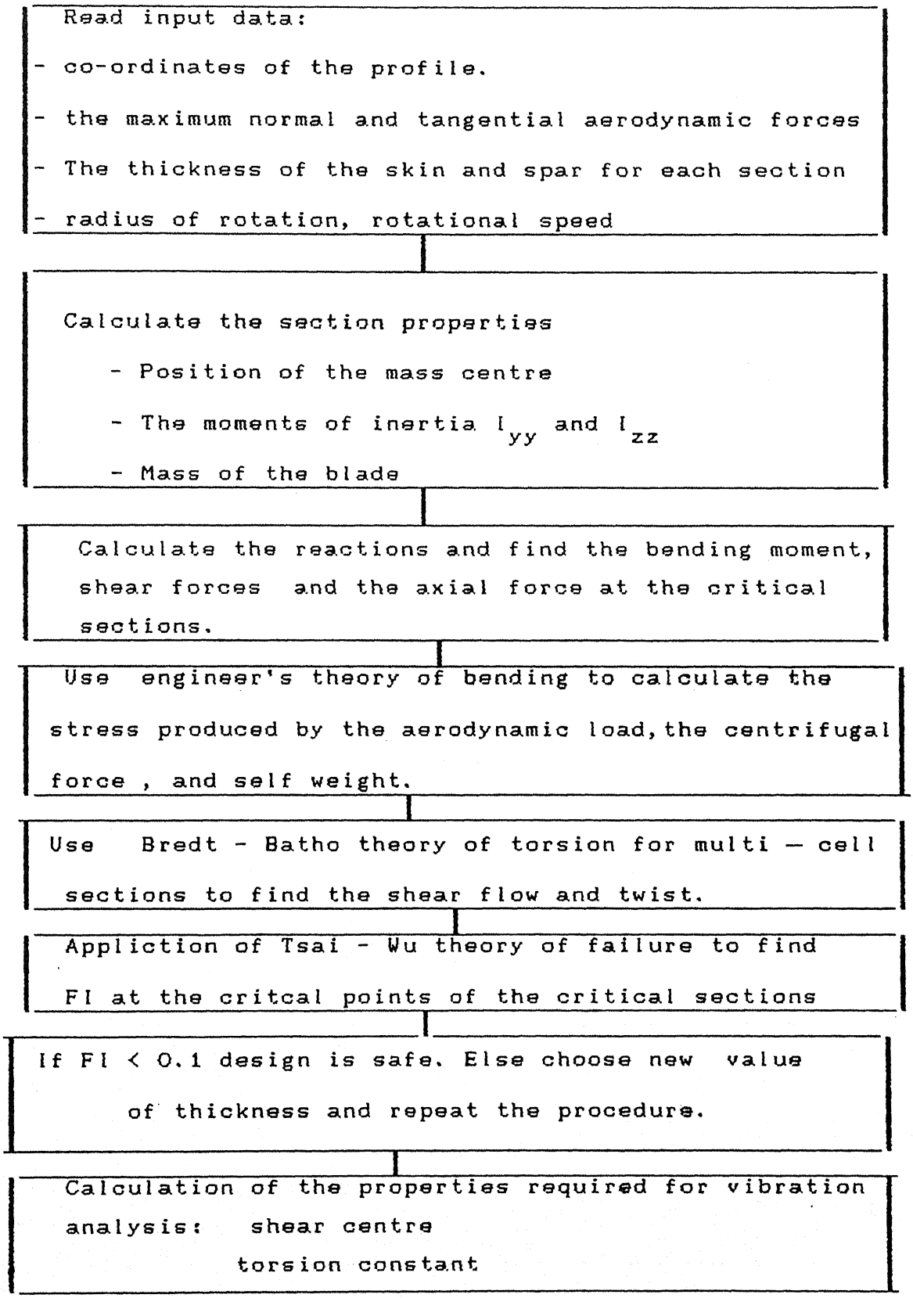
Read input data:
- co-ordinates of the profile.
- the maximum normal and tangential aerodynamic forces
- The thickness of the skin and spar for each section
- radius of rotation, rotational speed
Calculate the section properties
- Position of the mass centre
- The moments of inertia $I_{yy}$ and $I_{zz}$
- Mass of the blade
Calculate the reactions and find the bending moment, shear forces and the axial force at the critical sections.
Use engineer's theory of bending to calculate the stress produced by the aerodynamic load, the centrifugal force , and self weight.
Use Bredt - Batho theory of torsion for multi — cell sections to find the shear flow and twist.
Appliction of Tsai - Wu theory of failure to find FI at the critcal points of the critical sections
If FI < 0.1 design is safe. Else choose new value of thickness and repeat the procedure.
Calculation of the properties required for vibration analysis: shear centre
torsion constant

## 2.8 Results:

The material properties of the material used for the VGVAWT blade are given below in Table 2.2 [ 10 ].

Table 2.2: Properties of VGVAWT blade material

| Material used | E glass/ epoxy unidirectional fibre composite. |
|---|---|
| ELASTIC CONSTANTS ( Gpa ) | |
| Modulus of elasticity in fibre direction ( $E_1$ ) | 45 |
| Modulus of elasticity in the matrix direction ( $E_2$ ) | 12 |
| Modulus of Rigidity ( $\mu$ ) | 5.5 |
| STRENGTH PROPERTIES ( Mpa ) | |
| Ultimate tensile strength in fibre direction ( $X_t$ ) | 1020 |
| Ultimate compressive strength in the fibre direction ( $X_c$ ) | 620 |
| Ultimate tensile strength in the transverse direction ($Y_t$) | 40 |
| Ultimate compressive strength in the transverse direction($Y_c$) | 140 |
| In plane shear strength (S) | 70 |

Table 2.3 shows the stresses and the failure index ( FI ) at the most critical point of each of the three critical sections for various values of $t_1$.

Table 2.3: Stresses and failure index at the critical points of the VGVAWT blade.

The results are given for the following ratio of skin/spar thickness

$$\frac{t_4}{t_1} = 0.2, \quad \frac{t_2}{t_1} = 0.3, \quad \frac{t_3}{t_1} = 0.6$$

| $t_1$ (mm) | Maximum stress (Mpa) and FI | Point E spar thick. $t_1$ (mm) | Point B spar thick. $= t_2$ (mm) | Point c spar thick. $= t_3$ (mm) |
|---|---|---|---|---|
| 4 | $\sigma_{xx}$ | -72.989 | - 87.333 | -23.001 |
| | $\sigma_{xs}$ | 15.896 | 16.737 | 11.855 |
| | FI | 0.0754 | 0.0881 | 0.03439 |
| 5 | $\sigma_{xx}$ | -65.195 | -77.972 | -20.390 |
| | $\sigma_{xs}$ | 12.960 | 15.216 | 10.004 |
| | FI | 0.0594 | 0.0751 | 0.03437 |
| 6 | $\sigma_{xx}$ | -60.426 | -72.192 | -18.662 |
| | $\sigma_{xs}$ | 11.104 | 14.086 | 7.68 |
| | FI | 0.0566 | 0.0665 | 0.0183 |

At the points B and C there is a sudden change in the cross - section. This gives rise to a stress concentration at these points. There is no standard data available for estimating the

stress concentration effects for the present section. We assume the stress concentration factor to be 1.5. Now considering the effects of stress concentration, failure is said to occur when

$$FI < \frac{0.1}{1.5} \quad \text{i.e} \quad FI < 0.06666 \qquad \ldots 2.32$$

we see from the above table that this condition is satisfied at the most critical point of section B when the spar thickness $t_1$ = 6mm. For any other value of spar thickness ($t_1$) less than 6mm relation 2.32 the FI is grater than that required to prevent failure. Hence we choose the spar thickness in section AB ($t_1$) as 6mm.

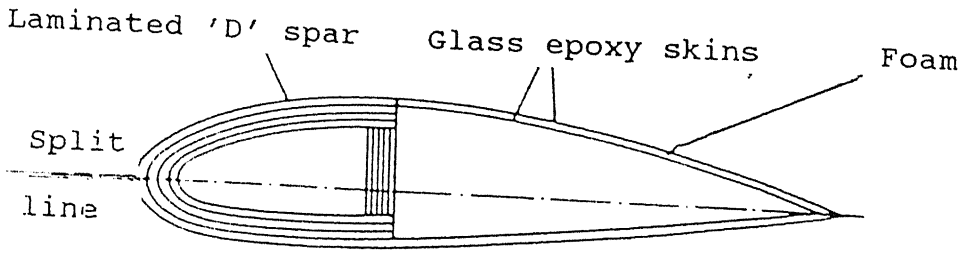


(a) Wood/epoxy blade construction

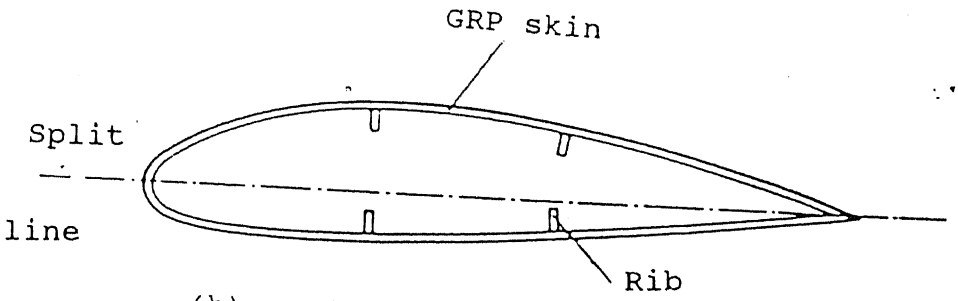


(b) GRP blade construction

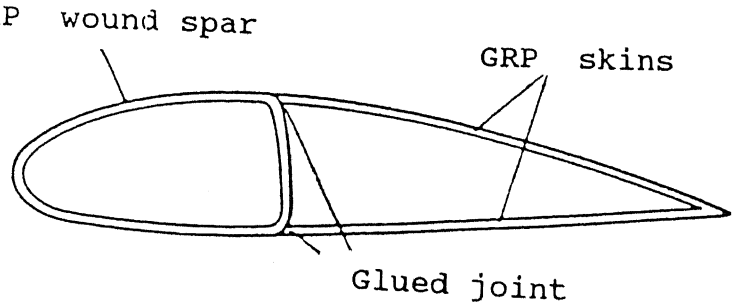


(c) Filament-wound spar blade construction

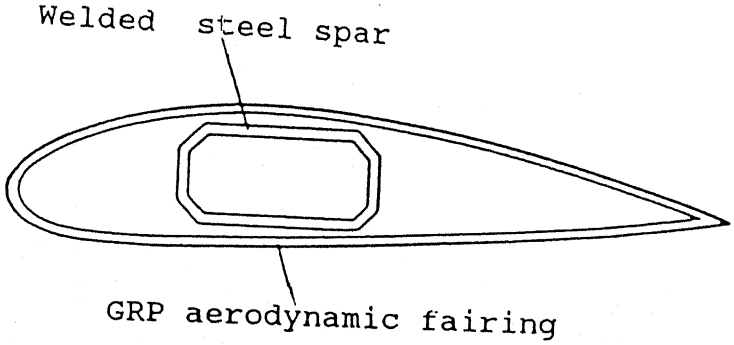


(d) Steel spar construction

Fig 2.1 : Typical Blade Constructions

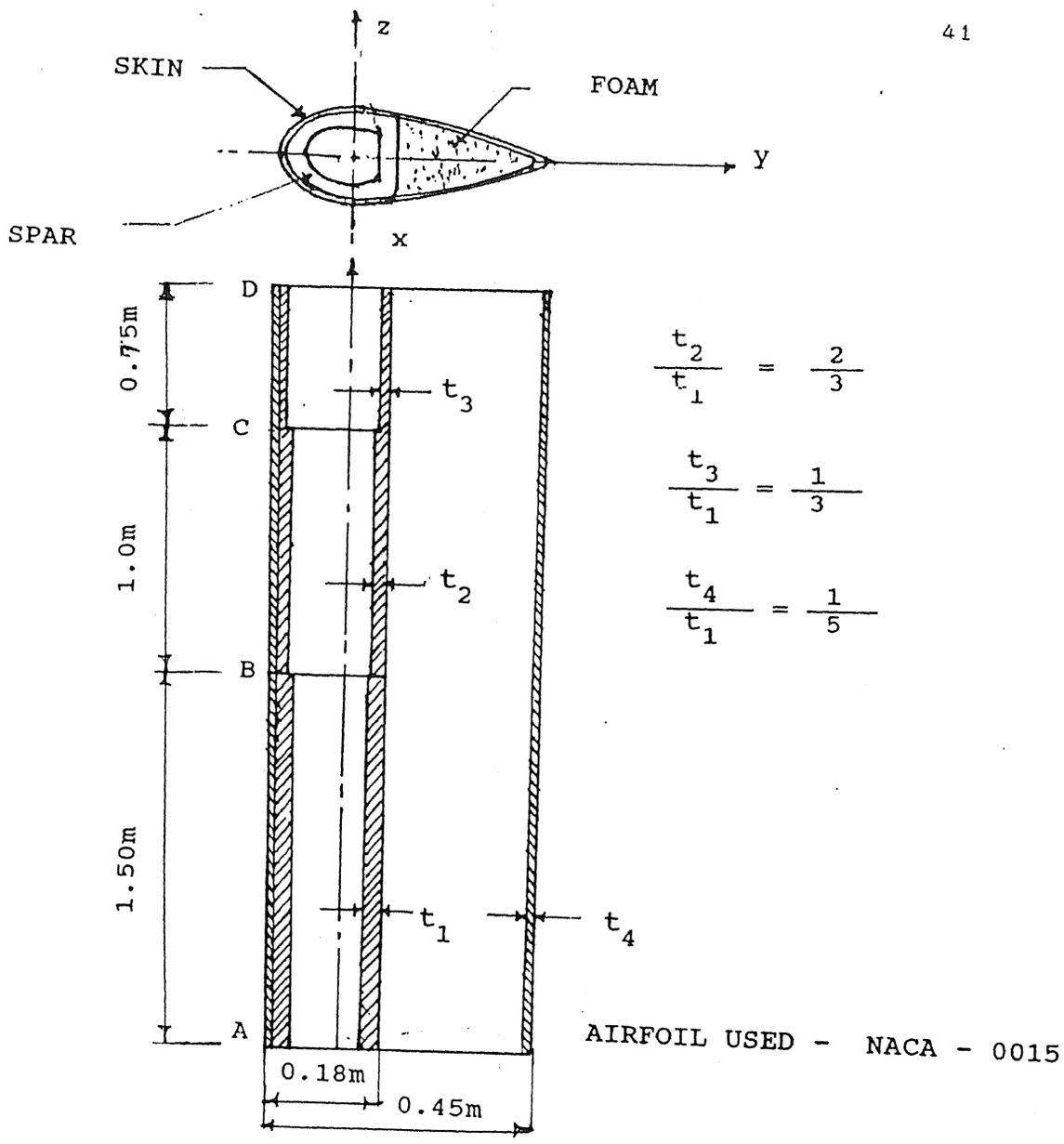


Fig 2.2 : Structural Details of the Blade

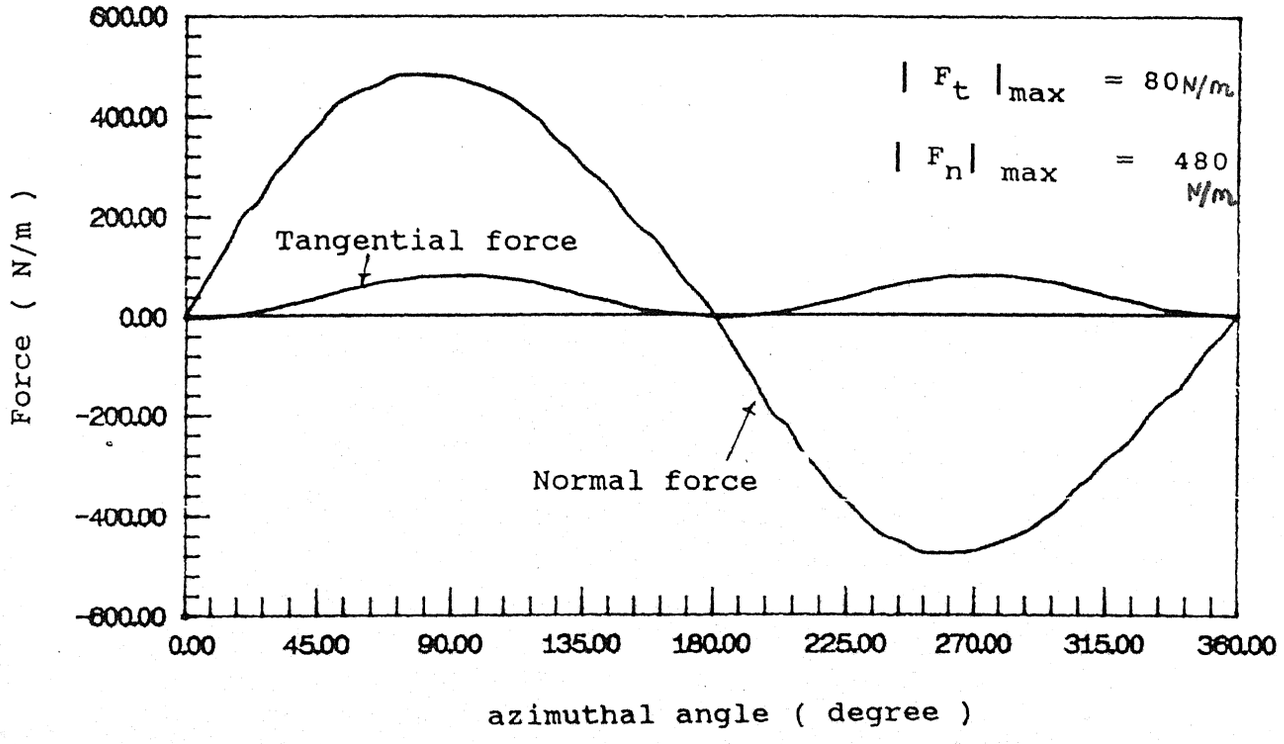

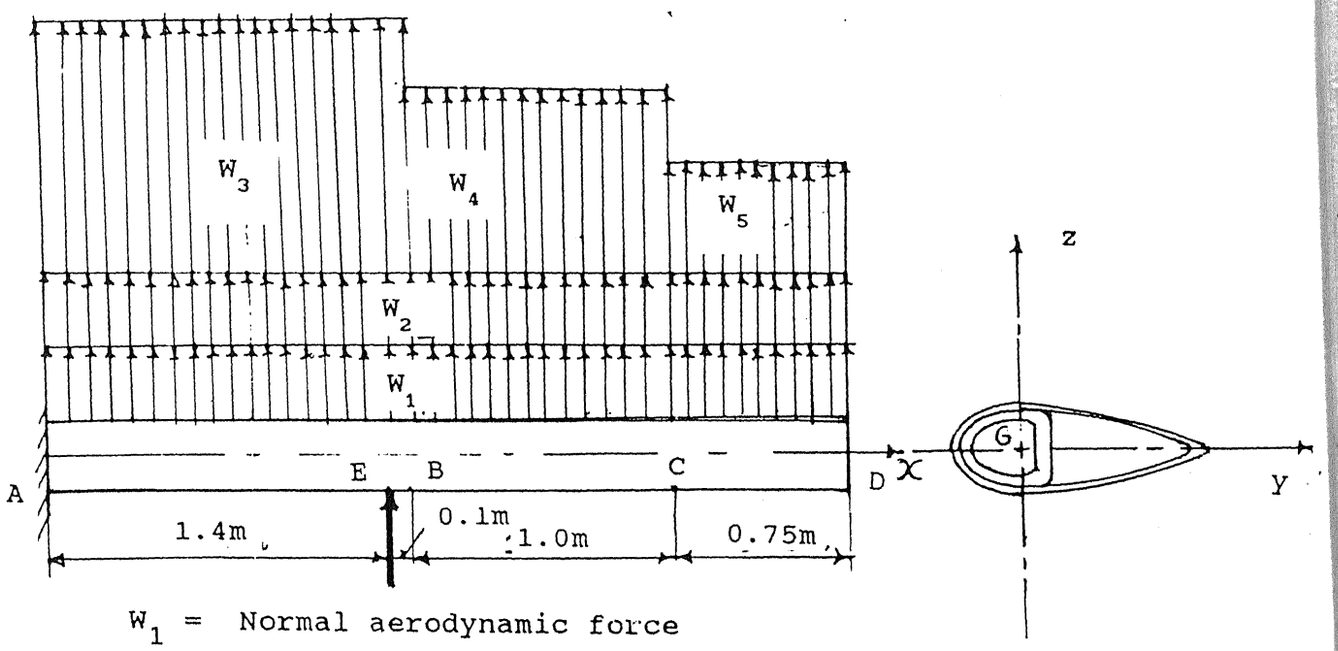


$W_1$ = Normal aerodynamic force

$W_2$ = Centrifugal force due to foam

$W_3$, $W_4$, $W_5$ = Centrifugal force due to self weight

Fig 2.4.a : Load Diagram In x - z Plane

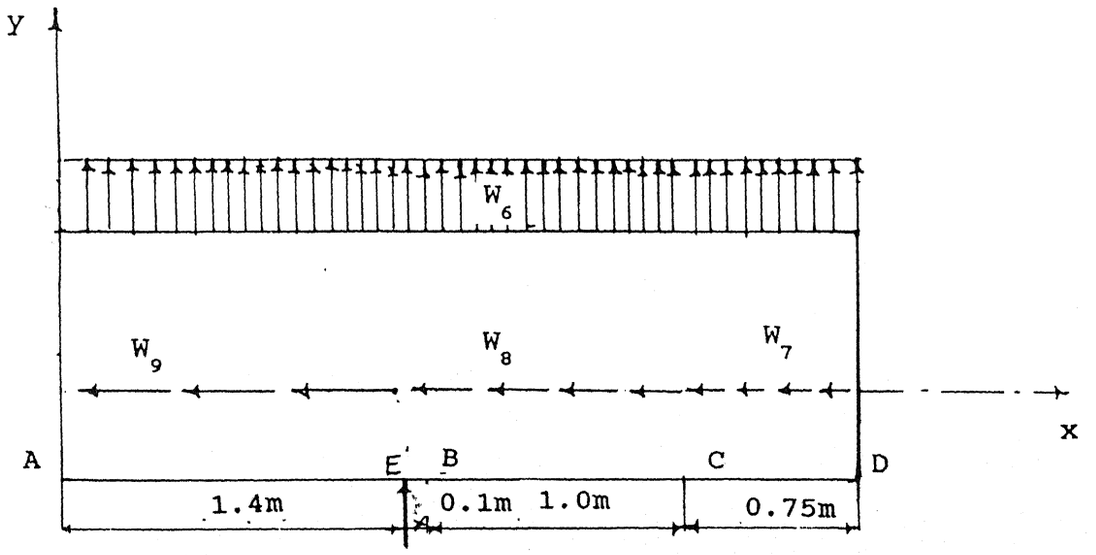


$W_6$ = Tangential aerodynamic force

$W_7$, $W_8$, $W_9$ = Gravitational force

Fig 2.4.b: Load Diagram in x - y Plane

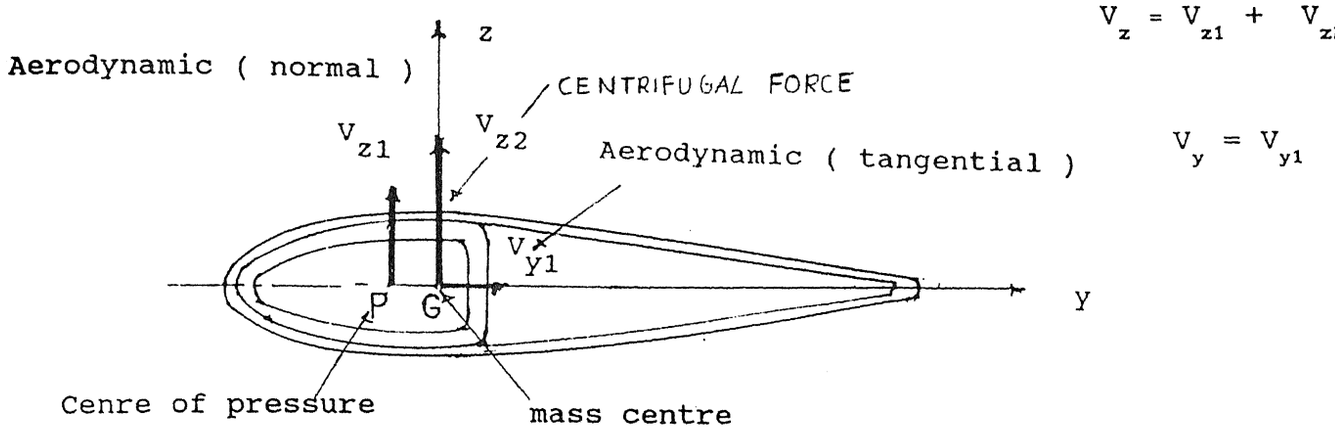


Fig 2.5: Shear Forces on the Section

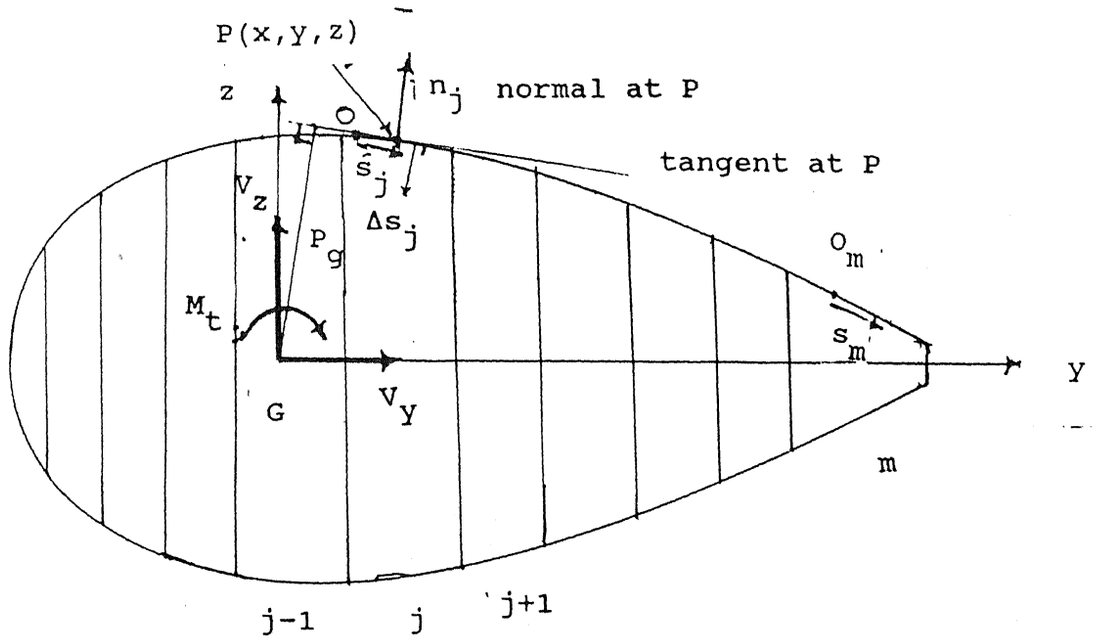


Fig 2.6: A General Multi-cell Section

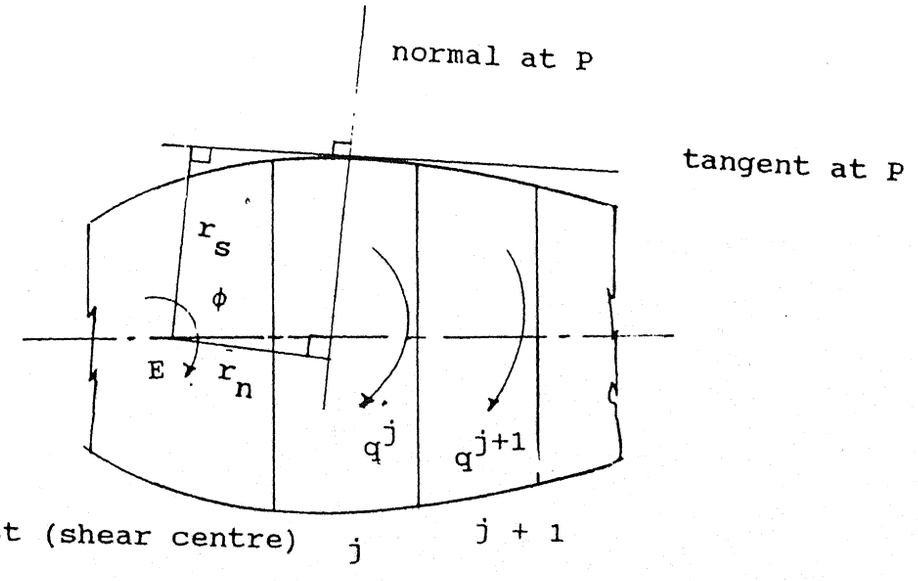


Fig 2.7 : Shear Flow in a Typical Multi-cell Section

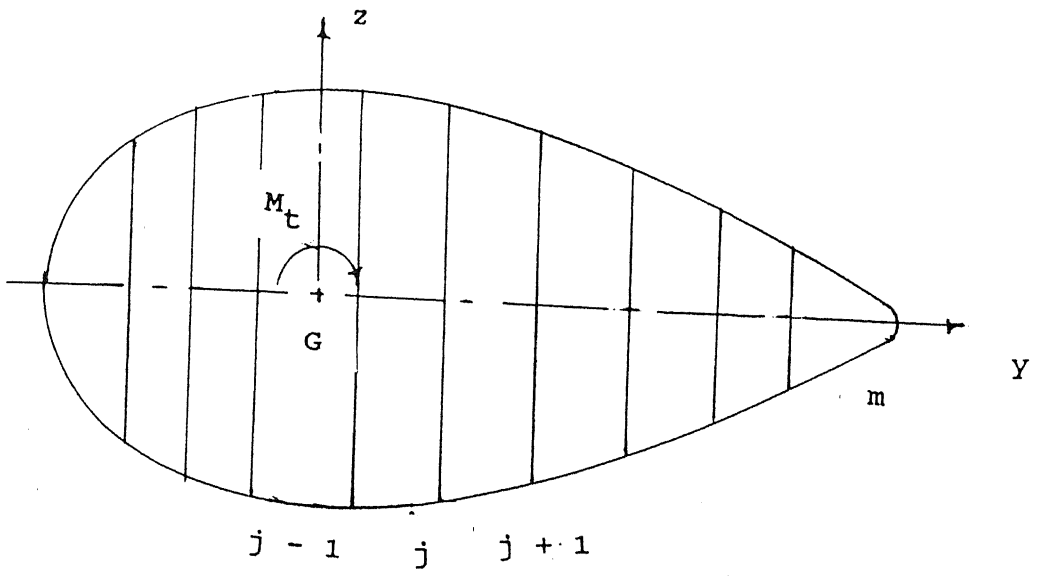


Fig 2.8 : A Multi-cell Section in Pure Torsion

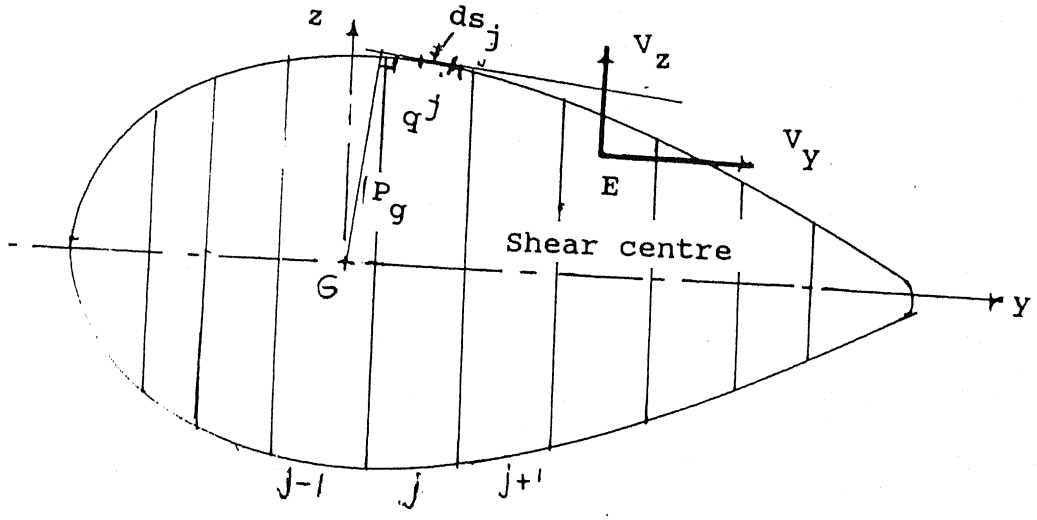


Fig 2.9 : A Multi-cell Section Subjected to shear Forces Passing Through the Shear Centre.

# CHAPTER 3
# VIBRATION ANALYSIS OF VGVAWT BLADE

This chapter deals with determination of the vibration charecteristics of the VGVAWT blade. The equations of motion governing the vibrations are developed using the Hamiltonian principle. The turbine blade is treated as a beam rotating about an axis, which is parallel to the length of the beam. The effects of shear deformation, rotary inertia and constrained warping have not been taken into account.

The finite element method is used to convert the equations of motion into a generalised matrix eigen value problem. The beam is discretized into a number of linear elements, with each node having five degrees of freedom. Natural frequencies and modes of vibration are determined by solving the eigen value problem. Parametric study is carried out to examine the effects of location of shear centre, location of hinge support, wall thickness and taper.

The periodic aerodynamic force acting on the blade is decomposed into Fourier components to determine the most dominant excitation frequencies. The variation of first few natural frequencies as well as the dominant excitation frequencies with the rotation speed is plotted as a campbell diagram to check for resonance.

## 3.1 Equations of motion for rotating beam

The equations of motion for a rotating beam of arbitrary cross - section are derived in reference [ 8 ].For the sake of completeness, this derivation has been reproduced below with

certain modifications. Figure 3.1 shows the cross - section of a beam in y-z plane where ( x, y, z ) is an inertial co-ordinate system with origin O at the trace of the rotation axis. Normally displacements are expressed with respect to a body - fixed co-ordinate system which rotates with the beam. Let ( $x_1$, $y_1$, $z_1$ ) be such a rotating system with origin at the centroid G at the beam. In this system $x_1$- axis is parallel to x - axis but not coincident. Further, ( $y_1$, $z_1$ ) are the principal inertial axes of the cross - section. Therefore $I_{y_1 z_1}$=0. Note that the co-ordinate system used in chapter 2 is identical to ( $x_1$, $y_1$, $z_1$ ). The angular velocity of the system is denoted by $\Omega$ .

Let the displacements of the particle which occupies the position P ( $x_1$, $y_1$, $z_1$ ) be ( $\bar{u}$, $\bar{v}$, $\bar{w}$) with respect to the co-ordinate system ( $x_1$, $y_1$, $z_1$). Then the co-ordinates of the displaced position P* become ( $x_1+\bar{u}$, $y_1+\bar{v}$, $w_1+\bar{w}$). For the sake of convenience the shear centre E is assumed in the third quadrant of the c-ordinate system ( $y_1$, $z_1$). Let ( $y_E$, $z_E$)be the distances between E and the centroid G parallel to the $y_1$and $z_1$respectively. To facilitate the derivation we introduce an auxiliary rotating co-ordinate system ( $x_2$, $y_2$, $z_2$). Like ( $x_1$, $y_1$, $z_1$), this also rotates with $\Omega$ but it has origin at O. The $x_2$ axis is coincident with x and the $y_2$ axis is so chosen that it is always along the line OE. Thus $y_2$- axis makes a constant ( time independent )angle $\alpha$ with the $y_1$axis. If the $y_1$axis itself can be chosen parallel to the line OE, then there is no need to introduce the auxiliary co-ordinate system. For a stationary beam under torsion, rotation of the beam cross -section takes place about the shear centre E (and not about G). Hence the eccentricity of the rotating beam with

respect to the axis of rotation is represented by the distance OE rather than OG. In our case, OG is the radius of the turbine which has been determined from aerodynamic considerations. The distance EG has been determined in chapter 2. From this the distance OE can be calculated.

From fig 3.1 the position vector $\overrightarrow{r}$ of the point $P^*$ can be expressed as the sum of four vectors $\overrightarrow{OE}$, $\overrightarrow{EG}$, $\overrightarrow{GP}$ and $\overrightarrow{PP^*}$. In the component form, it can be expressed as

$$\overrightarrow{r} = \bar{u}\,\hat{i} + r_y\,\hat{j} + r_z\,\hat{k} \qquad \ldots 3.1$$

where,

$$r_y = V \cos(\alpha + \Omega t) - W \sin(\alpha + \Omega t) + e \cos(\Omega t),$$
$$r_z = V \sin(\alpha + \Omega t) + W \cos(\alpha + \Omega t) + e \sin(\Omega t),$$
$$V = y_E + y_1 + \bar{v},$$
$$W = z_E + z_1 + \bar{w}. \qquad \ldots 3.2$$

The velocity of the particle P is given by

$$\text{vel} = \dot{\overrightarrow{r}} = \dot{\bar{u}}\,\hat{i} + \dot{r}_y\,\hat{j} + \dot{r}_z\,\hat{k} \qquad \ldots 3.3$$

where the superscript $\dot{}$ indicates the partial derivative with respect to time. Now, the kinetic energy of the beam is given by

$$K = \frac{1}{2}\rho \int_{vol} \left| \overrightarrow{vel} \right|^2 dA\, dx \qquad \ldots 3.4$$

where $\rho$ is the density of the beam material. Differentiating the expression 3.1 with time and substituting it in equation 3.4, we get,

$$K = \int_0^L \int_A \frac{1}{2} \rho \{ \dot{\bar{u}}^2 + \dot{\bar{v}}^2 + \dot{\bar{w}}^2 + \Omega [ V^2 + W^2 + e^2 + 2e ( V \cos \alpha - W \sin \alpha ) ] + 2\Omega [ -\dot{V} W + \dot{W} V + e ( \dot{V} \sin \alpha + \dot{W} \cos \alpha ) ] \} \, dA \, dx \quad \ldots 3.5$$

where A is the area of cross - section and L is the length of the beam.

Before writing the expression for potential or strain energy, we make some simplifying assumptions about the deformation pattern. These are the same as those made in chapter 2. Thus we use engineer's theory of bending and Bredt - Batho theory of torsion to get the expressions for bending and torsion deformation and stresses. Note that while doing so, we are neglecting the effect of shear forces on bending deformation. Further we assume that the effect of constrained warping on axial stress is small . Then, the expressions for the displacements, after neglecting the axial deformation, become

$$\begin{aligned} \bar{u} &= -v' y_1 - w' z_1, \\ \bar{v} &= v ( x, t ) - \theta ( x, t ) ( z_E + z_1 ), \\ \bar{w} &= w ( x, t ) + \theta ( x, t ) ( y_E + y_1 ). \end{aligned} \quad \ldots 3.6$$

Here, v and w are the bending deflections i.e. the translations of the cross - section along $y_1$ and $z_1$ axis respectively and $\theta$ is the rotation of the cross - section about the shear centre. Further the superscript ' represents the partial derivative with respect to

x. The expression for the non-zero stresses are given by

$$\sigma_{xx} = - E ( v'' y_1 + w'' z_1 ),$$
$$\sigma_{xsj} = \alpha_j \; t \mu \theta' \quad ( j = 1, 2 ) \qquad \ldots 3.7$$

where E and $\mu$ are the elastic properties of the blade material, t is the wall thickness and $\alpha_j$, which are constants, are the solution of the equation 2.19 and 2.20 of chapter 2. The superscript j refers to the cell number and s is the co-ordinate along the mid line of the wall.

Now, the expression for the strain energy of the beam can be written as

$$U = \frac{1}{2} \int_0^L \left( \int_A \left[ \frac{1}{2E} \sigma_{xx}^2 + \frac{1}{2\mu} \sigma_{xsj}^2 \right] dA \right) dx \qquad \ldots 3.8$$

Carrying out the integration over A, this expression reduces to

$$U = \frac{1}{2} \int_0^L \left[ E I_{z_1 z_1} (v'')^2 + E I_{y_1 y_1} (w'')^2 + \mu J (\theta')^2 \right] dx \qquad \ldots 3.9$$

Where, $I_{y_1 y_1}$ and $I_{z_1 z_1}$ are the moments of inertia about $y_1$ and $z_1$ axes respectively and J is the torsion constant.

By Hamilton's principle, we get

$$\delta \int_{t_1}^{t_2} ( U - K ) \, dt = 0 \qquad \ldots 3.10$$

Where,

$$\delta v = \delta w = \delta v' = \delta w' = \delta \theta = 0 \quad \text{at } t = t_1, \; t_2 \qquad \ldots 3.11$$

After integration by parts with t (once) and with x (twice) and using the conditions at $t_1$ and $t_2$ as well as the we get the following equations for the bending - torsional vibrations of the beam

$$EI_{z_1z_1}(v'''') + \rho A(\ddot{v}) - \rho I_{z_1z_1}(\ddot{v}'') - \rho A\,\Omega^2(v)$$

$$-2\rho A\,\Omega(\dot{w}) - \rho A\, z_E(\ddot{\theta}) - 2\rho A\,\Omega y_E(\dot{\theta}) + \rho A\,\Omega^2 z_E(\theta) = \rho A\Omega^2 f,$$

$$EI_{y_1y_1}(w'''') + \rho A(\ddot{w}) - \rho I_{y_1y_1}(\ddot{w}'') - \rho A\,\Omega^2(w)$$

$$+ 2\rho A\,\Omega(\dot{v}) + \rho A\, y_E(\ddot{\theta}) - 2\rho A\,\Omega z_E(\dot{\theta}) - \rho A\,\Omega^2 y_E(\theta) = \rho A\Omega^2 g,$$

$$\mu J(\theta'') - \rho I_p(\ddot{\theta}) + \rho I_p\,\Omega^2(\theta) + \rho A(z_E\,\dot{v}' - y_E\,\dot{w}')$$

$$- \rho A\,\Omega^2(z_E\,v - y_E\,w) - 2\rho A\,\Omega(z_E\,\dot{w} + y_E\,\dot{v}) = \rho A\,\Omega^2 eh\,. \qquad \ldots\ 3.12$$

In the above equation

$$f = y_E + e\cos\alpha\,,\quad g = z_E - e\sin\alpha\,,\quad h = z_E\cos\alpha + y_E\sin\alpha$$

and

$$I_p = I_{y_1y_1} + I_{z_1z_1} + A(y_E^2 + z_E^2)$$

is the polar moment of inertia referred to the shear centre. The boundary conditions obtained are as follows:

$$[\,v''' - (\rho/E)\,\ddot{v}'\,]\,\delta v\,\Big|_0^L = 0, \qquad [\,v''\,\delta v'\,]\,\Big|_0^L = 0$$

$$[\,w''' - (\rho/E)\,\ddot{w}'\,]\,\delta w\,\Big|_0^L = 0, \qquad [\,w''\,\delta w'\,]\,\Big|_0^L = 0$$

$$[\,\theta'\,\delta\theta'\,]\,\Big|_0^L = 0 \qquad \ldots\ 3.13$$

For the case of the turbine blade under consideration, $y_1$- axis is an axis of symmetry. Hence $z_E = 0$. Also due to its small influence, rotary inertia terms can be neglected. In other words, terms containing the cross derivatives of fourth order can be discarded. When this is done, we get the following equations

$$EI_{z_1 z_1} (v'''') + \rho A (\ddot{v}) - \rho A \Omega^2 (v) - 2 \rho A \Omega (\dot{w}) - 2 \rho A \Omega z_E (\dot{\theta}) = \rho A \Omega^2 f,$$

$$EI_{y_1 y_1} (w'''') + \rho A (\ddot{w}) - \rho A \Omega^2 (w) + 2 \rho A \Omega (\dot{v}) + \rho A y_E (\ddot{\theta} - \Omega^2 \theta) = \rho A \Omega^2 g,$$

$$\mu J (\theta'') - \rho I_p (\ddot{\theta}) + \rho I_p \Omega^2 (\theta) + \rho A y_E (-\dot{w} + 2 \Omega \dot{v} + \Omega^2 w) = \rho A \Omega^2 eh \quad \ldots 3.14$$

The boundary conditions for these differential equations are obtained by deleting the second term from the first and the third condition of 3.13 as these are the rotary inertia terms.

### 3.2 Formulation of the eigen value problem

We can use the method of seperation of variables to solve the system of equations 3.14. Let the solution be of the form

$$v = P(x)p(t) + v_o(x)$$

$$w = Q(x)q(t) + w_o(x)$$

$$\theta = R(x)r(t) + \theta_o(x) \qquad \ldots 3.15$$

where the functions $v_o$ , $w_o$ and $\theta_o$ represent the solution of the time - independent inhomogeneous part. The boundary conditions for $v_o$, $w_o$ and $\theta_o$ can be obtained from equations 3.13.

The equations governing the homogeneous part of the solution ( P(x)p(t) ...etc ) can be obtained by substituting 3.15 into 3.14 and by dividing by p(t), q(t) and r(t). We get the following system of equations,

$$EI_{z_1z_1}P'''' + \frac{\rho AP\dot{p}^{\cdot}}{p} - \rho A\,\Omega^2 P - \frac{2\rho A\Omega Q\dot{q}}{p} - \frac{2\rho A\Omega y_E R\dot{r}}{p} = 0 ,$$

$$EI_{y_1y_1}Q'''' + \frac{\rho AQ\dot{q}^{\cdot}}{q} - \rho A\Omega^2 Q + \frac{2\rho A\Omega P\dot{p}}{q} + \frac{\rho Ay_E R\dot{r}^{\cdot}}{q} - \frac{\rho A\Omega^2 y_E Rr}{q} = 0,$$

$$\mu JR'' - \frac{\rho I_p R\dot{r}^{\cdot}}{r} + \rho\Omega^2 I_p R - \frac{\rho Ay_E Q\dot{q}^{\cdot}}{r} + \frac{\rho A\Omega^2 y_E Qq}{r} - \frac{2\rho A\Omega y_E P\dot{p}}{r} = 0.$$

... 3.16

Since the free motion should be harmonic, p(t),q(t) and r(t) should satisfy the following relations.

$$\dot{p}^{\cdot} = -\phi^2 p , \qquad \dot{q}^{\cdot} = -\beta^2 q, \qquad \dot{r}^{\cdot} = -\eta^2 r \qquad \ldots 3.17$$

where $\phi$, $\beta$ and $\eta$ are real constants. In order to satisfy the

equations 3.16, the following relations must hold

$$\phi^2 = \beta^2 = \eta^2,$$

$$p = \dot{q} \qquad q = r \ . \qquad \ldots 3.18$$

We define the following terms

$$a^2 = \frac{\rho A}{E I_{z_1 z_1}} \ , \qquad c^2 = \frac{\rho A}{\mu J} \ ,$$

$$b^2 = \frac{\rho A}{E I_{y_1 y_1}} \ , \qquad d^2 = \frac{\rho I_p}{\mu J} \ ,$$

$$\lambda^2 = \phi^2 = \beta^2 = \eta^2. \qquad \ldots 3.19$$

By using 3.18 and 3.19 the system of equations 3.16 can be written as,

$$P'''' - a^2( \lambda^2 + \Omega^2 )P - 2a^2\Omega Q - 2a^2\Omega y_E R = 0 \ ,$$

$$Q'''' - b^2( \lambda^2 + \Omega^2 )Q - 2b^2\lambda^2\Omega P - b^2( \lambda^2 + \Omega^2 )y_E R = 0,$$

$$R'' + d^2 ( \lambda^2 + \Omega^2 ) R + c^2 y_E ( \lambda^2 + \Omega^2 )Q + 2c^2 y_E \lambda^2\Omega P = 0$$

$$\ldots 3.20$$

These equations show that, when the cross - section has both the axes of symmetry, the coupling is only between the two bending modes ( flap-wise and edge-wise ) and it is caused by the

rotational speed Ω. On the other hand, when Ω = 0 and the cross - section is completely unsymmetric, there is coupling between two bending modes as well as between each bending mode and torsion. The coupling between two ~~two~~ bending modes can be eliminated by choosing principal axes of inertia ( equation 3.12 ). Additionally if there is one axis of symmetry ( say $y_1$ ), then coupling between the bending about the perpendicular axis ( i.e $z_1$ ) and torsion also can be eliminated ( equation 3.20 ). When both Ω and asymmetry are present, there is one additional coupling term involving each bending mode and torsion. The equations 3.20 can be written in the matrix form as

$$[ A ]\{ X'''' \} + [ B ]\{ X'' \} + [ C ]\{ X \} - \lambda^2 [ D ]\{ X \} = \{0\} \quad \ldots 3.21$$

where,

$$[ X^T ] = [ P \quad Q \quad R ]$$

$$A = \begin{bmatrix} 1 & 0 & 0 \\ 0 & 1 & 0 \\ 0 & 0 & 0 \end{bmatrix}, \qquad B = \begin{bmatrix} 0 & 0 & 0 \\ 0 & 0 & 0 \\ 0 & 0 & 1 \end{bmatrix},$$

$$[ C ] = \begin{bmatrix} -a^2\Omega^2 & -2a^2\Omega & -2a^2\Omega y_E \\ 0 & -b^2\Omega^2 & -b^2\Omega^2 y_E \\ 0 & o^2\Omega^2 y_E & d^2\Omega^2 \end{bmatrix},$$

$$[\,D\,] = \begin{bmatrix} a^2 & 0 & 0 \\ 2b^2\Omega & b^2 & b^2 y_E \\ -2c^2 y_E \Omega & -c^2 y_E & -d^2 \end{bmatrix} . \qquad \ldots 3.22$$

The boundary conditions for P, Q and R can be obtained from equations 3.13 as follows

$$\left( P''' \; \delta P \right) \Big|_0^L = 0 , \qquad \left( P'' \; \delta P' \right) \Big|_0^L = 0$$

$$\left( Q''' \; \delta Q \right) \Big|_0^L = 0, \qquad \left( Q'' \; \delta Q' \right) \Big|_0^L = 0$$

$$\left( R' \; \delta R \right) \Big|_0^L = 0, \qquad \ldots 3.23$$

### 3.3 Finite element formulation.

As closed form solution of the system of equations 3.22 is difficult to obtain, one has to apply one of the approximate numerical methods such as Galerkin, Collocation, FDM, FEM etc to get the approximate solution. Since the results obtain by FEM converge to the exact solution with the refinement of the mesh, FEM is utilized to solve the system of equations.

The beam is descretized into finite number of two noded elements ( Fig 3.2.a). There are five degrees of freedom at each node. Over a typical element shown in Fig 3.2.b, { X } is approximated as,

$$\{ X^{e} \}^{T} = [ S ] \{ X^{ne} \}^{T} \qquad \ldots 3.24$$

where,

$$[ S ] = \begin{bmatrix} N_1 & N_2 & 0 & 0 & 0 & N_3 & N_4 & 0 & 0 & 0 \\ 0 & 0 & N_1 & N_2 & 0 & 0 & 0 & N_3 & N_4 & 0 \\ 0 & 0 & 0 & 0 & M_1 & 0 & 0 & 0 & 0 & M_1 \end{bmatrix},$$

and

$$\{ X^{ne} \}^{T} = \begin{bmatrix} P_1 & P_1' & Q_1 & Q_1' & R_1 & P_2 & P_2' & Q_2 & Q_2' & R_2 \end{bmatrix}$$

$$\ldots 3.25$$

Here $N_i$ ( i=1, to 4) and $M_i$ (i =1,2)are the shape functions of the local co-ordinate $\xi$. For the $e^{th}$ element the relation between $\xi$ and the global co-ordinate x is given by( Fig 3.2.b )

$$\xi = \frac{( x - x_c )}{L_e} \qquad \ldots 3.26$$

where,

$$L_e = \frac{( x_{e+1} - x_e )}{2}$$

$$x_c = \frac{( x_{e+1} + x_e )}{2} \qquad \ldots 3.27$$

The expressions for $N_i$'s and $M_i$'s which satisfy the convergence

criteria are

$$N_1 = \frac{1}{4}\,(\,2 - 3\xi + \xi^3\,)$$

$$N_2 = \frac{L_e}{4}\,(\,1 - \xi - \xi^2 + \xi^3\,)$$

$$N_3 = \frac{1}{4}\,(\,2 + 3\xi - \xi^3\,)$$

$$N_4 = \frac{L_e}{4}\,(\,-1 - \xi + \xi^2 + \xi^3\,)$$

$$M_1 = \frac{1}{2}\,(\,1 - \xi\,)$$

$$M_2 = \frac{1}{2}\,(\,1 + \xi\,) \qquad \ldots 3.28$$

Substituting approximation 3.24 in equation 3..21, we get the following residue for a typical element

$$\{\,\varepsilon^e\,\} = \{\,[\,A\,][\,S''''\,] + [\,B\,][\,S''\,] + [\,C\,][\,S\,]\,\}\{\,X^{ne}\,\} - \lambda^2[\,D\,][\,S\,]\{\,X^{ne}\,\} \qquad \ldots 3.29$$

Where, $\{\,\varepsilon^e\,\}$ is a non-zero residue vector. To minimise the residue, we use the galerkin method. Then we set

$$\int_{x_e}^{x_{e+1}} [\,S\,]^T\,\varepsilon^e\,dx = 0 \qquad \ldots 3.30$$

After performing the integration by parts we get the following equations

$$[\,K^e\,]\{\,X^{ne}\,\} - \omega\,[\,M^e\,]\{\,X^{ne}\,\} = \{\,R^e\,\} \qquad \ldots 3.31$$

where,

$\omega = \lambda^2$ is the eigen value,

$[\,K^e\,]$ is the element stiffness matrix,

$[\,M^e\,]$ is the element mass matrix,

and $\{ R^e \}$ is the element force vector.

The expressions for these are as follows :

$$[ K^e ] = \int_{x_e}^{x_{e+1}} \{ [ S^T ]'' [ A ] [ S ]'' - [ S^T ]' [ B ] [ S ]' + [ S^T ] [ C ] [ S ] \} dx \quad \ldots 3.32$$

$$[ M^e ] = \int_{x_e}^{x_{e+1}} \{ [ S^T ] [ D ] [ S ] \} dx \quad \ldots 3.33$$

$$[ R^e ] = \left| \{ [ S^T ]' [ A ] [ S ]'' - [ S^T ] [ A ] [ S ]''' - [ S^T ] [ B ] [ S' ] \} \{ X^{ne} \} \right|_{x_e}^{x_{e+1}} \quad \ldots 3.34$$

To evaluate the element stiffness and mass matrices, we change the variable from the global co-ordinate x to the local co-ordinate $\xi$ using equation 3.26. We see that

$$dx = L_e \, d\xi$$

$$\frac{d}{dx} = \frac{1}{L_e} \frac{d}{d\xi} \quad \text{and} \quad \frac{d^2}{dx^2} = \frac{1}{L_e^2} \frac{d^2}{d\xi^2} \quad \ldots 3.35$$

and the limits of integration change from $x_e$ and $x_{e+1}$ to -1 and 1 respectively. Thus a typical integral transforms to

$$\int_{x_e}^{x_{e+1}} f(x) \, dx = L_{e-1} \int_{-1}^{1} f( x_c + L_e \xi ) \, d\xi \quad \ldots 3.36$$

Using relations given in 3.35 and 3.36, the integrals 3.32 to

3.34 are first transformed and then integrated numerically using Gauss - Legendre integration scheme to find the stiffness and the mass matrices. The element matrices thus obtained, are assembled together to form the global stiffness and global mass matrices.

For the beam under consideration, the end $x_1 = 0$ is fixed while the end $x_1 = L$ is free. Then the geometric boundary conditions are

$$P = 0, \quad P' = 0, \quad Q = 0, \quad Q' = 0, \quad R = 0 \quad \text{at } x_1 = 0 \qquad \ldots\ldots 3.37.a$$

Then the ( natural ) conditions at $x_1 = L$ can be found from equations 3.23. They are

$$P = 0, \quad P'' = 0, \quad Q''' = 0, \quad Q' = 0, \quad R' = 0 \qquad \ldots 3.37.b$$

When there is an hinge support at an intermediate location, the additional geometric conditions at this support are

$$P = 0, \quad Q = 0, \quad R = 0 \qquad \ldots 3.37.c$$

When the element force vectors ( $R^e$) are assembled, the contributions to an interior node from the neighboring elements cancel each other. The contributions to the node at $x_1 = L$ become zero because of the boundary conditions 3.37.b. At the node $x_1 = 0$ the global force vector is unknown. However, when the geometric conditions are applied, the number of unknowns get reduced and then these equations with unknown right hand side can be discarded.

After application of the boundary conditions we get a eigen value problem of the form

$$[K_g]\{X_g\} = \omega [M_g]\{X_g\} \quad \ldots 3.38$$

where $[K_g]$ and $[M_g]$ are the modified global stiffness and assembled mass matrix respectively and $\{X_g\}$ is the matrix containing the global degrees of freedom. The natural frequencies of the system are obtained as square - root of the eigen values of the problem 3.38.

### 3.4 Solution

The beam under consideration ( i.e the VGVAWT blade with uniform cross - section ) is shown in Fig 3.3 along with the necessary details. We observe that the stiffness matrix $[K_g]$ and the mass matrix $[M_g]$ are unsymmetric matrices. To solve the equation 3.38 we use the NAG subroutine F02BJF. As the continuous system has been approximated by a set of finite elements, the infinite degrees of freedom corresponding to the actual system have been reduced to a finite number. Hence the approximate model is more stiff than the actual system. Obviously with the increase in the number of elements, the number of degrees of freedom increases, the overall stiffness of the approximate model decreases and consequently the eigen values converge to their true values.

During the computation of the results, it was experienced that as the number of elements was increased , the first eigen value showed a slight oscillation about the mean value, whereas the higher eigen values converged. It was conjectured that this

could be possibly due to

1) $I_{z_1 z_1} >> I_{y_1 y_1}$ leading to the ill-conditioning of the matrices.

2) The number of iterations in the NAG subroutine are fixed but unknown and the user cannot exercise any control over it. The eigen values are the roots of the polynomial given by

$$\left| [K_g] - \omega [M_g] \right| = 0 \qquad \ldots 3.39$$

The higher roots of the polynomial equation 3.39 can be obtained by neglecting the lower degree terms. But for finding lower eigen values particularly the lowest one, one has to consider all the terms. Consequently, higher roots can be computed with fewer number of iterations, while the first few roots are obtained after a considerable number of iterations. Therefore it is possible that the first eigen value does not converge within the number of iterations fixed by the subroutine itself.Finally it was decided to choose 33 elements ( Fig 3.2.a ).

## 3.5 Results and discussion

To check the validity of the finite element model, the solution pattern obtained from the same is compared with the one given in reference [ 8 ] for a beam hinged at both the ends. In our case, the cross - section of the beam has an airfoil shape as shown in Fig 3.3 while in reference [ 8 ] it has the shape of a channel. Thus both have one axis of symmetry. Further the geometric and the material properties are also different in these two cases. Figure

3.4 shows the validation of the first three natural frequencies with Ω. These frequencies are

1) first flap-wise bending ( bending about $y_1$ - axis )

2) First edge-wise bending ( bending about $z_1$ - axis )

3) first torsion

It is seen from Fig 3.4 that the edge-wise bending frequency increases with the increase in the rotational speed. The first flap-wise bending frequency decreases initially with the increase in the speed of rotation until it becomes zero at a particular speed. Beyond this speed the system does not vibrate in the first flap-wise bending mode. This is indicated by a negative eigen value (i.e an imaginary frequency ) beyond a particular speed. This is the first critical speed of the system. This bending mode of vibration again re-appears after a certain speed of rotation ( as indicated by a positive eigen value. ) This is one of the higher critical speeds of the system. The frequency corresponding to the first torsion mode decreases with the increase in the rotational speed and it becomes zero at a particular speed.

The results of reference [ 8 ] are reproduced in Fig 3.5. It can be seen that the trends of variation of the frequency with Ω are identical.

The blade of VGVAWT is a beam fixed at one end and hinged at an intermediate point. Before getting the results for the same, it was decided to study the trend of variation of frequency with Ω for a cantilever beam. These results are shown in Fig 3.6. It is observed that the trends are exactly the same as those for a beam hinged at both the ends. Finally the results for the blade of

VGVAWT ( uniform cross - section ) are shown in Fig 3.7. It is seen that the frequencies show the same trend with rotational speed. It is observed that, in this case the frequency of a particular mode lies in between the corresponding frequencies of a cantilever beam and the beam hinged at both the ends.

A parametric study was conducted to examine the effects of wall thickness, shear centre position, the hinge location and taper on the natural frequencies. It is observed that the frequencies do not change with the wall thickness. This can be explained as follows:

Note that all the geometric properties of the cross - section ( A, $I_{y_1y_1}$, $I_{z_1z_1}$, $I_p$ and J ) are linear functions of the wall thickness. As a result, the ratios $a^2$, $b^2$, $c^2$ and $d^2$ ( defined by equation 3.19 ) are independent of the wall thickness. Further, the shear centre location does not change with the wall thickness as it depends only on the shape of the cross - section and not on its size. Equation 3.20 shows that the dependence of the natural frequencies on the geometry of the cross - section is only through the ratios $a^2$, $b^2$, $c^2$, $d^2$ ( henceforth called the shape factors ) and the shear centre location $y_E$. Since these quantities do not depend on the wall thickness, the natural frequencies do not depend on the size but only on the shape, provided of course the thickness is small compared with the other cross - sectional dimensions.

If an airfoil different from NACA 0015 is used for the cross - section, the natural frequencies will change. Calculation of the shape factors $a^2$, $b^2$, $c^2$ , $d^2$ and the shear centre location for various airfoils is a very tedious task. Therefore, the parametric study with the shape as the parameter is not carried out. Instead,

only the effect of unsymmetry of the cross - section on the natural frequencies is studied by varying $y_E$. This variation is shown in Fig 3.8. It is seen that only the torsional frequency changes with the shear centre position. It decreases as the distance of the shear centre from the centroid increases. For effective functioning of the reef control mechanism, the location of the intermediate support ( hinge ) should be close to the base. The effect of changing the hinge location on the natural frequencies is shown in Fig 3.9. It shows that the frequencies increase with the increase in the support distance from the base. Since the hinge support should be at the mass centre of the beam, a decrease in the support distance can be achieved by bringing the mass centre closer to the base. This is possible only when there is a taper. One such arrangement ( stepped internal taper ) is discussed in chapter 2 (Fig 2.2). The effect of this taper on the natural frequencies is is illustrated in figures 3.10.a 3.10.b and 3.10.c. It is observed that the flap - wise bending and torsional frequencies decrease with the taper but the edge - wise bending frequency increases. The increase in the edge - wise frequency is due to the increase in $I_{z_1 z_1} / A$ over the tapered portions BC and CD (Fig 2.2).

### 3.6 Interference diagram.

The normal and tangential aerodynamic forces acting on the blade are periodic in nature. Here we concentrate on the normal component since it is the more predominant of the the two forces.As seen from fig 2.3 the normal force is an odd function of the azimuthal angle and has a period of $2\pi$ radians and can be

represented as a fourier sine series as

$$F_n(\phi) = \sum_{n=1}^{\infty} b_n \sin(n\phi)$$

$$= \sum_{n=1}^{\infty} b_n \sin(n\Omega t) \qquad \ldots 3.39$$

where,

$$b_n = \frac{1}{2\pi} \int_{-\pi}^{\pi} F_n(\phi) \sin(n\phi)\, d\phi \qquad \ldots 3.40$$

The coefficients $b_n$ can be found by using a suitable numerical integration scheme. Table 3.1 shows the first twenty five

coefficients.

Table 3.1: Fourier coefficients of the normal aerodynamic force

| Harmonic number | Fourier coefficient |
|---|---|
| 1 | 480.0088 |
| 2 | 39.2705 |
| 3 | ~~31.0524~~ 3·10524 |
| 4 | -0.3516 |
| 5 | -0.1399 |
| 6 | -2.5437 |
| 7 | 2.5079 |
| 8 | 1.5279 |
| 9 | -0.8061 |
| 10 | 1.8509 |
| 11 | -1.6293 |
| 12 | 0.4728 |
| 13 | -3.4863 |
| 14 | 3.0834 |
| 15 | -3.9945 |
| 16 | 4.3429 |
| 17 | -3.5123 |
| 18 | 0.9485 |
| 19 | -2.4508 |
| 20 | -0.9545 |
| 21 | 3.2530 |
| 22 | -2.0074 |
| 23 | 6.1122 |
| 24 | -5.1709 |
| 25 | -5.6367 |

It is seen from the above table that the first two harmonics are predominant. Thus, the most dominant excitation frequencies are $\Omega$ and $2\Omega$.

For a rotating body, the natural frequencies vary with the speed of rotation. Further, if the external force is a periodic function of the rotational speed and its multiples, a Campbell

be small. On the other hand, the margin between the lowest speed of interference ( 450 rpm ) and the operational speed ( 85 rpm ) is so large. that this small decrease would not cause any resonance.

When the ratio of the spar thickness to skin thickness is increased, the shear centre moves away from the centroid causing a decrease in the first torsional frequency ( Fig 3.8 ). However, that would not change the lowest speed of interference (Fig 3.11). Thus, again there would be no resonance.

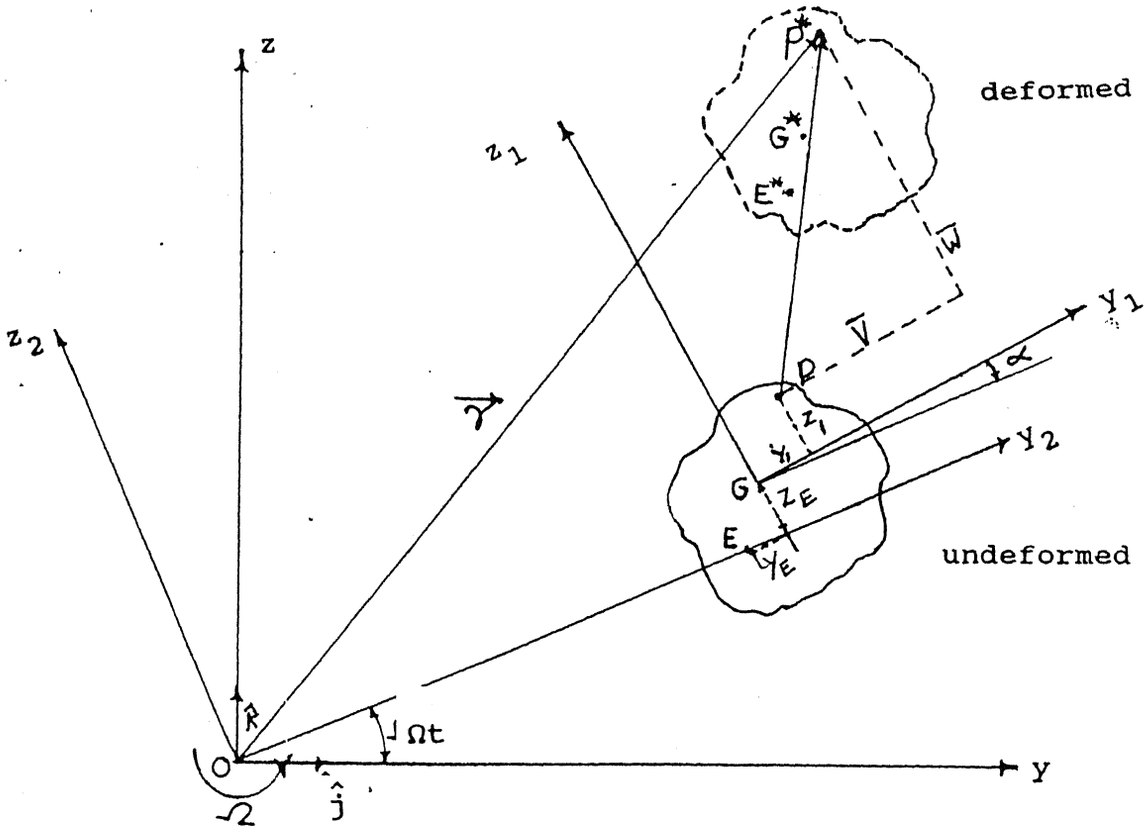


Fig 3.1 : A Typical Rotating Beam System.

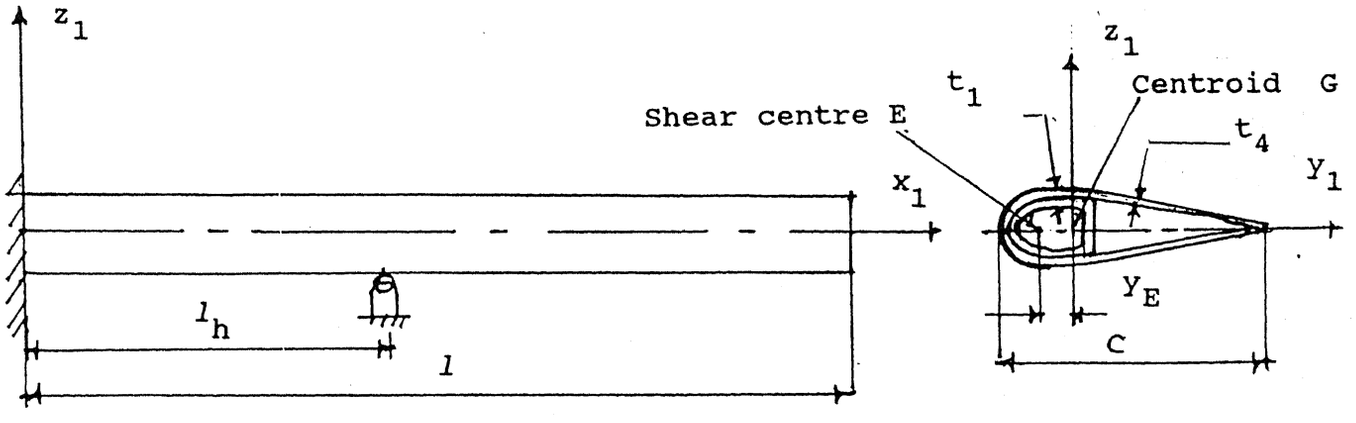


Cross-section shape = NACA 0015

$c = 0.45$ m, $\frac{t_4}{t_1} = 0.2$, $t_1 = 6$ mm

$l_h = 1.4$ m $\quad l = 3.25$ m

Fig 3.3: VGVAWT blade with Uniform Cross-section

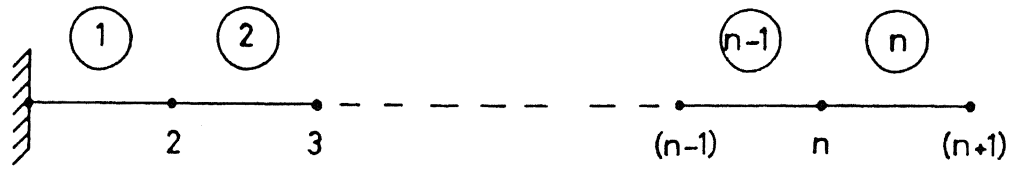


N.B. The encircled numbers represent the element numbers.

Fig 3.2.a : Descretization of the Beam into a Finite Number of Two-noded Elements.

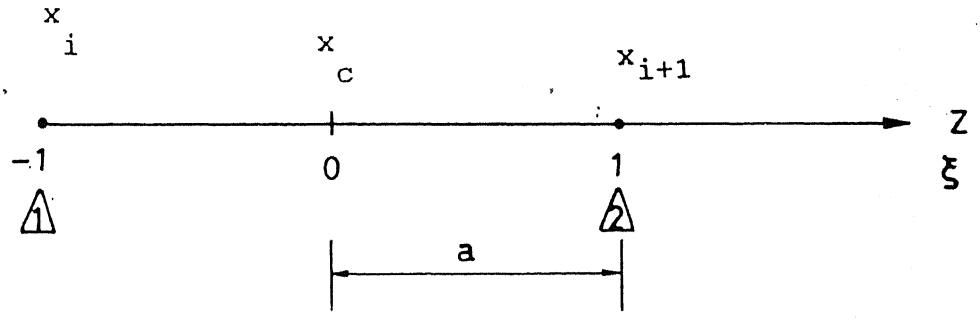


$i^{th}$ element

x -Global co-ordinate, ξ -Local co-ordinate

a -Half the length of the element

Numbers inscribed in the triangle represent local node numbers.

FIG. 3.2.b A TYPICAL TWO-NODED ELEMENT

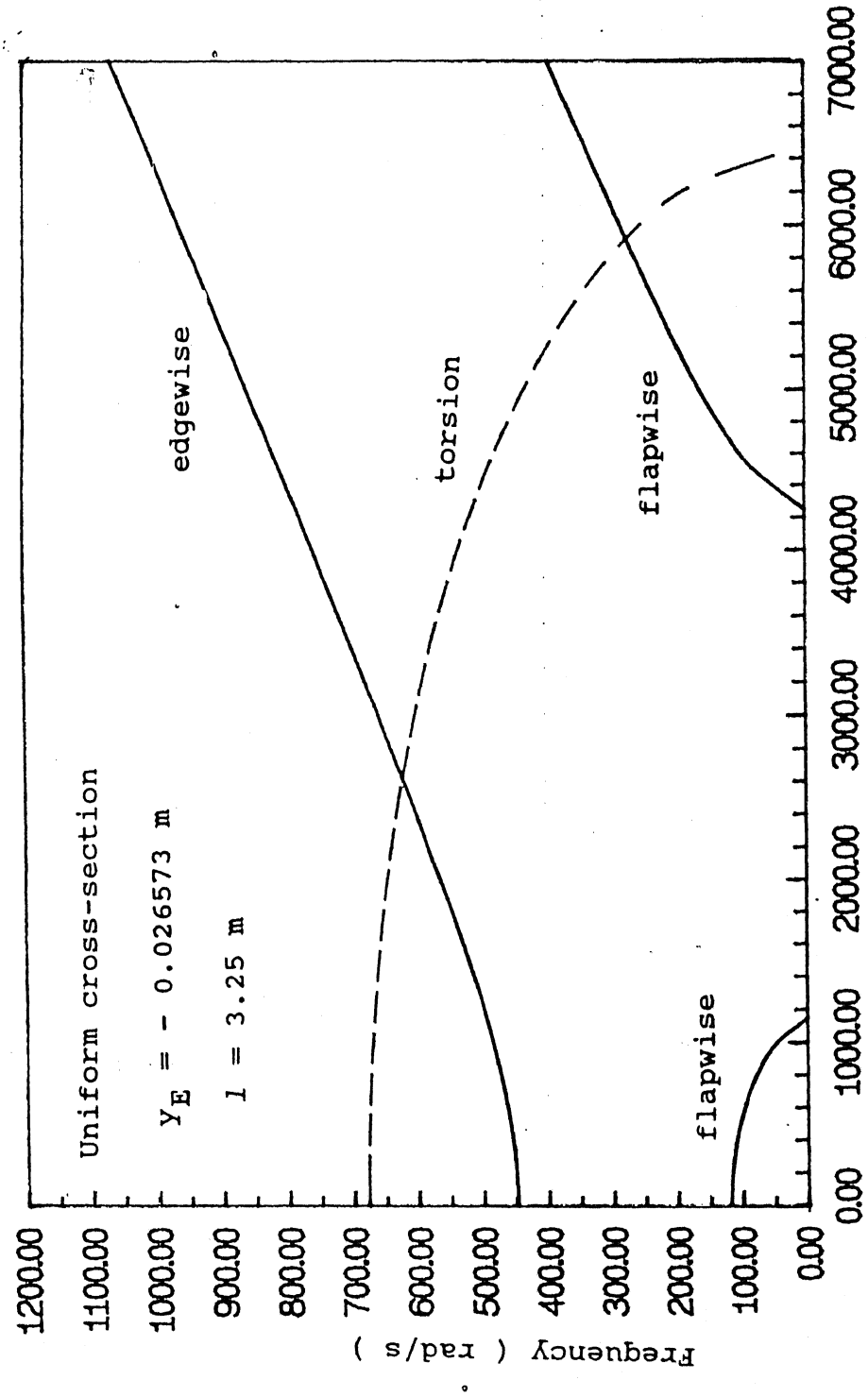


Fig .3.4 : Variation of Natural Frequencies with Rotational Speed for a Beam Hinged at Both Ends.

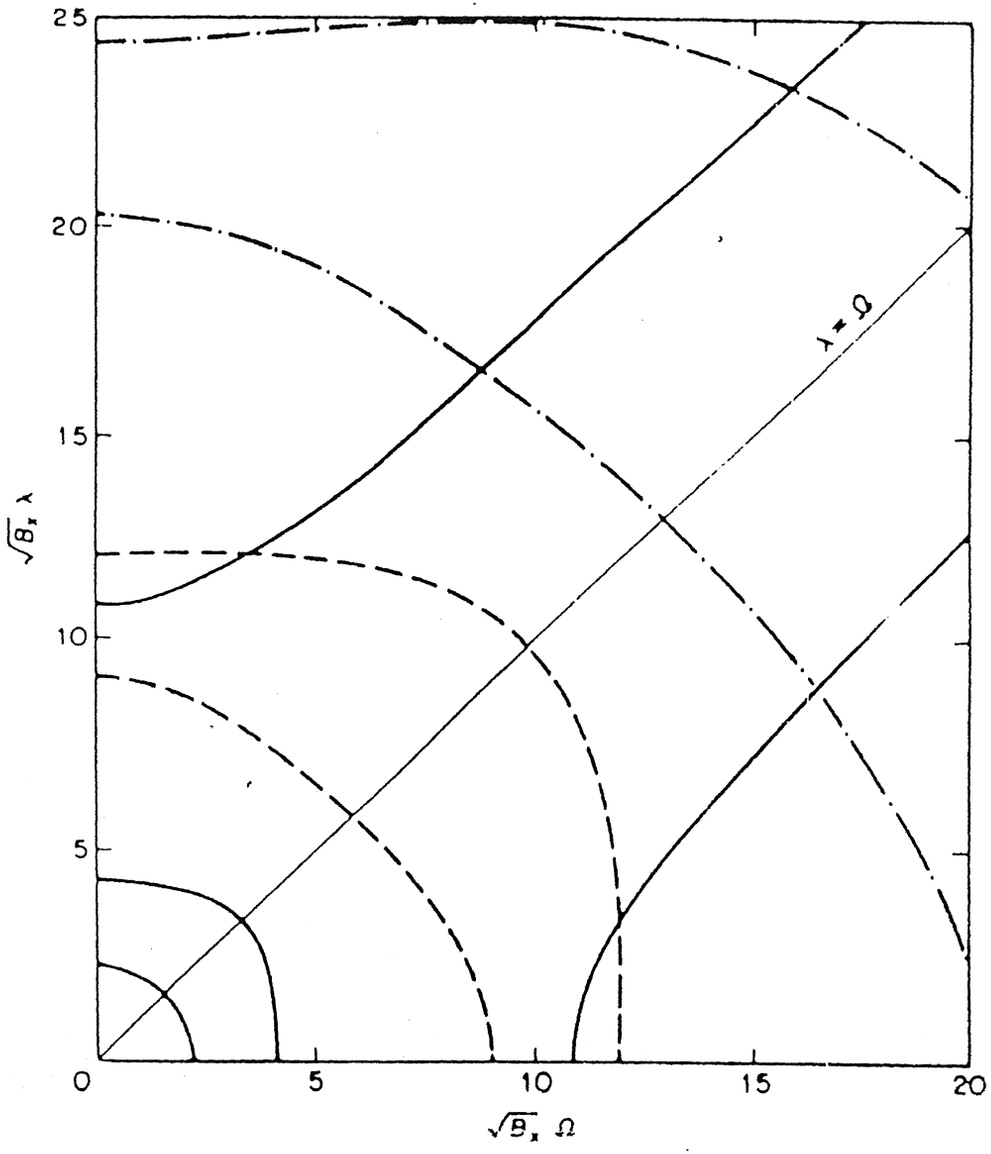


Fig 3.5 : Variation of Natural Frequencies with Rotational Speed for a Beam Hinged at Both Ends ( Ref [8] ).

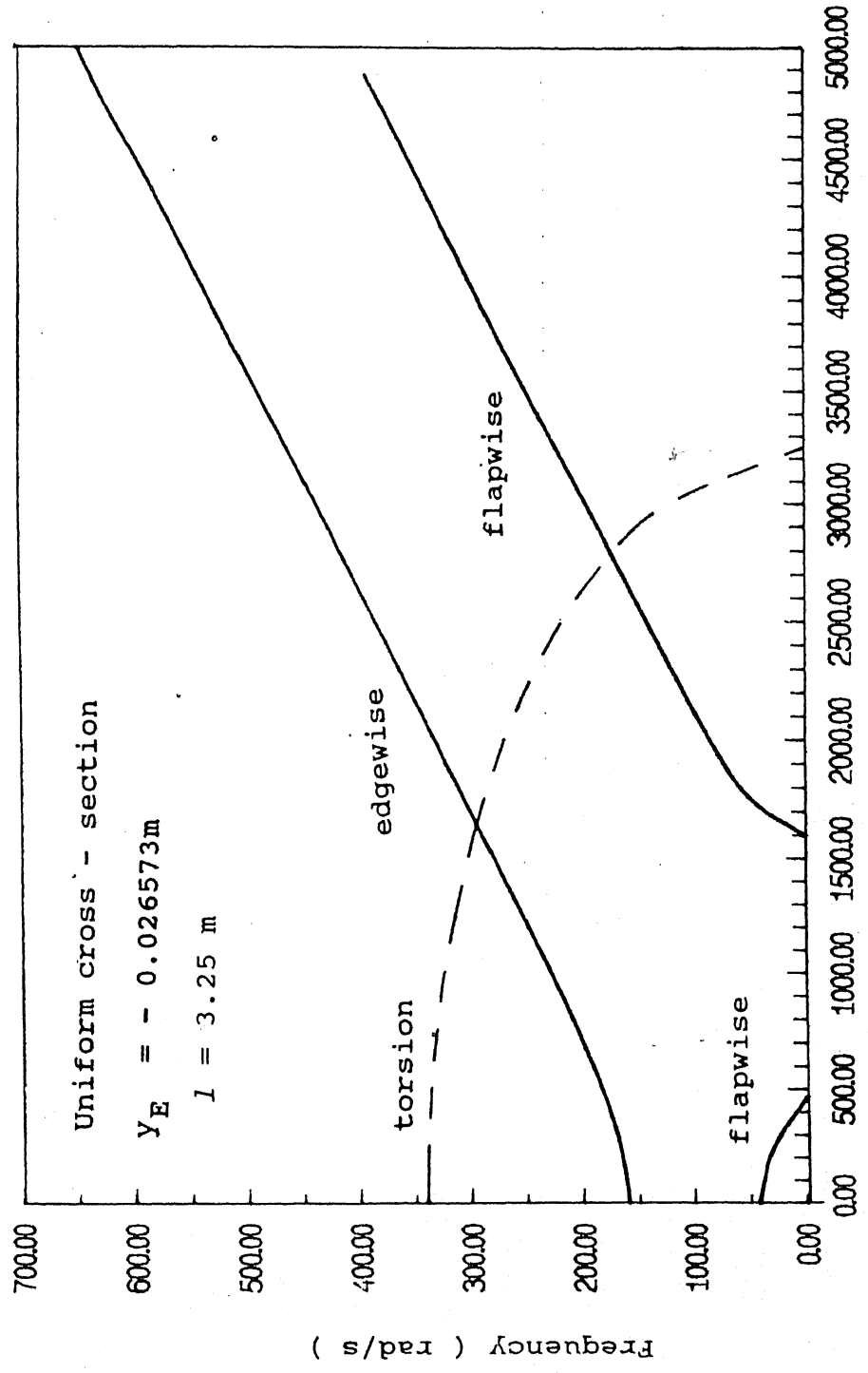


Fig 3.6 : Variation of Natural Frequencies with Rotational Speed for a Cantilever Beam.

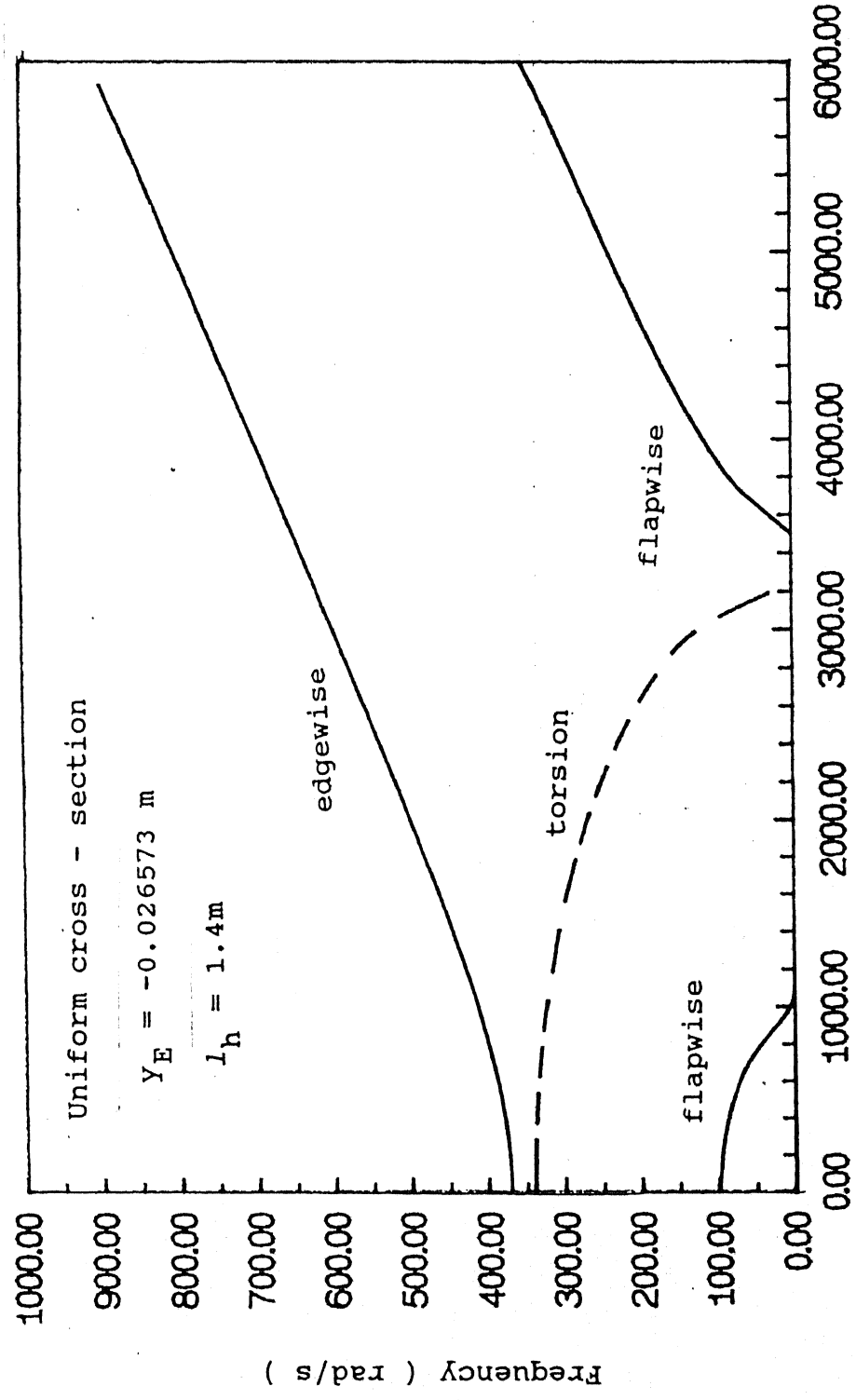


Fig 3.7 : Variation of Natural Frequencies with Rotational Speed for VGVAWT blade.

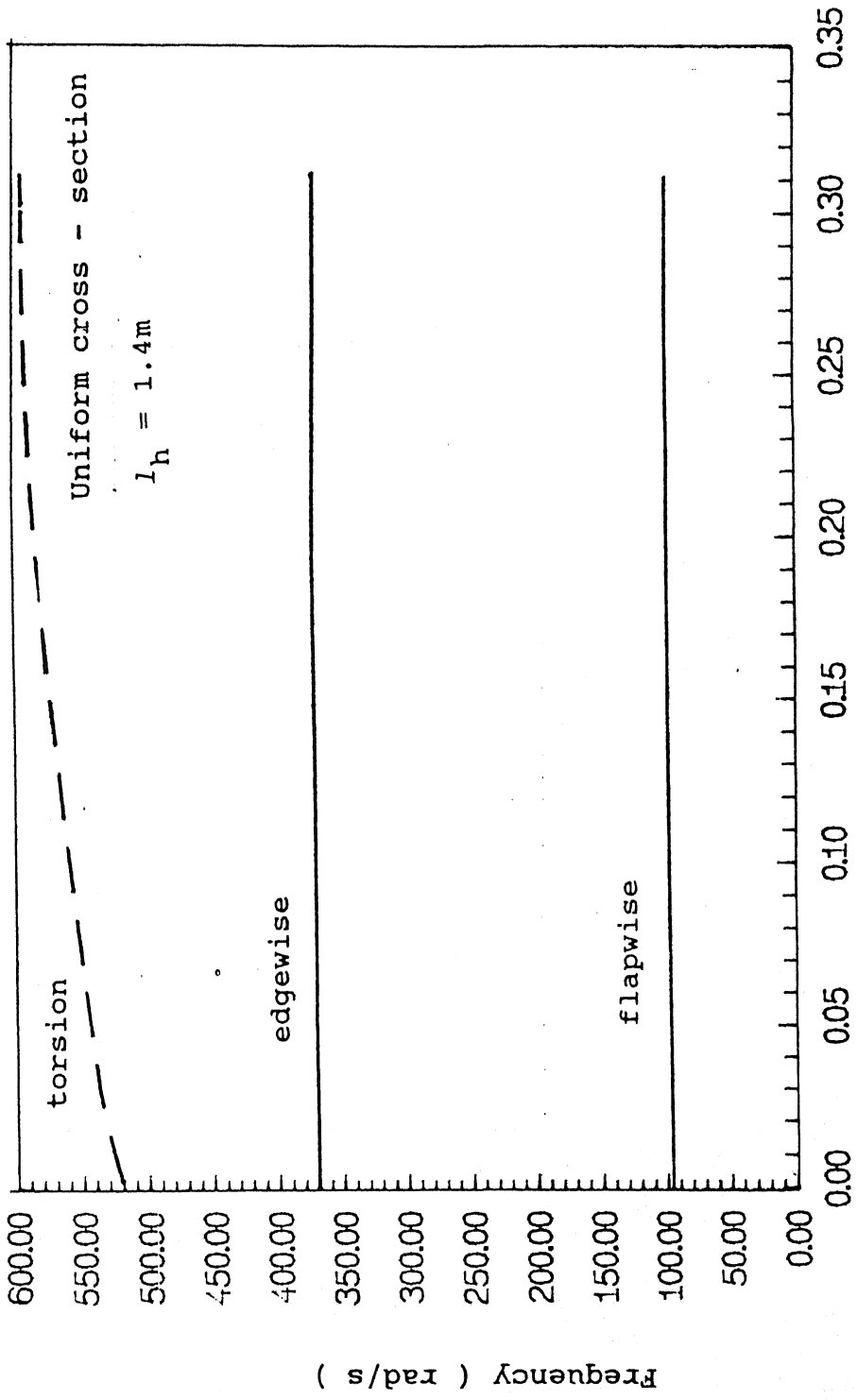


Fig 3.8 : Variation of Natural Frequencies with shear centre Loaction for VGVAWT blade.

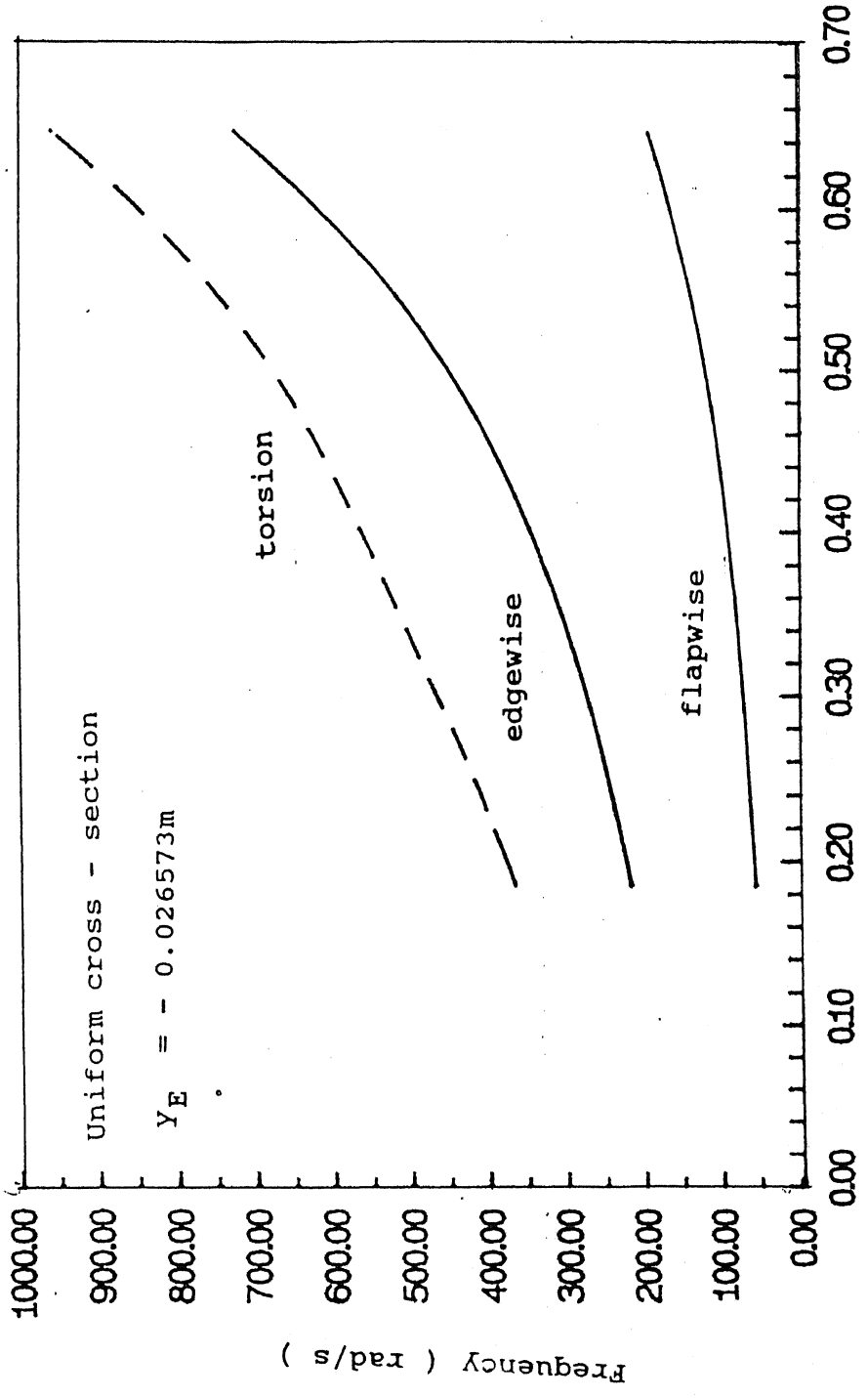


Fig 3.9 : Effect of the Hinge Loaction on the Natural Frequencies.

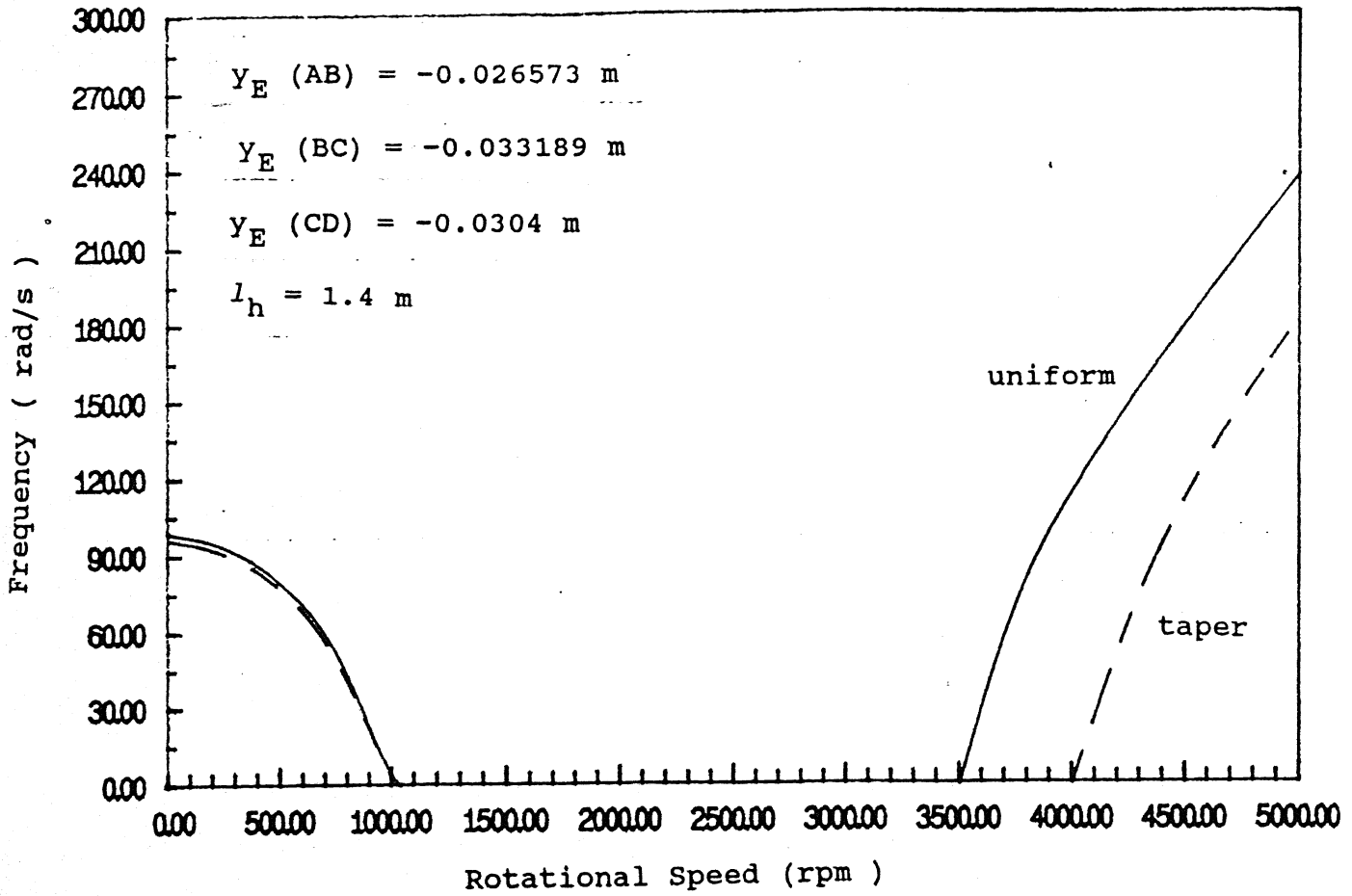


Fig 3.10.a : Effect of Taper on the First flapwise Frequency

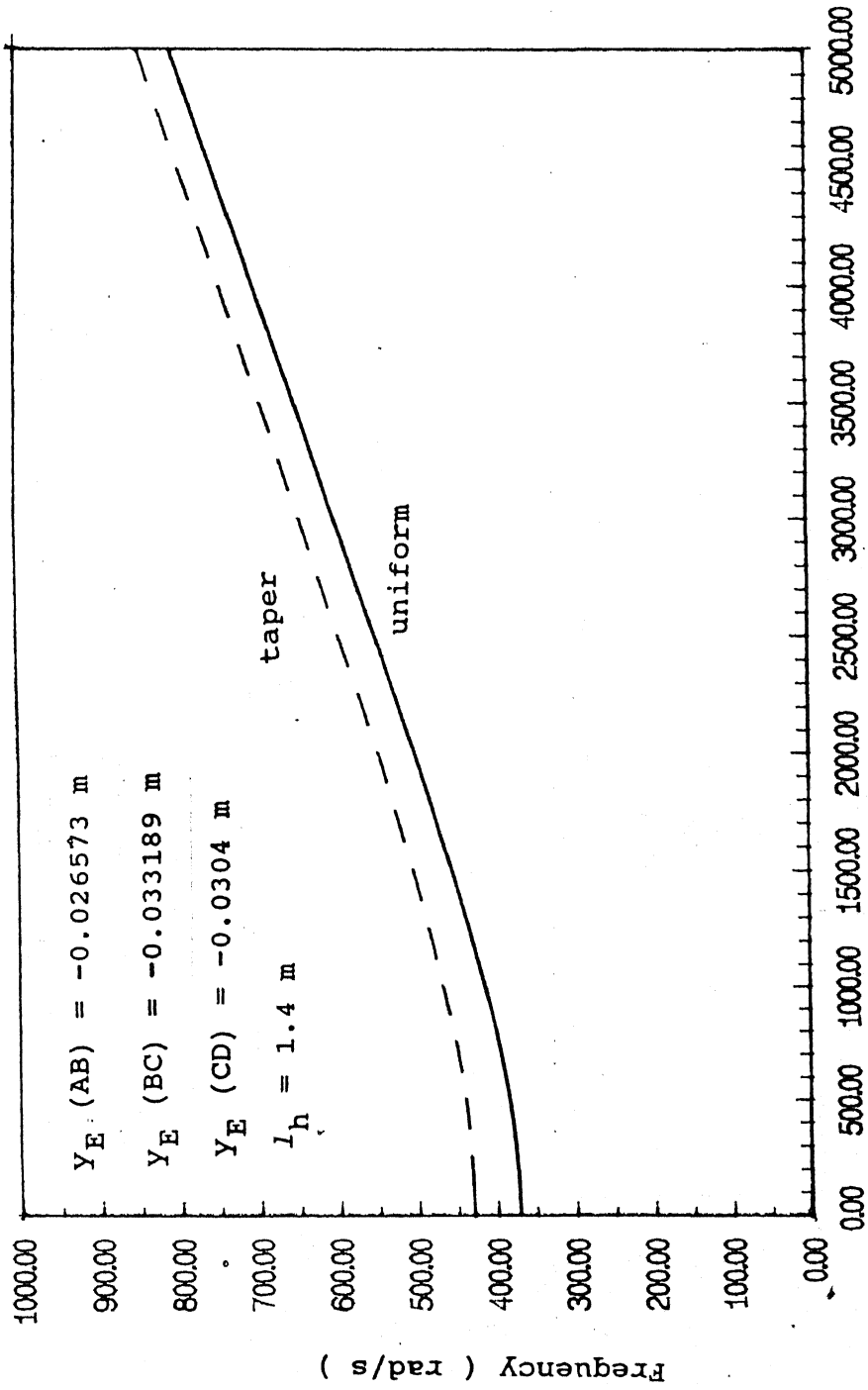


Fig 3.10.b : Effect of Taper on the First Edgewise Frequency

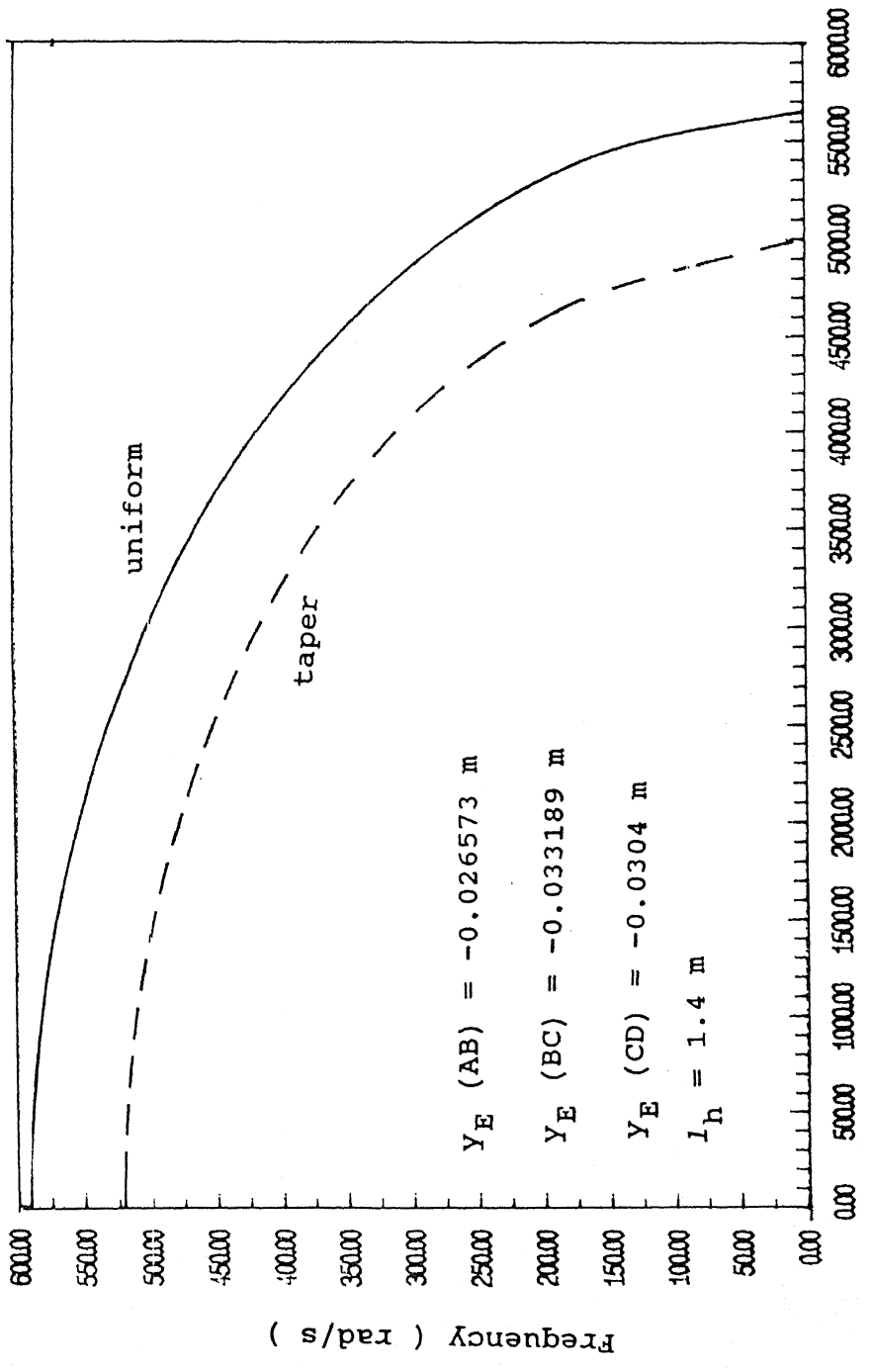


Fig 3.10.c : Effect of Taper on the First Torsional Frequency.

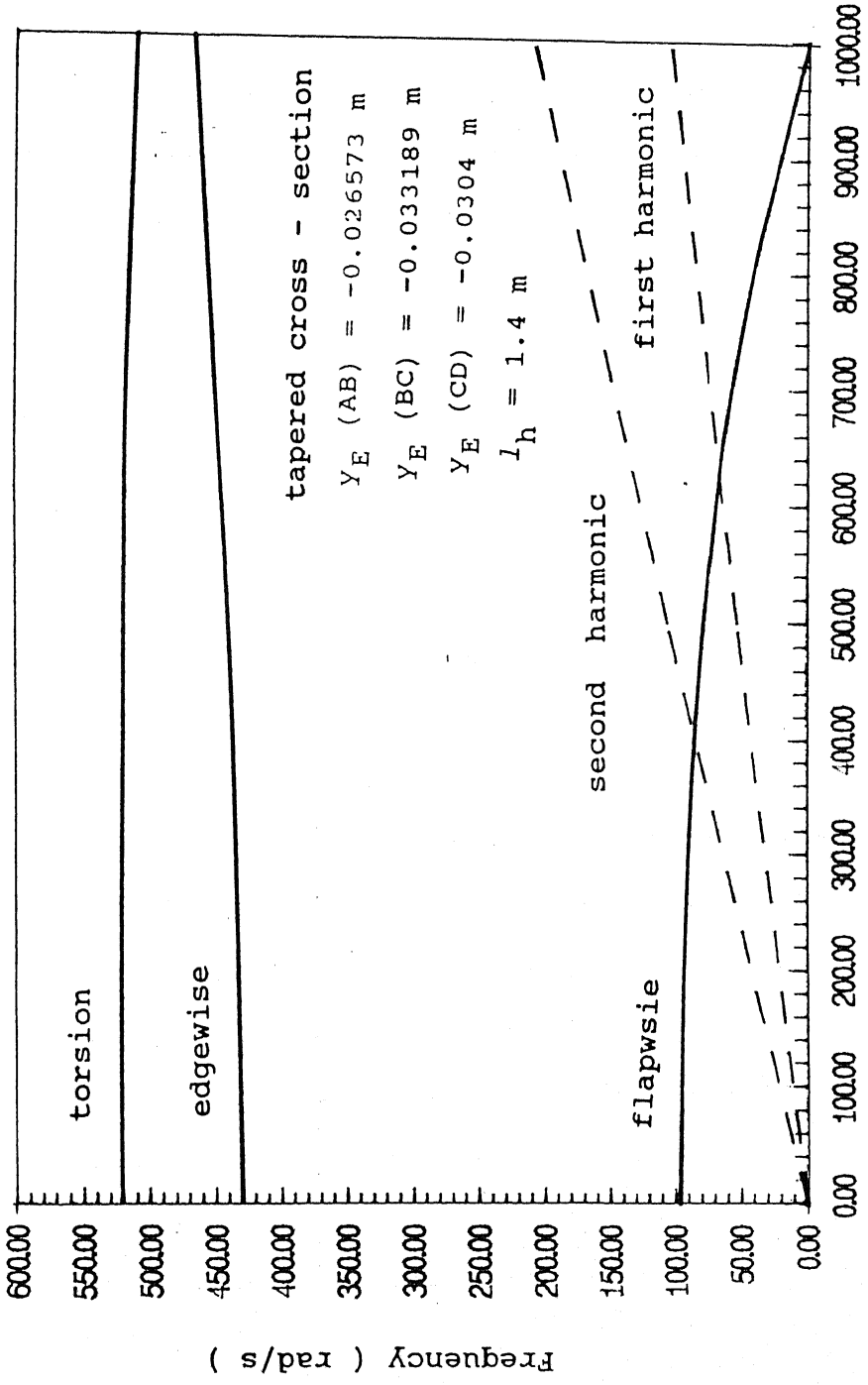


Fig 3.11 : Interference Diagram for VGVAWT blade.

CHAPTER 4

# ANALYSIS OF COMPOSITE BOX SHAPED SPAR

## 4.1 Introduction:

The wind turbines of high capacity generally rotate at high speeds. The blades of such turbines severe loading (both aerodynamic and centrifugal forces). In such cases the use of fibre wound D-shaped spar may not be sufficient to sustain the operating loads. Hence the spar is made of box shaped structure consisting of composite laminates stacked over each other.

Depending on the stacking sequence (layup), there are three different cases as shown in Fig 4.1. These are

1) Symmetric ply layup

2) Antisymmetric ply layup

3) cross ply layup

The present chapter deals with the static analysis of such composite box shaped spar, subjected to various types of load such as axial force, torque and bending load. In this case there is a coupling between different modes of deformation. This coupling depends on the structure of each laminate and on the ply stacking sequence. The variational finite element formulation is used to study the deformation of the spar.

## 4.2 Stiffness coefficients.

We assume that the spar carries a major portion of the load and hence the entire blade cross-section can be represented by

the spar for the purpose of static analysis. The spar is modelled as a rectangular box beam whose walls consist of laminated orthotropic composite plies.

### 4.2.2. Constitutive relations:

The box - beam geometry and co-ordinates are shown in Fig 4.2. The origin of the cross-section axes $\eta$ - $\xi$ is at the centroid of the beam. The deformation of the beam is described in terms of extension, bending, torsion and transverse shear. The effect of constrained warping is neglected. These assumptions yield displacements of the form

$$U = u(x) - \eta \left( v'(x) - \overset{\circ}{\gamma}_{x\eta}(x) \right) - \xi \left( w'(x) - \overset{\circ}{\gamma}_{x\xi}(x) \right), \quad ..4.1.a$$

$$V = v(x) - \xi\, \phi(x), \quad ...4.1.b$$

$$W = w(x) + \eta\, \phi(x). \quad ...4.1.c$$

In the above equations U, V, and W represent the total axial deformation (in the x direction), the total horizontal deformation (in the y direction) and the total vertical deformation (in the z direction) respectively. u, v and w represent the axial deformation due to extension, horizontal deformation due to bending and vertical deformation due to bending respectively. $\phi$ the twist while $\gamma$ represents the transverse shear strain in the cross section.

The rotation of the cross-section about the z axis ($\beta_z$) and that about the y axis ($\beta_y$) are given by

$$\beta_z = v'(x) - \gamma^o_{x\eta} , \qquad \ldots 4.2.a$$

$$\beta_y = w'(x) - \gamma^o_{x\xi} . \qquad \ldots 4.2.b$$

Substituting 4.2.a and 4.2.b in equations 4.1.a, 4.1.b and 4.1.c, we get the equations for displacements as

$$U = u(x) - \eta\, \beta_z(x) - \xi\, \beta_y(x), \qquad \ldots 4.3.a$$

$$V = v(x) - \xi\, \phi(x), \qquad \ldots 4.3.b$$

$$W = w(x) + \eta\, \phi(x). \qquad \ldots 4.3.c$$

Strains are determined by differentiating these displacement terms. Since the walls of the box - beam are assumed to be relatively thin, only the axial and in-plane shear strains are considered. The resulting strains are

$$\varepsilon_{xx} = \frac{\partial U}{\partial x} = u' - \eta\, \beta_z' - \xi\, \beta_y' , \qquad \ldots 4.4.a$$

$$\begin{aligned} \varepsilon_{x\xi} &= \frac{\partial U}{\partial \xi} + \frac{\partial W}{\partial x} \\ &= w' - \beta_y + \eta\, \phi' \\ &= \gamma^o_{x\xi} + \eta\, \phi' , \end{aligned} \qquad \ldots 4.4.b$$

$$\begin{aligned} \varepsilon_{x\eta} &= \frac{\partial U}{\partial \eta} + \frac{\partial V}{\partial x} \\ &= v' - \beta_z - \xi\, \phi' \\ &= \gamma^o_{x\eta} - \xi\, \phi' \end{aligned} \qquad \ldots 4.4.c$$

For a ply in the vertical beam wall, the elastic constitutive relations are

$$\begin{bmatrix} \sigma_{xx} \\ \sigma_{\xi\xi} \\ \sigma_{x\xi} \end{bmatrix} = \begin{bmatrix} \overline{Q}_{11} & \overline{Q}_{12} & \overline{Q}_{16} \\ \overline{Q}_{12} & \overline{Q}_{22} & \overline{Q}_{26} \\ \overline{Q}_{16} & \overline{Q}_{26} & \overline{Q}_{66} \end{bmatrix} \begin{bmatrix} \varepsilon_{xx} \\ \varepsilon_{\xi\xi} \\ \varepsilon_{x\xi} \end{bmatrix} \qquad \ldots 4.5.a$$

For a ply in the horizontal wall the relations are

$$\begin{bmatrix} \sigma_{xx} \\ \sigma_{\eta\eta} \\ \sigma_{x\eta} \end{bmatrix} = \begin{bmatrix} \overline{Q}_{11} & \overline{Q}_{12} & \overline{Q}_{16} \\ \overline{Q}_{12} & \overline{Q}_{22} & \overline{Q}_{26} \\ \overline{Q}_{16} & \overline{Q}_{26} & \overline{Q}_{66} \end{bmatrix} \begin{bmatrix} \varepsilon_{xx} \\ \varepsilon_{x\eta} \\ \varepsilon_{x\eta} \end{bmatrix} \qquad \ldots 4.5.b$$

The terms $\overline{Q}_{11}$, $\overline{Q}_{12}$ etc. are the reduced stiffness coefficients of a single ply which are related to the material properties by the relation [ 9 ]

$$\{ Q_R \} = [ T ] \{ Q \}, \qquad \ldots 4.6$$

where

$$[T] = \begin{bmatrix} m^4 & n^4 & 2m^2n^2 & 4m^2n^2 \\ n^4 & m^4 & 2m^2n^2 & 4m^2n^2 \\ m^2n^2 & m^2n^2 & -2m^2n^2 & (m^2 - n^2)^2 \\ m^2n^2 & m^2n^2 & m^4 + n^4 & -4m^2n^2 \\ m^3n & -mn^3 & (mn^3 - m^3n) & 2(mn^3 - m^3n) \\ mn^3 & -mn^3 & (m^3n - mn^3) & 2(m^3n - mn^3) \end{bmatrix} \qquad \ldots 4.7$$

$$\{ Q_R \}^T = \left| \overline{Q}_{11} \quad \overline{Q}_{22} \quad \overline{Q}_{66} \quad \overline{Q}_{12} \quad \overline{Q}_{16} \quad \overline{Q}_{26} \right| , \qquad \ldots 4.8$$

$$\{ Q \}^T = \left| Q_{11} \quad Q_{22} \quad Q_{12} \quad Q_{66} \quad \right| . \qquad \ldots 4.9$$

In expression 4.7,

$$m = \cos \theta , \quad n = \sin \theta \qquad \ldots 4.10$$

where $\theta$ is the angle made by the fibres with the x - axis ( Fig 4.3 ). The elements of $\{ Q \}$ are given by

$$Q_{11} = \frac{E_1}{( 1 - \nu_{12} \nu_{21} )} ,$$

$$Q_{12} = \frac{\nu_{21} E_1}{( 1 - \nu_{12} \nu_{21} )} ,$$

$$Q_{22} = \frac{E_2}{( 1 - \nu_{12} \nu_{21} )} ,$$

$$Q_{66} = G_{12} \qquad \ldots 4.11$$

where $E_1$ is the Young's modulus of the ply in the direction of the fibre, $E_2$ is the Young's modulus in the direction transverse to the fibre, $G_{12}$ is the in - plane shear modulus and $\nu_{12}$ and $\nu_{21}$ are the in - plane poisson's ratios. The poisson's ratio are related by

$$\frac{\nu_{12}}{E_1} = \frac{\nu_{21}}{E_2} \qquad \ldots 4.12$$

Adequate treatment of the transverse in - plane stresses

$\sigma_{\eta\eta}$ and $\sigma_{\xi\xi}$ and the strains $\varepsilon_{\eta\eta}$ and $\varepsilon_{\xi\xi}$ is important in composite box - beam analysis. Elastic properties within the composite plies change with the ply orientation angle and the poisson's ratio. The anisotropic elastic charecteristics of composite plies can result in highly two dimensional elastic behaviour. There are three methods to account for the in-plane elastic behaviour [9].

Method 1:

This is closest to the standard beam theory. Based on the initial kinematic assumptions of the beam we assume

$$\varepsilon_{\eta\eta} = \varepsilon_{\xi\xi} = 0 \qquad \ldots 4.13$$

and $\sigma_{\eta\eta}$ and $\sigma_{\xi\xi}$ have no effect on the net cross-section force and moments. This assumption is very similar in nature to the plane strain assumption. This assumption does not take into account the in -plane behaviour of the ply very accurately.

Method 2:

Here we assume

$$\sigma_{\eta\eta} = \sigma_{\xi\xi} = 0 \qquad \ldots 4.14$$

and $\varepsilon_{\eta\eta}$ and $\varepsilon_{\xi\xi}$ are removed from the constitutive relation by substitution. This assumption is similar in nature to the plane stress assumption. This is the method used in the present analysis.

Method 3:

This method treats the transverse in-plane behaviour in a more refined manner. Condition of in-plane stress and in-plane strain are imposed such that there are no in - plane forces or

moments.

Using method 2 and putting $\sigma_{\xi\xi} = 0$ in equation 4.5.a, we get the modified constitutive relation for a ply in the vertical wall

$$\begin{bmatrix} \sigma_{xx} \\ \sigma_{x\xi} \end{bmatrix} = \begin{bmatrix} \overline{Q'_{11}} & \overline{Q'_{16}} \\ \overline{Q'_{16}} & \overline{Q'_{66}} \end{bmatrix} \begin{bmatrix} \varepsilon_{xx} \\ \varepsilon_{x\xi} \end{bmatrix} \quad \ldots 4.15.a$$

Similarly substituting $\sigma_{\eta\eta} = 0$ in equation (4.2.e) we get the modified constitutive relations for a ply in the horizontal wall as

$$\begin{bmatrix} \sigma_{xx} \\ \sigma_{x\eta} \end{bmatrix} = \begin{bmatrix} \overline{Q'_{11}} & \overline{Q'_{16}} \\ \overline{Q'_{16}} & \overline{Q'_{66}} \end{bmatrix} \begin{bmatrix} \varepsilon_{xx} \\ \varepsilon_{x\eta} \end{bmatrix} \quad \ldots 4.15.b$$

where,

$$\overline{Q'_{11}} = \overline{Q_{11}} - \frac{(\overline{Q_{11}})^2}{\overline{Q_{22}}},$$

$$\overline{Q'_{16}} = \overline{Q_{16}} - \frac{(\overline{Q_{12}}\ \overline{Q_{26}})}{\overline{Q_{22}}},$$

$$\overline{Q_{66}} = \overline{Q_{66}} - \frac{(\overline{Q_{26}})^2}{\overline{Q_{22}}}. \quad \ldots 4.16$$

Substituting the relations for strain 4.4.a, 4.4.b and 4.4.c in equations 4.15.a and 4.15.b, we get the following equation for a ply in the vertical wall

$$\{ \sigma_v \} = [ V ] \{ \varepsilon \}^T \qquad \ldots 4.17.a$$

Similarly for a ply in the horizontal direction we get

$$\{ \sigma_H \} = [ H ] \{ \varepsilon \}^T \qquad \ldots 4.17.b$$

Here,

$$\{ \sigma_v \} = \begin{bmatrix} \overline{\sigma_{xx}} \\ \overline{\sigma_{x\xi}} \end{bmatrix} \qquad \ldots 4.18$$

$$\{ \sigma_h \} = \begin{bmatrix} \overline{\sigma_{xx}} \\ \overline{\sigma_{x\eta}} \end{bmatrix} \qquad \ldots 4.19$$

$$\{ \varepsilon \}^T = \begin{bmatrix} \underline{u'} & \gamma^o_{x\eta} & \gamma^o_{x\xi} & \phi' & \beta_y' & \underline{\beta_z'} \end{bmatrix} \qquad \ldots 4.20$$

$$[ V ] = \begin{bmatrix} \overline{\overline{Q_{11}'}} & 0 & \overline{\overline{Q_{16}'}} & \eta\,\overline{\overline{Q_{16}'}} & -\xi\,\overline{\overline{Q_{11}'}} & -\eta\,\overline{\overline{Q_{11}'}} \\ \underline{\overline{Q_{16}'}} & 0 & \overline{\overline{Q_{66}'}} & \eta\,\overline{\overline{Q_{66}'}} & -\xi\,\overline{\overline{Q_{16}'}} & -\eta\,\underline{\overline{Q_{16}'}} \end{bmatrix} \qquad \ldots 4.21$$

$$[ H ] = \begin{bmatrix} \overline{\overline{Q_{11}'}} & \overline{\overline{Q_{16}'}} & 0 & -\xi\,\overline{\overline{Q_{16}'}} & -\xi\,\overline{\overline{Q_{11}'}} & -\eta\,\overline{\overline{Q_{11}'}} \\ \underline{\overline{Q_{16}'}} & \overline{\overline{Q_{66}'}} & 0 & -\xi\,\overline{\overline{Q_{66}'}} & -\xi\,\overline{\overline{Q_{16}'}} & -\eta\,\underline{\overline{Q_{16}'}} \end{bmatrix} \qquad \ldots 4.22$$

The net forces and moments acting over the cross-section are defined to the stresses in the beam walls by equilibrium as follows,

$$F_x = \int\int \sigma_{xx}\, dA$$

$$F_y = \int\int \sigma_{x\eta}\, dA$$

$$F_z = \int\int \sigma_{x\xi}\, dA$$

$$M_x = \int\int ( \eta\, \sigma_{x\xi} - \xi\, \sigma_{x\eta} )\, dA$$

$$M_y = - \int\int \sigma_{xx}\, \xi\, dA$$

$$M_z = - \int\int \sigma_{xx}\, \eta\, dA \qquad \ldots 4.23$$

where, $F_x$, $F_y$ and $F_z$ represent the net force in the x, y and z directions respectively, while $M_x$, $M_y$ and $M_z$ are the moments about the x-axis , y-axis and z-axis respectively. Substituting the relations 4.17.a and 4.17.b into 4.23, we get

$$\{ F \} = [ D ] \{ \varepsilon \} \qquad \ldots 4.24$$

where,

$$\{ F \}^T = \lfloor F_x \quad F_y \quad F_z \quad M_x \quad M_y \quad M_z \rfloor$$

$$\ldots 4.25$$

and [ D ] is the symmetric stiffness matrix whose elements are given

$$D_{11} = \int_H\int \overline{Q_{11}'}\, dA + \int_V\int \overline{Q_{11}'}\, dA$$

$$D_{12} = \int_H\int \overline{Q_{16}'}\, dA$$

$$D_{13} = \int_V\int \overline{Q_{16}'}\, dA$$

$$D_{14} = \int_V\int \eta\, \overline{Q_{16}'}\, dA - \int_H\int \xi\, \overline{Q_{16}'}\, dA$$

$$D_{15} = -\int_V \int \xi \overline{Q_{11}'}\, dA - \int_H \int \xi \overline{Q_{11}'}\, dA$$

$$D_{16} = -\int_V \int \eta \overline{Q_{11}'}\, dA - \int_H \int \eta \overline{Q_{11}'}\, dA$$

$$D_{22} = \int_H \int \overline{Q_{66}'}\, dA$$

$$D_{23} = 0$$

$$D_{24} = -\int_H \int \xi \overline{Q_{66}'}\, dA$$

$$D_{25} = -\int_H \int \xi \overline{Q_{16}'}\, dA$$

$$D_{26} = -\int_H \int \eta \overline{Q_{16}'}\, dA$$

$$D_{33} = \int_V \int \overline{Q_{66}'}\, dA$$

$$D_{34} = \int_V \int \eta \overline{Q_{66}'}\, dA$$

$$D_{35} = -\int_V \int \eta \overline{Q_{66}'}\, dA$$

$$D_{36} = -\int_V \int \xi \overline{Q_{16}'}\, dA$$

$$D_{44} = \int_V \int \eta^2 \overline{Q_{66}'}\, dA + \int_H \int \xi^2 \overline{Q_{66}'}\, dA$$

$$D_{45} = \int_H \int \xi^2 \overline{Q_{16}'}\, dA + \int_V \int \eta\, \xi \overline{Q_{16}'}\, dA$$

$$D_{46} = \int_H \int \eta\, \xi \overline{Q_{16}'}\, dA - \int_V \int \eta^2 \overline{Q_{16}'}\, dA$$

$$D_{55} = \int_H \int \xi^2 \overline{Q_{11}'}\, dA + \int_V \int \xi^2 \overline{Q_{11}'}\, dA$$

$$D_{56} = \int_V \int \eta\, \xi \overline{Q_{11}'}\, dA + \int_H \int \eta\, \xi \overline{Q_{11}'}\, dA$$

$$D_{66} = \int_V \int \eta^2 \overline{Q_{11}'}\, dA + \int_H \int \eta^2 \overline{Q_{11}'}\, dA$$

... 4.26

In the above equations, the suffix H and V represent the integration over the horizontal and vertical wall respectively. The integrals in 4.26 can be numerically integrated to find the stiffness coefficients. For the present case of box-beam, it is possible also develope analytical relations for the stiffness coefficients.

**4.3 Finite element formulation**

The beam is divided into a number of elements. The strain energy of a typical e th element can be expressed as

$$U^e = \frac{1}{2} \int_{x_e}^{x_{e+1}} \{ \varepsilon \}^T [ D ] \{ \varepsilon \}\, dx$$

... 4.27

where [ D ] and { $\varepsilon^e$ } are given by equations 4.5and 4.3.h respectively.Using relations 4.1.d and 4.1.e the matrix { $\varepsilon^e$ } can be expressed as

$$\{ \varepsilon \} = \{ P \} + \{ Q \} \qquad \ldots 4.28$$

where,

$$\{ P \}^T = \begin{bmatrix} u & v & w & \phi & \beta_y' & \beta_z' \end{bmatrix},$$

$$\{ Q \}^T = \begin{bmatrix} 0 & -\beta_z & -\beta_y & 0 & 0 & 0 \end{bmatrix}.$$

....4.29

Thus, we have 6 degrees of freedom, namely u, v, w, $\phi$, $\beta_y$ and $\beta_z$. These can be expressed in the vector form as

$$\{ X \}^T = \left| \underline{u} \quad v \quad w \quad \phi \quad \beta_y \quad \underline{\beta_z} \right| \qquad \ldots 4.30$$

We notice that in equation 4.26 the highest order of derivative of any degree of freedom is two. Thus, for convergence, completeness in 1) u, u' 2) v, v', 3) w, w', 4) $\phi$, $\phi'$, 5) $\beta_y$, $\beta_y'$ and 6) $\beta_z$, $\beta_z'$ is required and the compatibility of u, v, w, $\phi$, $\beta_y$ and $\beta_z$ is required. Hence two noded elements with linear shape functions can be used. The vector { X } at any point can be expressed as

$$\{ X^{ne} \} = [ S ] \{ X^{ne} \} \qquad \ldots 4.31$$

where,

$$[S] = \left| \begin{array}{cccccccccccc} \underline{N_1} & 0 & 0 & 0 & 0 & 0 & N_2 & 0 & 0 & 0 & 0 & \underline{0} \\ 0 & N_1 & 0 & 0 & 0 & 0 & 0 & N_2 & 0 & 0 & 0 & 0 \\ 0 & 0 & N_1 & 0 & 0 & 0 & 0 & 0 & N_2 & 0 & 0 & 0 \\ 0 & 0 & 0 & N_1 & 0 & 0 & 0 & 0 & 0 & N_2 & 0 & 0 \\ 0 & 0 & 0 & 0 & N_1 & 0 & 0 & 0 & 0 & 0 & N_2 & 0 \\ \underline{0} & 0 & 0 & 0 & 0 & N_1 & 0 & 0 & 0 & 0 & 0 & \underline{N_2} \end{array} \right| \qquad \ldots 4.32$$

is the shape function matrix and

$$\{ X^{ne} \}^T = \left| \underline{u_1, v_1, w_1, \phi_1, \beta_{y_1}, \beta_{z_1}, u_2, v_2, w_2, \phi_2 \beta_{y_2}, \beta_{z_2}} \right| \qquad \ldots 4.33$$

is the vector of elemental degrees of freedom. Here $N_1$ and $N_2$ are the shape functions and can be expressed in terms of the local co-ordinate $\alpha$. For the e th element, the relationship between $\alpha$ and the global co-ordinate x is given by

$$\alpha = \frac{x - x_c}{L} \qquad \ldots 4.34$$

where,

$$L = \frac{x_{e+1} - x_e}{L} \qquad \ldots 4.35$$

is the half length of the element and

$$x_c = \frac{x_{e+1} + x_e}{2} \qquad \ldots 4.36$$

is the global co-ordinate of the mid-point of the element e.

The expressions for $N_1$ and $N_2$ which satisfy the convergence criteria are

$$N_1 = \frac{1}{2} ( 1 - \alpha )$$

$$N_2 = \frac{1}{2} ( 1 + \alpha ) \qquad \ldots 4.37$$

From expressions 4.28 and 4.29 the vector $\{ \varepsilon \}$ can be expressed as

$$\{ \varepsilon \}^T = [ B ] \{ X^{ne} \} \qquad \ldots 4.38$$

where

$$[ B ] = [ B ]_1 + [ B ]_2 \qquad \ldots 4.39$$

$$[B]_1 = \begin{bmatrix} N_{1,\alpha} & 0 & 0 & 0 & 0 & 0 & N_{2,\alpha} & 0 & 0 & 0 & 0 & 0 \\ 0 & N_{1,\alpha} & 0 & 0 & 0 & 0 & 0 & N_{2,\alpha} & 0 & 0 & 0 & 0 \\ 0 & 0 & N_{1,\alpha} & 0 & 0 & 0 & 0 & 0 & N_{2,\alpha} & 0 & 0 & 0 \\ 0 & 0 & 0 & N_{1,\alpha} & 0 & 0 & 0 & 0 & 0 & N_{2,\alpha} & 0 & 0 \\ 0 & 0 & 0 & 0 & N_{1,\alpha} & 0 & 0 & 0 & 0 & 0 & N_{1,\alpha} & 0 \\ 0 & 0 & 0 & 0 & 0 & N_{1,\alpha} & 0 & 0 & 0 & 0 & 0 & N_{1,\alpha} \end{bmatrix}$$

... 4.40

$$[B]_2 = \begin{bmatrix} 0 & 0 & 0 & 0 & 0 & 0 & 0 & 0 & 0 & 0 & 0 & 0 \\ 0 & 0 & 0 & 0 & 0 & -N_1 & 0 & 0 & 0 & 0 & 0 & -N_2 \\ 0 & 0 & 0 & 0 & -N_1 & 0 & 0 & 0 & 0 & 0 & -N_2 & 0 \\ 0 & 0 & 0 & 0 & 0 & 0 & 0 & 0 & 0 & 0 & 0 & 0 \\ 0 & 0 & 0 & 0 & 0 & 0 & 0 & 0 & 0 & 0 & 0 & 0 \\ 0 & 0 & 0 & 0 & 0 & 0 & 0 & 0 & 0 & 0 & 0 & 0 \end{bmatrix}$$

...4.41

where the subscript ,$\alpha$ represents differentiation w.r.t $\alpha$. Substituting in 4.27, we get the expression for the strain energy as

$$U^e = \frac{1}{2} \{ X^{ne} \}^T [ K^e ] \{ X^{ne} \} \qquad \ldots 4.42$$

$$[K^e] = \int_{x_e}^{x_{e+1}} [B]^T [D] [B] \, dx \qquad \ldots 4.43$$

is the elementary stiffness matrix. To perform the above integration numerically, the variable x needs to be transformed to the local variable $\alpha$ using the relation 4.34.

When the elemental stiffness matrices $[K^e]$ are assembled, we get the global stiffness matrix $[K_g]$. The global finite element equations become

$$[K_g] \{X_g\} = \{F_g\} \qquad \ldots 4.44$$

where, $\{X_g\}$ is the vector of global degrees of freedom and $\{F_g\}$ is the global force vector. Here it is assumed that the external forces consist of only the concentrated forces and/or moments. A node is placed at the point of application of every concentrated force or moment. Thus $\{F_g\}$ is found by putting the values of the external forces and moments in the approximate rows.

### 4.2 Results and Discussion

The analysis was carried out for a cantilever beam. The response of the structure was studied for three layups of the plies namely cross-ply layup, antisymmetric layup and symmetric layup. The following three types of loading were considered:

a) Unit tip axial force

b) Unit tip bending force

c) Unit tip torque

The details of the beam are shown in table 4.1 ( Ref. [4] )

a) Cross - ply layup :

Table 4.2 shows the tip deflections for a cross - ply layup. As expected, the various modes of deformation are uncoupled. To study the effects of constrained warping, the analysis was carried for a beam of having a L/d ratio 29. In this case the values of c and d chosen for this case are 52.324 mm and 26.035 mm respectively [ 4 ]. Table 4.3 shows the tip twist under unit torque. It is seen that tip twist is underestimated by about 14% if warping is neglected.

Table 4.1: Dimensions and Material properties of the composite box - beam

| | |
|---|---|
| Length of the beam ( L ) | 762.00 mm |
| Outer depth of the box - beam cross - section ( d ) | 13.64 mm |
| Outer width of the box - beam cross - section ( c ) | 24.20 mm |
| Ply thickness ( t ) | 0.127 mm |
| Elastic modulus in the direction of the fibre ( $E_1$ ) | 142.045 Gpa |
| Elastic modulus in the direction perpendicular to fibre ( $E_2$ ) | 9.796 Gpa |
| In - plane shear modulus ( $G_{12}$ ) | 6.001 Gpa |
| Poisson's ratio in the direction of the fibres ( $\nu_{12}$ ) | 0.42 |

Table 4.2: Response of a cross - ply composite box - beam

| Loading | u (mm) | v (mm) | $\phi$ (mm) |
|---|---|---|---|
| a) Unit tip axial force | 0.000807 | 0.0 | 0.0 |
| b) unit tip bending force | 0.0 | 4.072 | 0.0 |
| c) Unit tip torque | 0.0 | 0.0 | 0.00334 |

Table 4.3 Tip twist under unit tip torque for cross - ply layup composite box - beam

| Case | twist ( radian ) |
|---|---|
| without warping | 0.0003749 |
| with warping ( ref [4] ) | 0.000425 |

b) symmetric layup

Figure 4.4 shows the variation of tip twist with the ply orientation angle ( $\theta$ ) under unit tip torque. It is observed that the tip twist reaches its minimum value at $\theta = 30^{o}$. The same graph also shows the result from reference [ 4 ] which indicates the effect of constrained warping. When this effect is neglected, the tip twist is underestimated up to $\theta = 36^{o}$ and overestimated beyond that up to $\theta = 85^{o}$. The maximum error in the estimation of the twist is about 45 %. When the effect of constrained warping is included, the location of minimum twist shifts from $\theta = 30^{o}$ to $\theta = 45^{o}$ and the graph becomes symmetric about the line $\theta = 45^{o}$.

Figure 4.5 shows the variation of tip twist with the ply orientation angle ( $\theta$ ) under unit tip bending load. It is seen that the effect of bending - twist coupling is more predominant for the range $15^{o} < \theta < 60^{o}$. Further, the coupling effect is quite strong as the twist due to unit bending load is almost of the same order as that due to unit torque ( Fig 4.4 ). The result of reference [ 4 ] which includes the effect of constrained warping is also shown in Fig 4.5. It is observed that, when the effect of constrained warping is neglected, the tip twist is underestimated by as much as 70 %.

Figure 4.6 shows the variation of tip bending deflection with the ply orientation angle ( $\theta$ ) under unit tip bending load. As expected, the tip deflection increases with $\theta$. This happens because the effective Young's modulus along the beam length decreases with $\theta$. The same trend is observed in Fig 4.7 which shows the variation of the tip extension with $\theta$ under unit tip axial load. In both the graphs, the maximum rate of increase occurs at around $\theta = 45^{o}$.

c) Antisymmetric layup

Figure 4.8 shows the variation of the tip twist with the ply orientation angle ( $\theta$ ) under unit tip torque. For this case also, the minimum value of the tip twist occurs at $\theta = 30^{o}$. The same graph also shows the results from the reference [ 4 ] which includes the effect of constrained warping. When this effect is neglected, the tip twist is underestimated for all values of $\theta$. The maximum estimation error is about 25 %.

The effect of extension - twist coupling is shown in Fig 4.9.a in the form of variation of tip twist with $\theta$ under unit tip axial load. The coupling effect is more predominant for $15 < \theta < 45^{o}$. The result of reference [ 4 ] which includes the effect of constrained warping is shown in Fig 4.9.b. It is seen that, when this effect is excluded, the tip twist is underestimated by as much as 99 %. However, even after including this effect, the order of tip twist increases to 0.001 radians which is about 25 % of the tip twist due to unit tip torque. Therefore the coupling effect is rather weak for the antisymmetric layup.

Figure 4.10 shows the effect of varying the ply angle ( $\theta$ ) on the tip bending deflection under unit tip bending force. It is observed that the bending deflection increases gradually with $\theta$ upto $\theta = 60^{o}$ after which it remains more or less constant. The same trend is observed in Fig 4.11 which shows the variation of the tip extension under unit tip axial load.

d) Comparison

Comparison of Figures 4.4 and 4.8 show that the tip twist under unit tip torque is more or less same for both the symmetric and antisymmetric layup. For most values of $\theta$, the tip twist for symmetric / antisymmetric layup is less than that for the cross-ply layup ( Table 4.2 ). The tip bending deflection of the antisymetric layup is always smaller than that of the symmetric layup except for $\theta = 0$ ( Figures 4.6 and 4.10 ). For $\theta = 90^{o}$, it is less than one-third of the value of the symmetric layup. Further, the maximum tip bending deflection of the antisymmetric layup is less than the tip bending deflection of the cross - ply layup ( refer to table

4.2 ). Similar trend is observed for tip extension ( see Figures 4.7, 4.11 and table 4.2 ). Thus for the same material and geometric properties, the antisymmetric layup is more stiff.

As stated earlier, the additional twist produced by the coupling effect is much less in antisymmetric layup ( Fig 4.9 ) than in the symmetric layup ( Fig 4.5 ). Thus, the coupling effect is weak in antisymmetric layup. It is totally absent in the cross-ply layup.

When the effect of constrained warping is neglected, the maximum error in the estimation of the tip twist under unit tip torque is more for symmetric layup than for antisymmetric layup. The total twist consists of the twist due to the torque and the additional twist produced by coupling effect. As stated earlier, in the symmetric layup, this additional twist is almost of the same order as the twist due to torque. On the other hand, it is vary small in the antisymmetric layup. Further, when the effect of constrained warping is included, the additional twist in the symmetric layup,becomes much larger than the the twist due to torque ( Figures 4.4. and 4.5 ). But in the case of antisymmetric layup, the additional twist even after considering the effect of constrained warping, never becomes even as large the twist due to torque ( Figures 4.8 and 4.9.b ). Thus the effect of constrained warping is less severe for antisymmetric layup.

c) Conclusions:

1) The antisymmetric layup is more stiff than the symmetric layup. Additionally, the coupling effect is quite weak in the antisymmetric layup. Further, in a typical turbine blade, the axial

forces are quite small compared to transverse forces. Then the coupling does not have any effect. Finally the effect of constrained warping is also less in the antisymmetric layup compared to symmetric layup. As a result the antisymmetric layup is better than the symmetric layup.

2) Tip twist is maximum at about $\theta = 30^{o}$ in the antisymmetric layup. Further, tip bending deflection and tip extension are smaller upto $\theta = 45^{o}$. Thus a suitable range for ply orientation is from $\theta = 15^{o}$ to $\theta = 45^{o}$.

3) For the antisymmetric layup, neglecting the effect of constrained warping may not led to serious errors either in values or in trends in stress / vibration analysis of wind turbine blades.

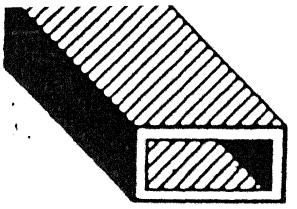

Symmetric Layup Beam

- Bending-Torsion Coupling
- Extension-Shear Coupling

Cross-Ply Layup Beam

- Alternating Plies at 0 and 90 deg
- No Elastic Couplings

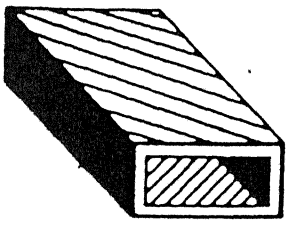

Anti-Symmetric Layup Beam

- Extension-Torsion Coupling
- Bending-Shear Coupling

Fig 4.1 : Composite layup designations.

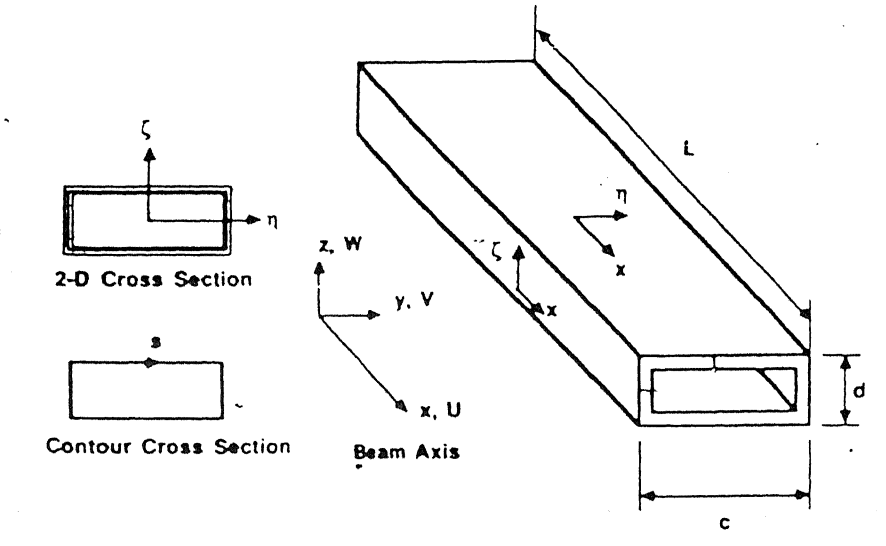


Fig 4.2 Box-beam configuration and coordinates.

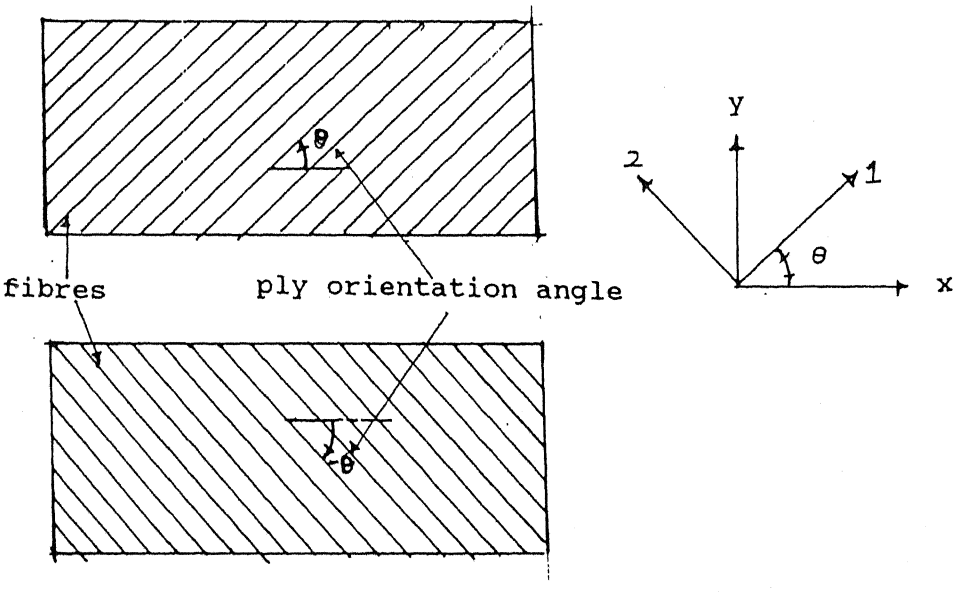


Fig 4.3 : Illustration of Ply Oreintation Angle.

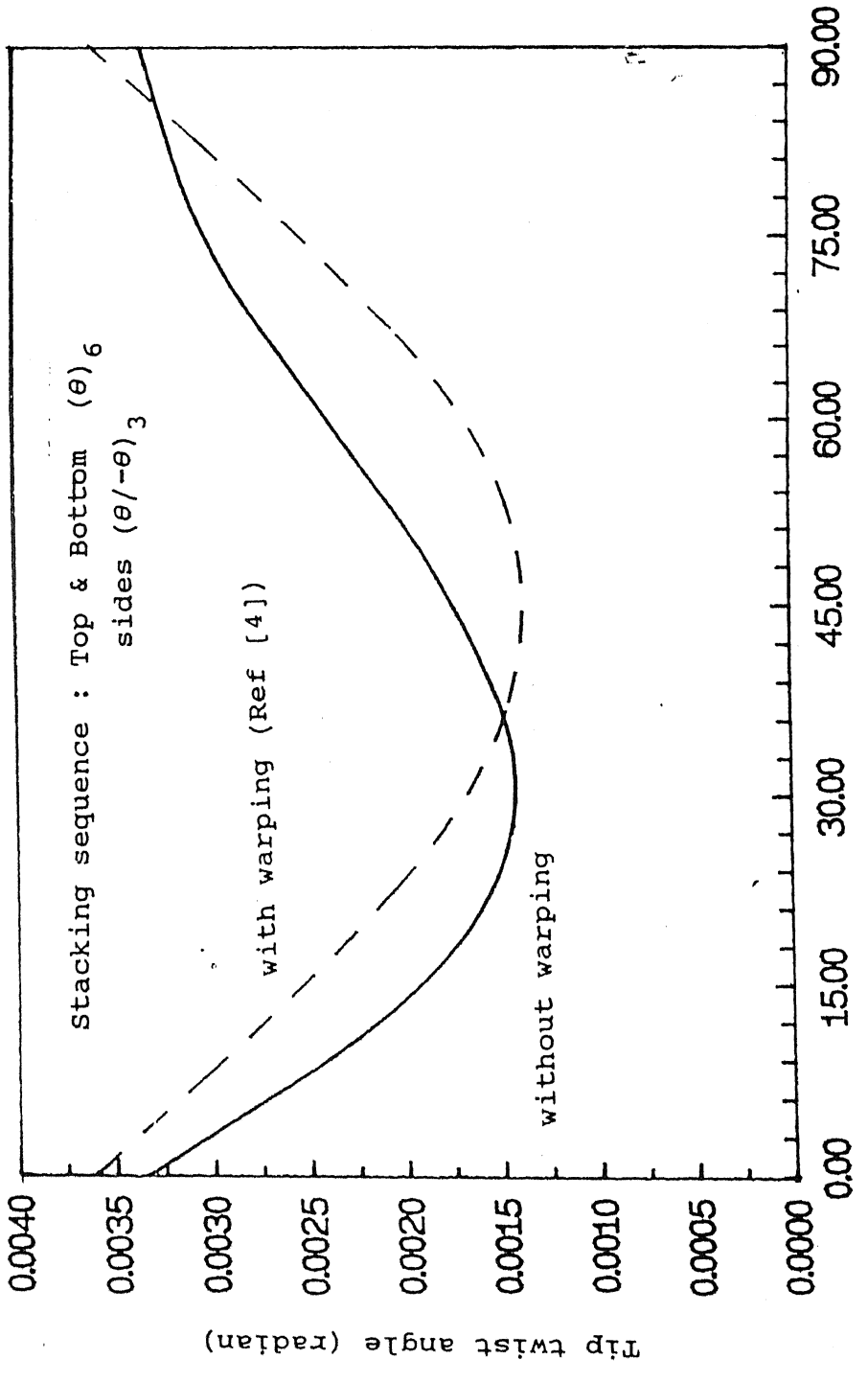


Fig 4.4: Tip Twist of Symmetric Layup Under Unit Tip Torque

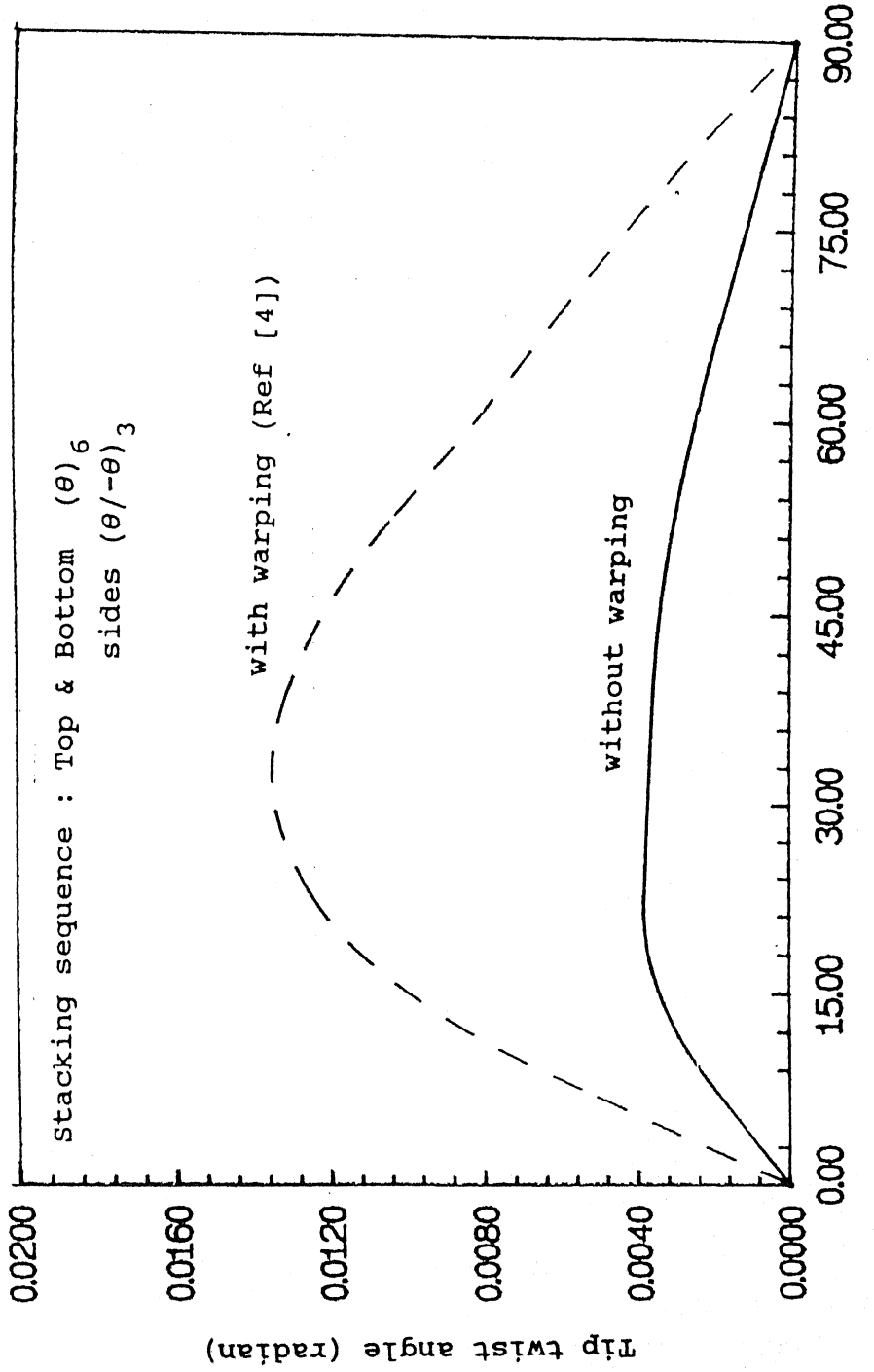


Fig 4.5: Tip Twist of Symmetric Layup Under Unit Tip Bending Load.

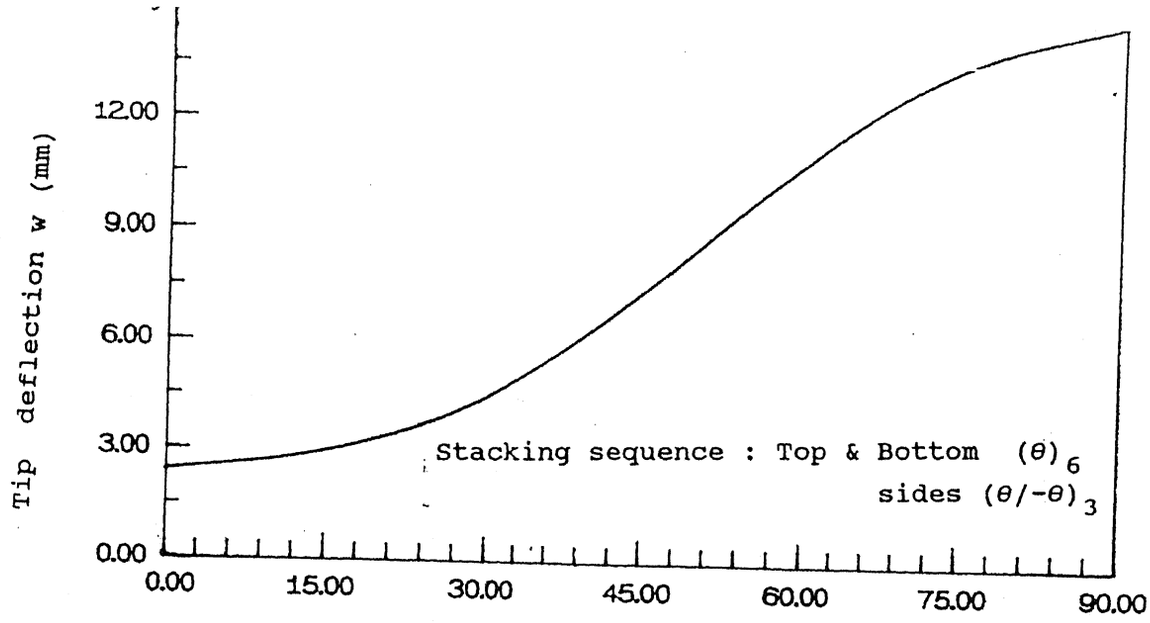


Fig 4.6: Tip Deflection of Symmetric Layup Under Unit Tip Bending Load.

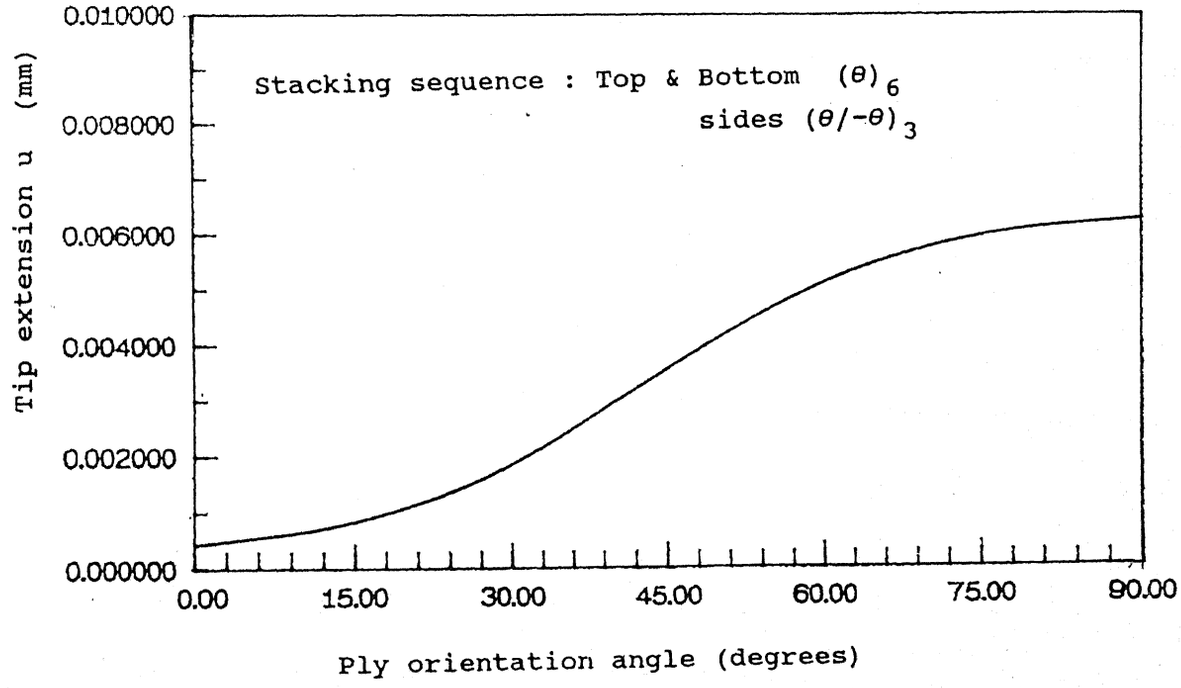


Fig 4.7: Tip Extension of Symmetric Layup Under Unit Tip Axial Load.

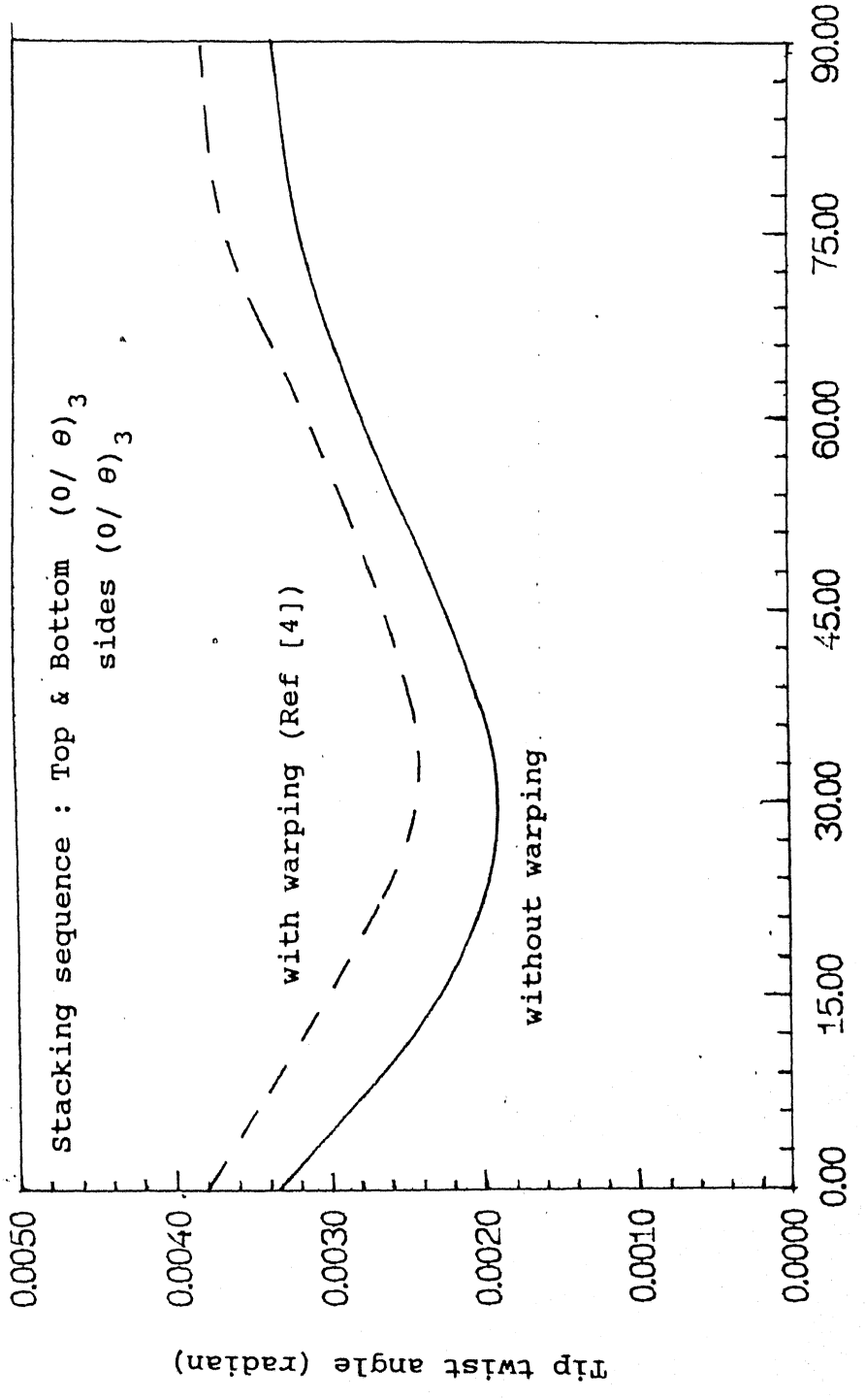


Fig 4.8: Tip Twist of Antisymmetric Layup Under Unit Tip Torque

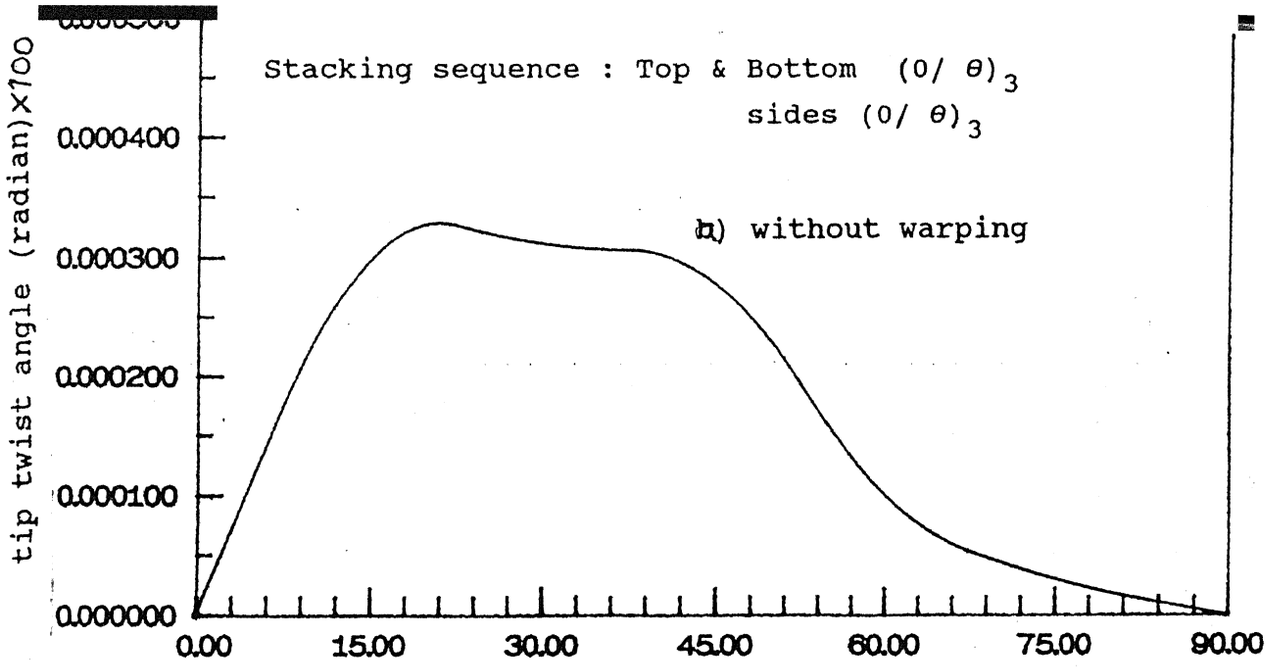


Fig 4.9 Tip Twist of Antisymmetric Layup Under Unit Tip Axial Load.

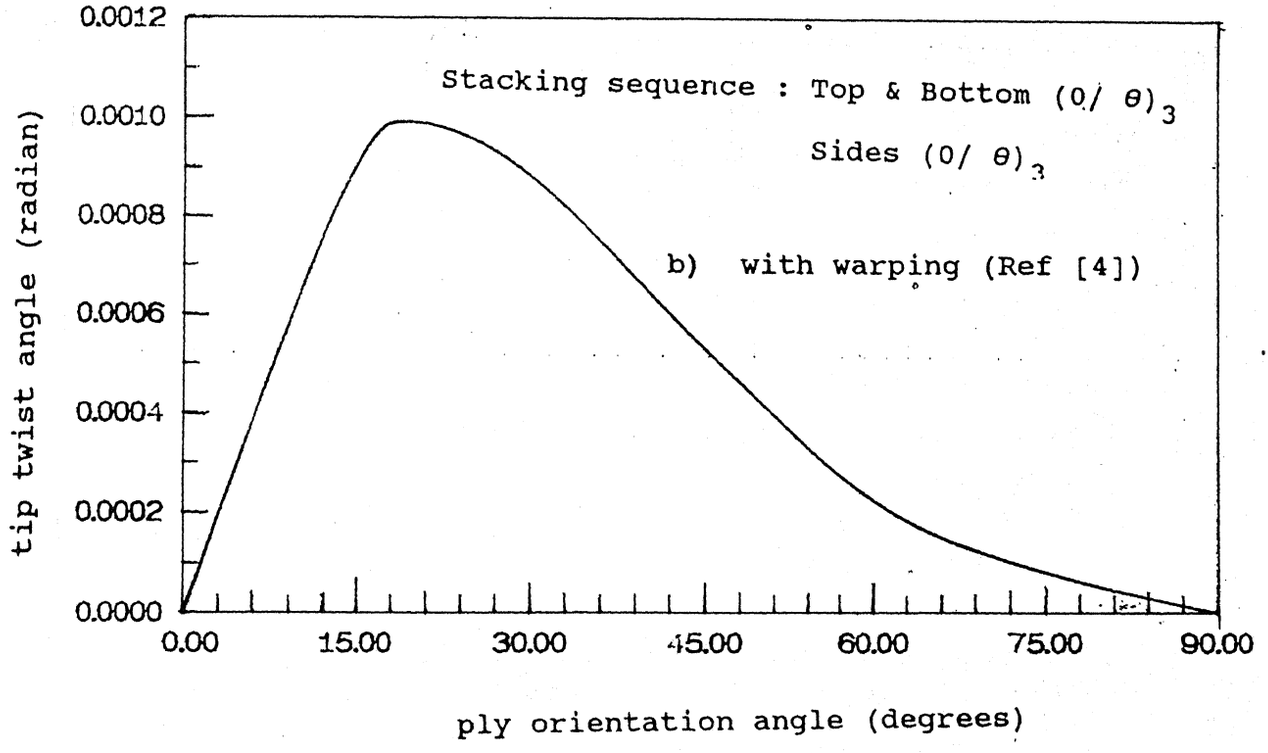


Fig 4.9b Tip Twist of Antisymmetric Layup Under Unit Tip Axial Load.

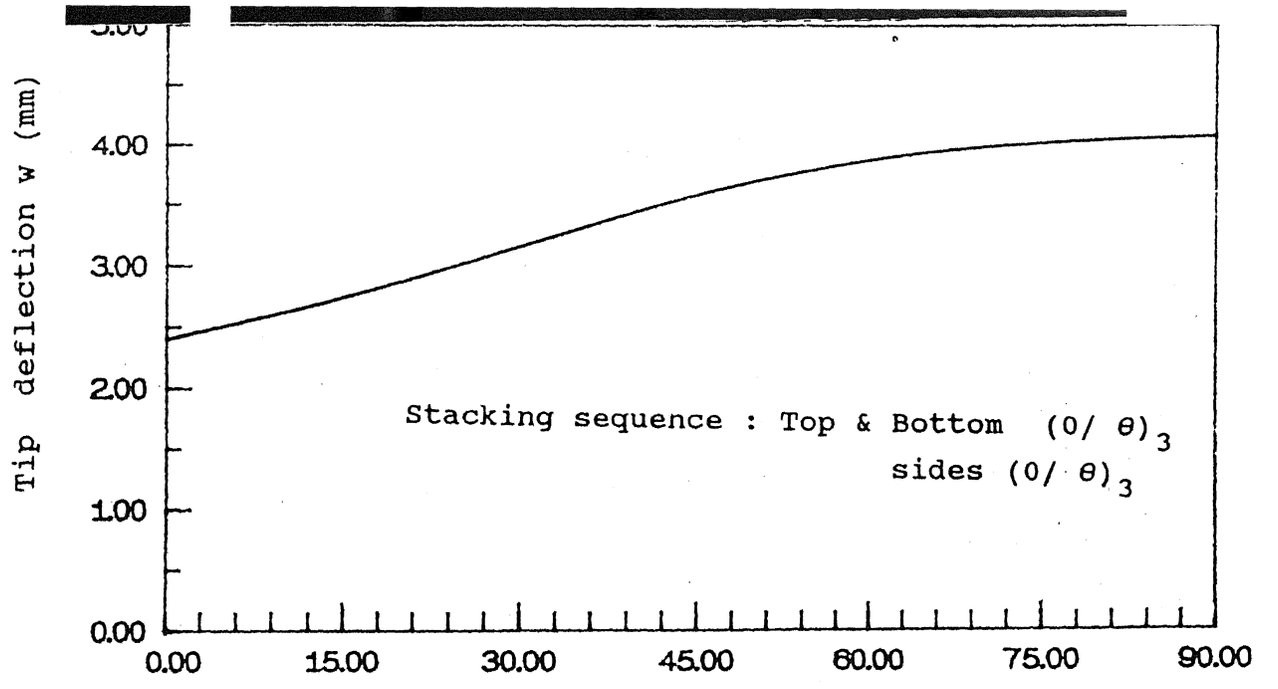


Fig 4.10: Tip Deflection of Antisymmetric Layup Under Unit Tip Bending Load.

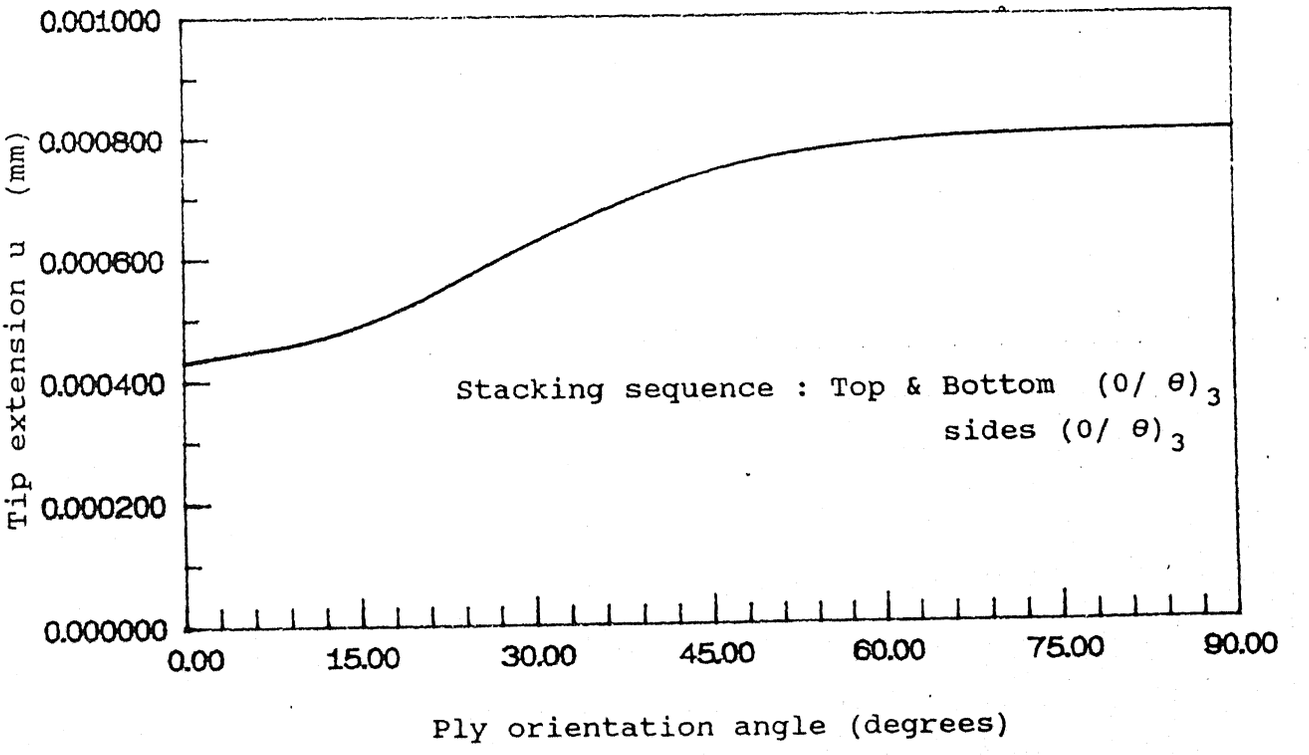


Fig 4.11: Tip Extension of Antisymmetric Layup Under Unit Tip Axial Load.

# CHAPTER 5

## SUMMARY OF RESULTS AND CONCLUSIONS

For the VGVAWT blade, a standard 2 cell structure consisting of a D-shaped thick-walled spar and thin walled skin is chosen. A stepped internal taper is introduced to bring down the mass centre of the blade. Uni - directional fabric is used as the blade material. The stresses at the critical section are determined using Engineer's theory of bending and Bredt - Batho theory of torsion of multi - cell sections. Reasonable values are chosen for various thickness ratios. Finally the spar thickness in the untapered portion is determined using Tsai - Wu failure criterion for composite materials.

The finite element method is used to obtain the natural frequencies and mode shapes of the VGVAWT. The periodic aerodynamic force acting on the blade is resolved into Fourier components to determine the most dominant excitation frequencies. The campbell ( or interference ) diagram is constructed to check for resonance. It is shown that there is no resonance at the operational speed and hence the structural design of VGVAWT blade is satisfactory from resonance point of view also. Further, if a small change is made either in structural details (i.e various thickness ratios ) or in the distance of the intermediate support, then also the structure is safe against resonance. Parametric study of the natural frequencies lead to the following conclusions

1) In a thin walled beam, the natural frequencies do not change with thickness.

2) The natural frequencies under consideration increase with

the increase in the distance of the support from the base.

3) As the shear centre distance from the mass centre increases, the torsion frequency decreases. There is very little effect on the flap - wise and edge - wise bending frequencies.

When a wind turbine is to be designed for high capacity, the spar has to be modelled as a composite box - beam. The static behaviour of this beam is studied for three different stacking sequences : cross - ply layup, antisymmetric layup and symmetric layup. Shear deformation and appropriate coupling effects are taken into account. The study leads to the following conclusions

1) The antisymetric layup is more stiff than the other two layups. Compared to the symmetric layup, the effect of constrained warping and the coupling effect are small in the antisymmetric layup. Thus the antisymmetric layup is better than the symmetric layup. 2) For the antisymmetric layup, the ply orientation angle should be between $15^{o}$ and $45^{o}$ to minimise the deflections.

3) If the effect of constrained warping is neglected, the stress / vibration analysis of antisymmetric layup are still expected to give reasonable values / trends.

**Suggestions for future work**

1. The effects of shear deformation and constrained warping should be included in the stress analysis of the VGVAWT blade.

2.a) The effects of shear deformation and constrained warping should be included in the vibration analysis of the VGVAWT blade.

b) The flexibility of the cross - arm and the tower should be included in the vibration study.

c) The effects of various airfoil shapes ( NACA and NASA series ) on the natural frequencies should be studied.

3) The effects of constrained warping, stacking sequence and ply orientation angle on the natural frequencies of rotating composite box - beam should be studied.

REFERENCES

1(a). Ghosh,K.,

"Centrifugal reef control of variable geometry vertical axis wind turbine",

Proceedings of world renewable energy congress reading, UK, 1990

1(b). Megson,T.H.G ,

" Linear analysis of thin walled elastic structures ",

John Wiley & Sons, New York, 1974.

2. Chandra,R., Stemple,A.D and Chopra,I. ,

" Thin - Walled composite beams under bending, torsional and extensional loads ",

Journal of Aircraft, Vol 27, No 7, July 1990, pp 619 - 626.

3. Stemple,A.D., Lee,S.W ,

" Finite-element model for composite beams with arbitrary cross-sectional warping.",

AIAA Journal, Vol 26, No 12 , December 1988, pp 1512 - 1520.

4. Smith,E.C and Chopra,I,

" Formulation and evaluation of an analytical model for composite box-beams ",

Journal of The American Helicopter Soc.,July 1991, pp 23-35.

5. Chandra,R., Chopra,I.,

" Structural behaviour of two-cell composite rotor blades with elastic couplings ",

AIAA Journal, Vol 30, No 12, December 1992, pp 2914 - 2921.

6. Carnegie,W.,

" The application of the variational method to derive the equations of motion of vibrating cantilever blading under rotation"

Bulletin of Mech. Engg. Education, Vol 6, 1967, pp 29 - 38.

7. Chandra,R. and Chopra,I.,

" Experimental- theoretical investigation of the vibration charecteristics of rotating composite box-beams ",

Jnl. of Aircraft, Vol 29, No 4, July - Aug. 1992, pp 657 - 664.

8. Filipich,C.P, and Rosales,M.B,

" Free flexural-torsional vibrations of a uniform spinning beam ",

Journal of Sound and Vibration, Vol 141 (3), 1990, pp 375 - 387.

9. Selvaraj,K.,

" Aerodynamic design of centrifugally controlled variable geometry vertical axis wind turbine "

M.tech Thesis, Dept. of Aerospace Engg., IIT Kanpur, April 1992.

10. Datoo,M.H,

" Mechanics of fibrous composites "

Elsevier Science Publishers Ltd, Essex, 1991.

11. Zweben,C., Hahn,H.T. and Chow,T.W.,

" Mechanical behaviour and properties of composite materials "

Technomic Publications Ltd, Pennsylvania, 1989.